# R

## RADARSAT-2

RADARSAT-2, the second in a series of Canadian spaceborne Synthetic Aperture Radar (SAR) satellites, was built by MacDonald Dettwiler, Richmond, Canada. RADARSAT-2, jointly funded by the Canadian Space Agency and MacDonald Dettwiler, represents a good example of public–private partnerships. RADARSAT-2 builds on the heritage of the RADARSAT-1 SAR satellite, which was launched in 1995. RADARSAT-2 will be a single-sensor polarimetric C-band SAR (5.405 GHz).

RADARSAT-2 retains the same capability as RADARSAT-1. Morena et al., 2004 For example, the RADARSAT-2 has the same imaging modes as RADARSAT-1, and as well, the orbit parameters will be the same thus allowing co-registration of RADARSAT-1 and RADARSAT-2 images. Furthermore, radiometric and geometric calibration is maintained thus permitting correlation of time series data for applications such as long-term change detection (Luscombe and Thomson, 2001).

The following features of the RADARSAT-2 system are thought to be the most significant in terms of their impact on existing and new applications.

*Polarization modes*. Three polarization modes: Selective, Polarimetry, Selective Single.
*Resolution*. 3 m ultra-fine mode and a 10-m Multi-Look Fine mode.
*Programming lead time*. Programming is defined as the minimum time between receiving a request to program the satellite and the actual image acquisition. Routine image acquisition planning is base-lined at 12–24 h, and emergency acquisition planning is base-lined at 4–12 h.
*Processing*. Routine processing is base-lined at 4 h; emergency processing is base-lined at 3 h; and 20 min for processing a single scene.
*Re-visit*. Re-visit is defined as the capability of the satellite to image the same geographic region. Re-visit is improved through the use of left- and right-looking capability.
*Georeference*. Image location knowledge of $<$300 m at down-link and $<$100 m post-processing.

## RADARSAT-2 polarimetry modes

The RADARSAT-2 polarimetric capability is considered to be the most significant in terms of increasing the information content of the SAR imagery, and is subsequently discussed in more detail. To date, SAR data have been widely available from single channel (single frequency and polarization) spaceborne radars including ERS-1 and 2, JERS-1, and RADARSAT-1. RADARSAT-2 provides polarized data, and is the first spaceborne commercial SAR to offer polarimetry data.

The intent here is not to outline polarimetry theory, but to present the concepts in an intuitive manner so that those not familiar with polarimetry can understand the benefits of polarimetry and the information available in polarimetry data. Many articles are available that discuss polarimetry theory, applications, and provide excellent background information (Ulaby and Elachi, 1990; Touzi *et al*. 2004). Notwithstanding the inherent complexity of polarimetry, polarimetry in its simplest terms refers to the orientation of the radar wave relative to the earth's surface and the phase information between polarization configurations.

RADARSAT-1 is horizontally polarized meaning the radar wave (the electric component of the radar wave) is horizontal to the earth's surface (Figure R1). In contrast, the ERS SAR sensor was vertically polarized, implying the radar wave was vertical to the earth's surface. Spaceborne SAR sensors such as RADARSAT-2, ENVISAT, and the Shuttle Imaging Radar have the capability to send and receive data in both horizontal (HH) and vertical (VV) polarizations. Both the HH and VV polarization configurations are referred to as co-polarized modes. A second mode, the cross-polarized mode, combines horizontal send with vertical receive (HV) or vice versa (VH). As a rule, the law of reciprocity applies and HV $\cong$ VH (Ulaby and Elachi, 1990).

A unique feature of RADARSAT-2 is the availability of polarimetry data, meaning that both the amplitude and the phase information are available. The amplitude information is familiar to SAR users, but the phase information is likely new and rather nonintuitive. In its simplest term, phase can be thought of as the travel time for the SAR signal: the travel time is the two-way time between the sensor and the earth, and includes any propagation delays as a result of surface or volume scattering. It is the propagation delays and the scattering properties of the HH and VV polarization configurations that make polarimetry data so powerful.

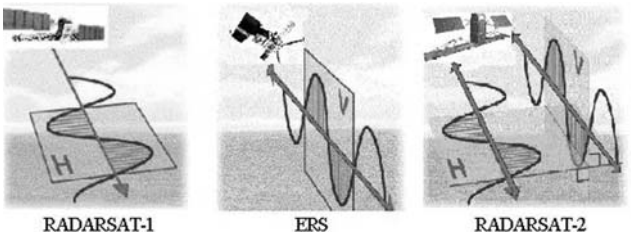


**Figure R1** Orientation of horizontal (H) and vertical (V) polarization. Typical transmit and receive polarizations are HH, VV, and HV (adapted from the CCRS website).

**Table R1** RADARSAT-2 modes. Beam mode name, swath width, swath coverage, and nominal resolution

| | Beam mode | Nominal swath width (km) | Swath coverage to left or right of ground track (km) | Approximate resolution Rng × Az ($m^2$) |
|---|---|---|---|---|
| Selective Polarization | Standard | 100 | 250–750 | 25 × 28 |
| | Wide | 150 | 250–650 | 25 × 28 |
| Transmit H or V | Low incidence | 170 | 125–300 | 40 × 28 |
| Receive H or V or (H and V) | High incidence | 70 | 750–1000 | 20 × 28 |
| | Fine | 50 | 525–750 | 10 × 9 |
| | ScanSAR wide | 500 | 250–750 | 100 × 100 |
| | ScanSAR narrow | 300 | 300–720 | 50 × 50 |
| Polarimetry | | | | |
| Transmit H and V on alternate pulses | Standard QP | 25 | 250–600 | 25 × 28 |
| Receive H and V on every pulse | Fine QP | 25 | 400–600 | 11 × 9 |
| Selective Single Polarization | | | | |
| Transmit H or V | Multiple fine | 50 | 400–750 | 11 × 9 |
| Receive H or V | Ultra-fine wide | 20 | 400–550 | 3 × 3 |

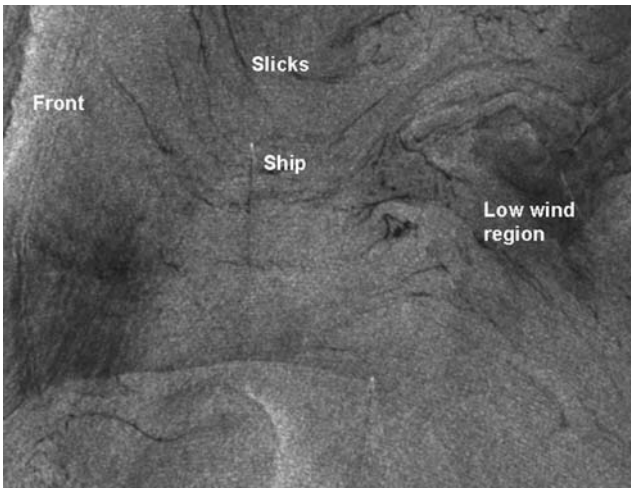


**Figure R2** RADARSAT-1 SAR image acquired September, 1998 off the coast of Alaska. Typical ocean features and targets are shown. (Canadian Space Agency, 1998).

The RADARSAT-2 program has adopted the following terms to define the polarization modes (Table R1): Selective Polarization, Polarimetry, and Selective Single Polarization. Selective Polarization and Selective Single Polarization modes imply the availability of amplitude data, but no interchannel phase data. For example, amplitude data may be HH, VV, or HV imagery. In contrast, the polarimetry mode (also called quad-polarized) implies the availability of both amplitude and interchannel phase information. The amplitude information is the same as the Selective Polarization and Selective Single Polarization modes, but adds phase information, such as the co-polarized phase difference.

## Marine applications

Marine applications of SAR data can be divided into three main categories: atmospheric phenomena, ship detection, and ocean features (Figure R2).

Atmospheric phenomena include the effect of large-scale atmospheric features such as hurricanes on the ocean surface. Although SAR images through the hurricane cloud-structure, the variability of the hurricane wind speed produces changes in the ocean surface-roughness that the radar detects. For example, the low-wind regime at the eye of the hurricane looks very different than the outer high-wind edges. The radar sensitivity to wind-induced roughness can also be used to map ocean-surface wind speed and direction. The use of VV polarization will be the preferred polarization configuration, largely due to a better radar response relative to HH or HV configurations.

Ship detection is optimal under low wind conditions, HH polarization, and large incidence angles. When co-polarized data and small incidence angles are used, there is increased radar return from the ocean surface, thus reducing the contrast between the ocean and the ship. The use of cross-polarized data (e.g., HV), however, enhances ship detection at small incidence angles due to the weaker return from the ocean surface, but similar return from the ship. Through the application of target decomposition algorithms, quad-polarized data can be used for ship detection and classification (Yeremy *et al.*, 2001).

Ocean features include the detection of eddies, fronts, slicks, currents, surface waves, and internal waves. Radar return from the ocean surface is due to Bragg scattering. Bragg scattering is stronger for VV polarization, thus VV polarization is predominantly used versus HH or HV. The use of quad-polarized data will add significantly to the information content of the SAR imagery.

Gordon C. Staples

## Bibliography

CASI, 2004. *Canadian J. of Remote Sensing, RADARSAT-2* Special Issue, **30**(3): 365 pp.

Luscombe, A., 2001. *RADARSAT-2 Product Specification*, Richmond, Canada: MacDonald Dettwiler RN-SP-50–9786.

Morena, L., James, K., and Beck, K., 2004. An Introduction to the RADARSAT-2 mission, *Canadian Journal of Remote Sensing*, **30**(3): 221–234.

Ulaby, F., and Elachi, C. (eds.), 1990. *Radar Polarimetry for Geoscience Applications*. Norwood, MA: Artech House.

Yeremy, M., Campbell, J., Mattar, K., and Potter, T., 2001. Ocean Surveillance with Polarimetric SAR. *Canadian Journal of Remote Sensing*, **27**(4): 328–344.

## Cross-references

Remote Sensing of Coastal Environments
Synthetic Aperture Radar Systems

# RATING BEACHES

## Introduction

Beaches are the number one recreational destination for Americans and Europeans, and a beach culture has developed worldwide. Nothing restores the body and soul like a stay at the beach. We are naturally drawn to the rhythmic pounding of the waves as if returning to our primordial beginnings. Recreational opportunities abound, and everyone, but perhaps children most of all, loves sand.

People are flocking to the shore in ever-increasing numbers for sun and fun. But most want much more from a beach experience—people are searching for real getaway places where they can escape from urban confinement and everyday pressures. The shore offers freedom from the

"hemmed-in" feeling as we gaze out from the beach at the seemingly endless sea. The fresh, salty air invigorates the body as the sheer beauty and dynamic interplay between the waves and beach captures our imagination and refreshes our psyche.

So what do people look for in a beach? Water quality is probably the first concern. Polluted water can ruin any beach; the washing ashore of medical wastes along northern New Jersey beaches a decade ago nearly wrecked the local coastal economy as tourism plummeted. Coastal waters are the recipient of much of the nation's wastewater. Already stressed by pollution from upland sources, coastal environments are also adversely affected by the onslaught of contaminants from coastal development and wastes dumped at sea. Sewage-associated wastes are an eyesore, particularly along parts of the US urbanized northeast coast, where inadequate treatment systems still exist. The Gulf coast states, especially Louisiana, have the greatest accumulation of ship galley wastes on their beaches. All of these materials degrade nearshore coastal waters and foul beaches (Center for Marine Conservation, 1990). While concern about pollution is mounting as coastal development continues, some areas are addressing long-standing problems (e.g., construction of the massive Boston Harbor sewerage system). Actually, US beaches are generally quite clean compared to those in many countries, where pollution concerns receive far less attention and funding.

There is a worldwide coastward migration of the population, which itself is burgeoning at over 6 billion at present. What some oceanographers refer to as the ring around the bathtub is some of the most expensive real estate in the world. These areas are rapidly urbanizing, and there is much public concern about the quality of coastal areas. For example, it is estimated that by the year 2010, the coastal population will increase almost 60% in the United States. (NOAA, 1990). As the population trend continues, many of the qualities that attracted people initially are diminishing.

Crowded beaches such as Jones Beach, New York, where the sunbathing towels run together like a gigantic patchwork quilt, accommodate a huge number of people, but few would rate this as the best beach. If coastal communities are too successful in encouraging development, as Ocean City, Maryland has been in the last few decades, then overall quality also drops.

Beach weather and water temperature can greatly limit planned activities. The rugged beauty and sereneness of Oregon's beaches appeal to the wilderness enthusiasts, but the water is much too cold for swimming, and frequent rainy days can spoil any plans for sunbathing. While the picturesque Northwest Pacific coast may be described as the most beautiful, others prefer the palm-treed beachscapes of Hawaii. Which is the most beautiful beach? Shakespeare correctly noted that "Beauty lies in the eyes of the beholder." But all of us can probably agree on a few basic characteristics, which include the physical condition, biological quality, and human use and development of beaches.

## Beach awards and ratings

Beach awards and evaluation systems in Europe have been identified as a valuable tool for promotion of beach tourism (Williams and Morgan, 1995). The proliferation of awards and awarding bodies in the United Kingdom, however, has led to low public awareness and distrust of their validity. Those currently in use in the United Kingdom include the European Blue Flag Award (administered by the Foundation for Environmental Education in Europe; FEEE, 1997), the Seaside Award given by the Tidy Britain Group, and the Good Beach Guide, a book published annually by the Marine Conservation Society (MCS, 1997). All of these awards are based on a limited number of factors and do not approach coverage of all measurable aspects of the beach environment (Williams and Morgan, 1995).

Over 2,000 beaches in 18 countries presently participate in the European Blue Flag Award with the numbers growing through time. Only one-third of beach users have a reasonable understanding of the award criteria, which are largely based on water quality; 11% recognized the Blue Flag itself and 7% actually thought the symbol represented danger (Williams and Morgan, 1995).

The Seaside Award was introduced in the United Kingdom in 1992 and is administered by the Tidy Britain Group (a NGO with some government funding). The award criteria are similar to the Blue Flag (e.g., water quality, beach cleanliness, and high standards of facilities and management). While the Blue Flag Award requires strict water quality standards, the Seaside Award system is less rigid so that more UK beaches qualify for this recognition (Williams and Morgan, 1995).

The Good Beach Award is published annually by the MCS and available for sale to the general public at bookstores. Beaches must exhibit a high standard of water quality and a low probability of sewage contamination (which is a major problem for many European beaches). Over 1,000 UK beaches were assessed, and 136 were recommended in 1997. There must be no sewage outfalls adjacent to the beach, bathing must be safe, and there must be no excessive marine litter or sewage—related debris (Williams and Morgan, 1995).

During the past decade, researchers in the United States (Leatherman, 1991, 1997) and Williams and Morgan (1995) in the United Kingdom have devised beach rating systems that attempt to take into account all measurable beach aspects. The two rating surveys are quite similar; beaches are scored for 50 parameters on a scale from one to five (Table R2). In the United States, 650 public recreational beaches were evaluated by Leatherman (1991) and 182 UK beaches were rated by Williams and Morgan (1995). Kapalua on Maui, Hawaii was the first National Winner in 1991 with a score of 92%, and Porthmeir along the English Cornwell coast was listed as the top UK beach in 1995 (at 86%).

For a number of the criteria, a beach user's preference was assumed (e.g., wide beaches are preferable to narrow ones). Quantitative values were attributed to all categories to the extent possible, but some were judged on a purely subjective basis (e.g., vistas far and near). No weighting was attached to the 50 parameters relative to each other in either scheme (Leatherman, 1991; Williams and Morgan, 1995).

## US beaches ratings

A beach rating survey was designed to provide an objective appraisal of the major public recreational beaches along the US Atlantic, Gulf, and Pacific coasts. About 650 beaches were evaluated nationwide on the basis of 50 criteria with a sliding scale to quantify the elusive quality factor. In-state coastal experts provided information and assisted Leatherman (1991) in this evaluation. Only the open ocean and Gulf coast beaches were rated. Therefore, seashores along Long Island Sound in New York and Connecticut were not considered nor were the many small beaches in major bays such as the Chesapeake and San Francisco. Puget Sound is perhaps the most desirable coastal property in the State of Washington, but here again it is an inland marine water body. In addition, Alaska's long coastline with many sandy to cobbly beaches was not evaluated, although the Valdez oil spill spotlighted this area's scenic beauty and the small pocket beaches where the oil tended to accumulate and pool.

A battery of factors were arrayed in order to allow for a quantitative comparison of the various beaches. The relevant criteria are those which influence beach quality as broadly defined. The factors considered in this analysis are of three types: physical, biological, and human use and impacts (Table R2). These ranged from 1 (poor) to 5 (excellent). This approach follows that developed by Leopold (1969) in her quantitative comparison of aesthetic factors for rivers.

The survey was designed to reflect general beach usage with swimming water (see especially factors 5–14) being of primary importance. A water temperature scale for optimal and tolerable conditions for swimming and bathing (Figure R3) was also designed to aid in quantifying factor 5 of the questionnaire (see Table R2). In general, pristine beaches with limited development scored much better than the overdeveloped and overcrowded urban resort areas. A profile can be developed for each beach based on the 50 factors evaluated; Figure R4 illustrates this graphical representation for Kapalua on Maui, Hawaii—the top-rated beach nationally in 1991. For visual comparison, one of the nation's worst beaches (Pike's Beach in the New York City area) is presented (Figure R5). This rating of America's best beaches has been conducted for the past 10 years, and the results have appeared in the popular media. Specialty categories were determined by using a subset of the data. Figure R6 illustrates the ranking for the US northeast region as presented in America's Best Beaches (Leatherman, 1998).

Some coastal specialists have questioned the objectiveness of the beach rating scale. For example, white and pink sand are the most highly rated, while gray sand is assigned the lowest rating. While pure white sand does cause much glare, the sugar-white beaches of the Florida panhandle are considered the most beautiful by sunglass-wearing tourists. Also, the pink sand beaches of Bermuda are something to behold. Others have pointed out that the 50 parameters are all equally weighted and that some factors are more important than others. This consideration was partly dealt with by using a suite of factors that are all related to one variable such as pollution (Table R2, factors 21, 23, 27, 29–31, 43, 44, and 48) or beach safety (Table R2, factors 10–14, 21, 23, 28, 40, 41, and 49). Therefore, multiple factors are used to delineate important criteria in rating beaches.

**Table R2** Beach rating questionnaire

| | 1 | 2 | 3 | 4 | 5 |
|---|---|---|---|---|---|
| *Physical factors* | | | | | |
| 1. Beach width at low tide | ☐ narrow <10 m | ☐ 10–30 m | ☐ 30–60 m | ☐ 60–100 m | ☐ 100+ m wide |
| 2. Beach material | ☐ cobbles | ☐ sand/cobbles | ☐ coarse sand | ☐ | ☐ fine sand |
| 3. Beach condition or variation | ☐ erosional | ☐ | ☐ stable | ☐ | ☐ depositional |
| 4. Sand softness | ☐ hard | ☐ | ☐ | ☐ | ☐ soft |
| 5. Water temperature | ☐ cold/hot | ☐ | ☐ | ☐ | ☐ warm (70–85°F) |
| 6. Air temprature (midday) | ☐ <60°F >100°F | ☐ | ☐ | ☐ | ☐ 80–90°F |
| 7. Number of sunny days | ☐ few | ☐ | ☐ | ☐ | ☐ many |
| 8. Amount of rain | ☐ large | ☐ | ☐ | ☐ little | ☐ |
| 9. Wind speeds | ☐ high | ☐ | ☐ | ☐ | ☐ low |
| 10. Size of breaking waves | ☐ high/dangerous | ☐ | ☐ | ☐ | ☐ low/safe |
| 11. Number of waves/ width of breaker zone | ☐ none | ☐ 1 | ☐ 2 | ☐ 3 | ☐ 4+ |
| 12. Beach slope (underwater) | ☐ steeply sloping bottom | ☐ | ☐ | ☐ | ☐ gently sloping bottom |
| 13. Longshore current | ☐ strong | ☐ | ☐ | ☐ | ☐ weak |
| 14. Rip currents present | ☐ often | ☐ | ☐ | ☐ | ☐ never |
| 15. Color of sand | ☐ gray | ☐ black | ☐ brown | ☐ light tan | ☐ white/pink |
| 16. Tidal range | ☐ large (>4 m) | ☐ 3–4 m | ☐ 2–3 m | ☐ 1–2 m | ☐ small (<1 m) |
| 17. Beach shape | ☐ straight | ☐ | ☐ | ☐ | ☐ pocket |
| 18. Bathing area bottom conditions | ☐ rocky, cobbles, mud | ☐ | ☐ | ☐ | ☐ fine sand |
| *Biological factors* | | | | | |
| 19. Turbidity | ☐ turbid | ☐ | ☐ | ☐ | ☐ clear |
| 20. Water color | ☐ gray | ☐ | ☐ | ☐ | ☐ aquablue/turquoise |
| 21. Floating/suspended human material (sewerage, scum) | ☐ plentiful | ☐ | ☐ | ☐ | ☐ none |
| 22. Algae in water | ☐ infested | ☐ | ☐ | ☐ | ☐ absent |
| 23. Red tide | ☐ common | ☐ | ☐ | ☐ | ☐ none |
| 24. Smell (seaweed, rotting fish) | ☐ bad odors | ☐ | ☐ | ☐ | ☐ fresh salty air |
| 25. Wildlife (e.g., shore birds) | ☐ none | ☐ | ☐ | ☐ | ☐ plentiful |
| 26. Pests (biting files, ticks, mosquitos) | ☐ common | ☐ | ☐ | ☐ | ☐ no problem |
| 27. Presence of sewerage/runoff outfall lines on/across the beach | ☐ several | ☐ | ☐ | ☐ | ☐ none |
| 28. Seaweed/jellyfish on the beach | ☐ many | ☐ | ☐ | ☐ | ☐ none |
| *Human use and impacts* | | | | | |
| 29. Trash and litter (paper, plastics, nets, ropes, planks) | ☐ common | ☐ | ☐ | ☐ | ☐ rare |
| 30. Oil and tar balls | ☐ common | ☐ | ☐ | ☐ | ☐ none |
| 31. Glass and rubble | ☐ common | ☐ | ☐ | ☐ | ☐ rare |
| 32. Views and vistas local scene | ☐ obstructed | ☐ | ☐ | ☐ | ☐ unobstructed |
| 33. View and vistas far vista | ☐ confined | ☐ | ☐ | ☐ | ☐ unconfined |
| 34. Buildings/urbanism | ☐ overdeveloped | ☐ | ☐ | ☐ | ☐ pristine/wild |
| 35. Access | ☐ limited | ☐ | ☐ | ☐ | ☐ good |

**Table R2** (*Continued*)

| | 1 | 2 | 3 | 4 | 5 |
|---|---|---|---|---|---|
| 36. Misfits (nuclear power station; offshore dumping) | present | | | | none |
| 37. Vegetation (nearby) trees, dunes | none | | | | many |
| 38. Well-kept grounds/ promenades or natural environment | no | | | | yes |
| 39. Amenities (showers, chairs, bars, etc.) | none | | | | some |
| 40. Lifeguards | none | | | | present |
| 41. Safety record (deaths) | some | | | | none |
| 42. Domestic animals (e.g., dogs) | many | | | | none |
| 43. Noise (cars, nearby highways, trains) | much | | | | little |
| 44. Noise (e.g., crowds, radios) | much | | | | little |
| 45. Presence of seawalls, riprap, concrete/ rubble | large amount | | | | none |
| 46. Intensity of beach use | overcrowded | | | | ample open space |
| 47. Off-road vehicles | common | | | | none |
| 48. Floatables in water (garbage, toilet paper) | common | | | | none |
| 49. Public safety (e.g., pickpockets, crime) | common | | | | rare |
| 50. Competition for free use of beach (e.g., fishermen, boaters, waterskiers) | many | | | | few |

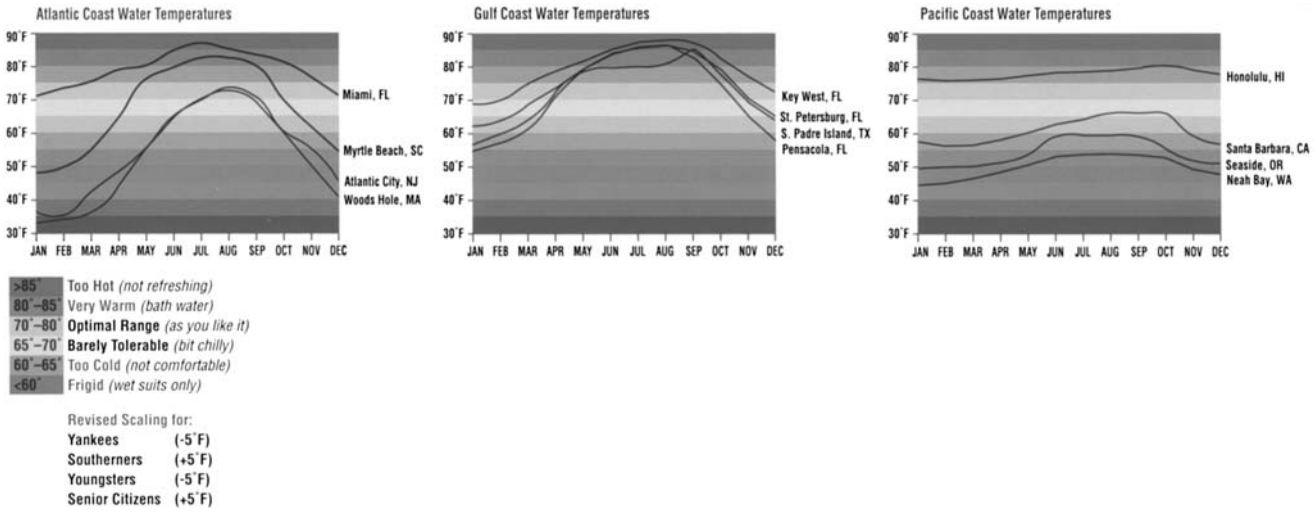


**Figure R3** Water temperature scale for bathing and swimming.

America's most famous beaches were rarely rated the best ones for overall quality. For instance, the beaches at world famous Waikiki Beach in Honolulu, Hawaii have experienced progressive erosion to the point that the beach simply does not exist in some sections. Coney Island in New York city was a very popular beach in the 1960s, but crime and other problems have taken their toll.

## Beach users survey

Morgan (1999) developed a questionnaire to query recreational beach users in Wales, UK. Overall, scenic quality was rated as the most important factor in the beach environment, but it must be remembered that Welsh beaches are "cold water" and not that conducive to swimming. Sand and water quality were also highly rated in this innovative study.

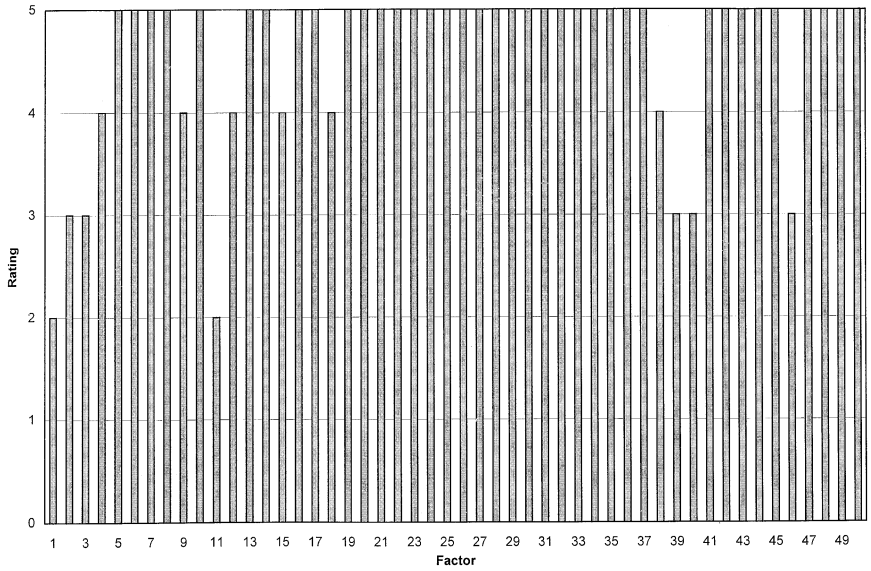


**Figure R4** Beach profile for top-rated Kapalua Bay Beach, Maui, Hawaii.

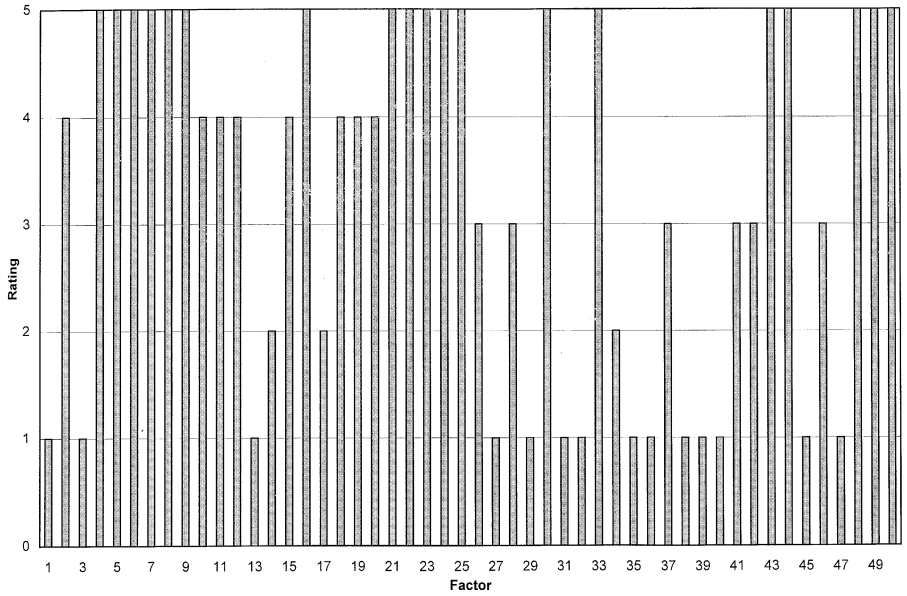


**Figure R5** Beach rating profile for Pikes Beach, New York. Note that the "sawtooth" graph indicates a less aesthetically pleasing and overall lower quality beach.

There were many observed differences in beach user preferences, depending upon the type of beach (e.g., urban to rural) that the user preferred to visit. Some vacationers wanted all the amenities and "creature comforts" of a beach resort (e.g., good hotels and restaurants, many water-based activities, and nightlife) compared to others who preferred the natural characteristics of a beach (e.g., fauna and flora, scenery, and camping). Morgan (1999) found that high environmental quality was a prerequisite for all beach users, emphasizing the high level of public concern for this aspect.

## Summary

Various beach awards have been ongoing in Europe for decades, but the use of scientific criteria and ratings have evolved subsequently to the efforts begun in the US beaches are always changing because of storm impact, beach nourishment, pollution problems, etc. so the rankings vary year to year.

Stephen P. Leatherman

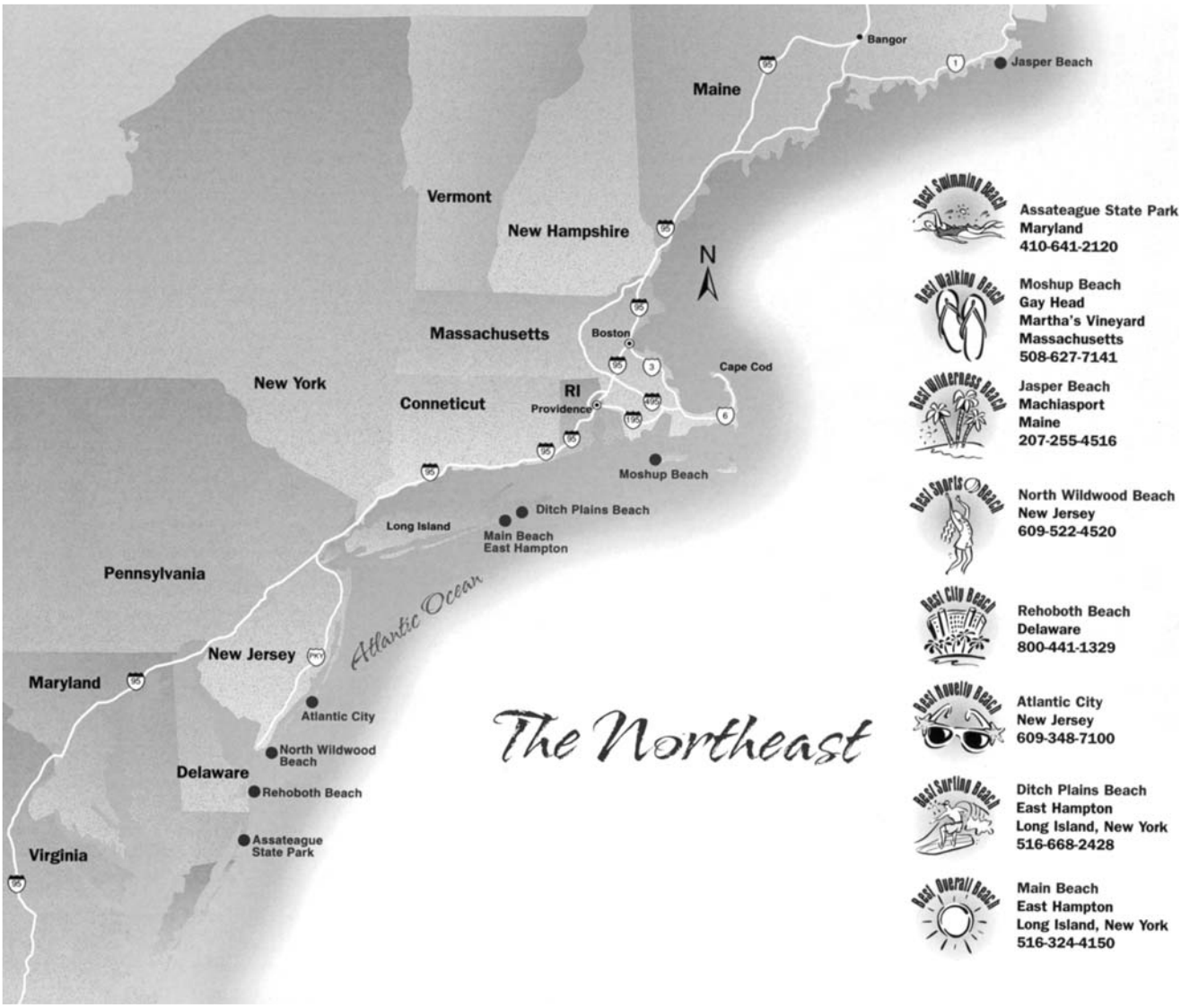


**Figure R6** US beaches have been evaluated by region and category (Leatherman, 1998). Each region offers a different venue and recreational advantage. While swimming is the favorite activity of most beachgoers, many people just enjoy walking along beaches for the exercise or to enjoy the scenery. Purists prefer wilderness beaches, but many vacationers are looking for creature comforts; the top city beaches offer all the amenities.

## Bibliography


Center for Marine Conservation, 1990. *Cleaning North America's Beaches*. Washington, DC.

FEEE, 1997. *The Blue Flag Awards of 1997*. Foundation for Environmental Education in Europe.

Leatherman, S.P., 1991. *Top 20 Beaches in Continental U.S. and Hawaii*. College Park, MD: University of Maryland.

Leatherman, S.P., 1997. Beach rating: a methodological approach. *Journal of Coastal Research*, **13**(1): 253–258.

Leatherman, S.P., 1998. *America's Best Beaches*. Laboratory for Coastal Research. Miami: Florida International University.

Leopold, L.B., 1969. Quantitative comparison of some aesthetic factors among rivers. Denver: U.S. Geological Survey Circular 620.

Marine Conservation Society, 1997. *Readers Digest Good Beach Guide*, London: David & Charles.

Morgan, R., 1999. Preferences and priorities of recreational beach users in Wales, U.K. *Journal of Coastal Research*, **15**(3): 653–667.

National Oceanic and Atmospheric Administration, 1990. *50 Years of Population Change Along the Nation's Coasts, 1960–2010*. Rockville, MD: National Ocean Service.

Williams, A.T., and Morgan, R., 1995. Beach awards and rating systems. *Shore and Beach*, **63**(4): 29–33.


## Cross-references


Beach Sediment Characteristics
Cleaning Beaches
Environmental Quality
Human Impact on Coasts
Lifesaving and Beach Safety
Marine Debris, Onshore, Offshore, and Seafloor Litter
Reclamation
Surfing
Water Quality

# RECLAMATION

Although normally associated with the rehabilitation of land, reclamation in the coastal context refers to the exclusion of marine or estuarine water from formerly submerged land. The basic idea of reclamation is to win land from the sea, to displace water and to create new land (Plant *et al.*, 1998, p. 563). The resulting land surface normally extends from the existing coastline and should be well above the level reached by the sea. Reclamation differs from the building up of shallow offshore grounds to form *artificial islands* (*q.v.*) (Kondo, 1995). It also differs from *polders* (*q.v.*) (CUR, 1993, p. 230, 244) in which the level of land subject to seasonal or permanent high water level is protected by dikes, and flood control and water management are important aspects.

## Historical and geographical brief

The origins of reclamation probably date back to humankind's efforts in reclaiming land from estuaries and along coasts for their homes, livestock, and crops. For example, in the first few centuries, artificial clay mounds ("terps") were constructed by people in the lower parts of the Netherlands (Pilarczyk, 2000). It is likely that reclamation initially involved the draining of low-lying land and marshes. A survey of reclamation in temperate countries shows reclamation was primarily for agricultural purposes. Later, expanding population and increasing needs for industrial expansion and dock development led to a more focused objective of gaining land from the sea. It started with small-scale reclamation in almost all of the larger cities and ports situated on estuaries and coast throughout the world (Cole and Knights, 1979) (Figure R7). In fact, the reclamation of estuaries was better addressed, especially in the second-half of the 19th century to provide dock and harbor facilities to meet world trade expansion during the period of rapid industrialization in Europe and the United States (Kendrick, 1994).

Any mention of gaining land from the sea cannot avoid the Netherlands because of the massive scale of reclamation in a country where the battle against the sea has become an integral part of the way of life. Reclamation was carried out in conjunction with poldering and the construction of sea defense works. Many lessons were learnt not only in engineering aspects but also in the physical and economic planning of reclaimed land. Another country in which reclamation of its estuaries and low-lying coastal areas has been carried extensively is Japan, which has at least 400 years of reclamation history. It has considerable experience in the consolidation and settlement of fill material, particularly in the treatment of soft foundations, such as the wide application of the sand drain method and the sand compaction method (Watari *et al.*, 1994).

The need for reclaimed land for various developments varies worldwide and becomes particularly crucial around existing ports and cities and in countries where land scarcity is a factor, for example, in Singapore and Hong Kong (Walker, 1988) (Figure R7). Faced with land scarcity, Singapore has resorted to large-scale reclamation from the 1960s although reclamation dated back to the 19th century. Through various projects, it has reclaimed about 10% of its area, which totaled 647 $km^2$ in 1998. Under the Concept Plan to accommodate a population of 4 million from the present 3.2 million, another 100 $km^2$ have to be reclaimed. This would amount to 25% in land area since the 1960s (Figure R8). With current technology, it is not cost-effective to reclaim in waters deeper than 15 m. Another limitation is that reclamation encroaches into the sea space for shipping lanes and anchorage.

## Reclamation methods

Land won from the sea is normally carried out by raising the level of previously submerged land above sea level using materials dredged from the sea or excavated from the land. The reclaimed site is where reclamation is to take place and eventually forms the platform for required land use. The borrow area is where such material is obtained for reclamation and the disposal area is where material, unsuitable for fill, is to be disposed.

Depending on the type of landfill, there are two major types of reclamation and each has its advantages and disadvantages (Plant *et al.*, 1998, p. 197, 561; CUR, 1993, p. 244).

1. In the "drained" reclamation, fill is placed on the reclaimed site. The advantage is that existing soft marine material can be left in place, reducing the amount of fill required. The disadvantage is the longer time required for settlement and a greater uncertainty in the duration and rate of consolidation. This could increase the costs in follow-up structures to accommodate a larger settlement. Artificial drainage is required to reduce drainage paths and accelerate settlement (Plant *et al.*, 1998, p. 561).
2. In the "dredged" reclamation, landfill by is by replacement, in which soft marine material is removed and replaced by imported fill. This means a larger volume of fill but the advantage of faster consolidation. The Hong Kong International Airport at Chek Lap Kok is an example of "dredged" reclamation in which three-quarters of the airport platform was reclaimed from the sea using a combination of dredging mud from the seabed, borrowing marine sand, excavation of islands, and construction of seawalls.

Site conditions have a strong influence on reclamation and factors such as climate, site access and site geology are important (Plant *et al.*, 1998, p. 15). Inaccurate information on these factors has led to delays, disruptions, disputes, and operational failures. For example, heavy

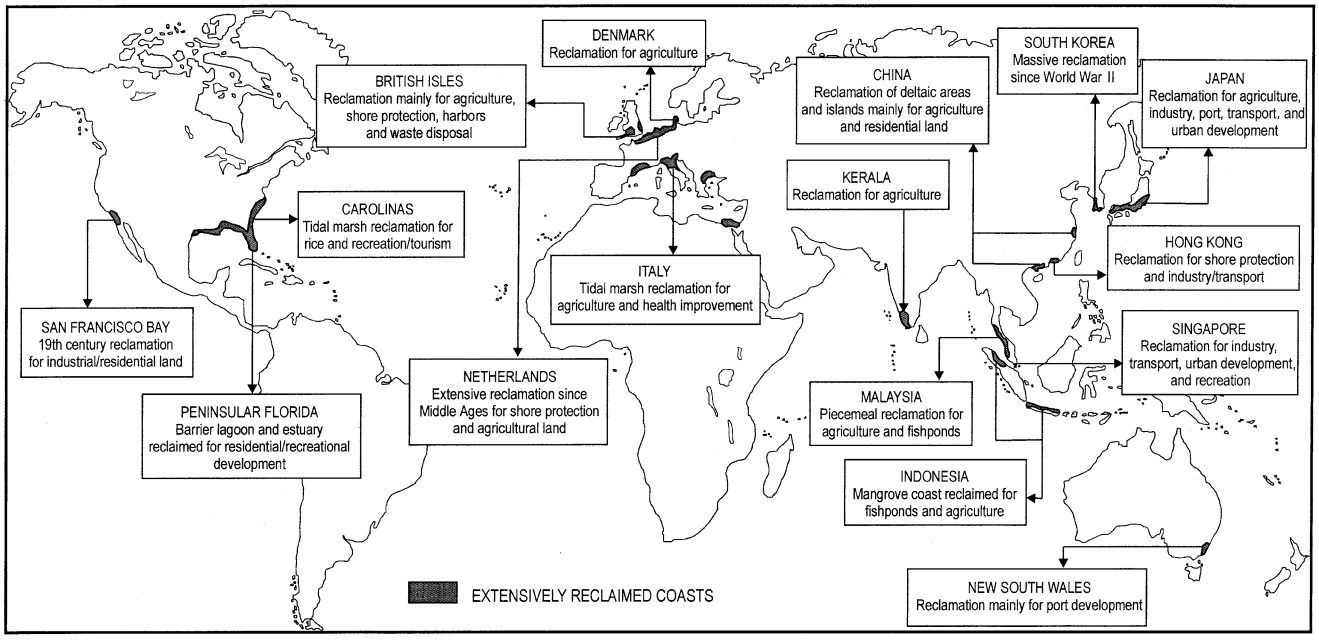


**Figure R7** Major reclaimed coasts in the world.

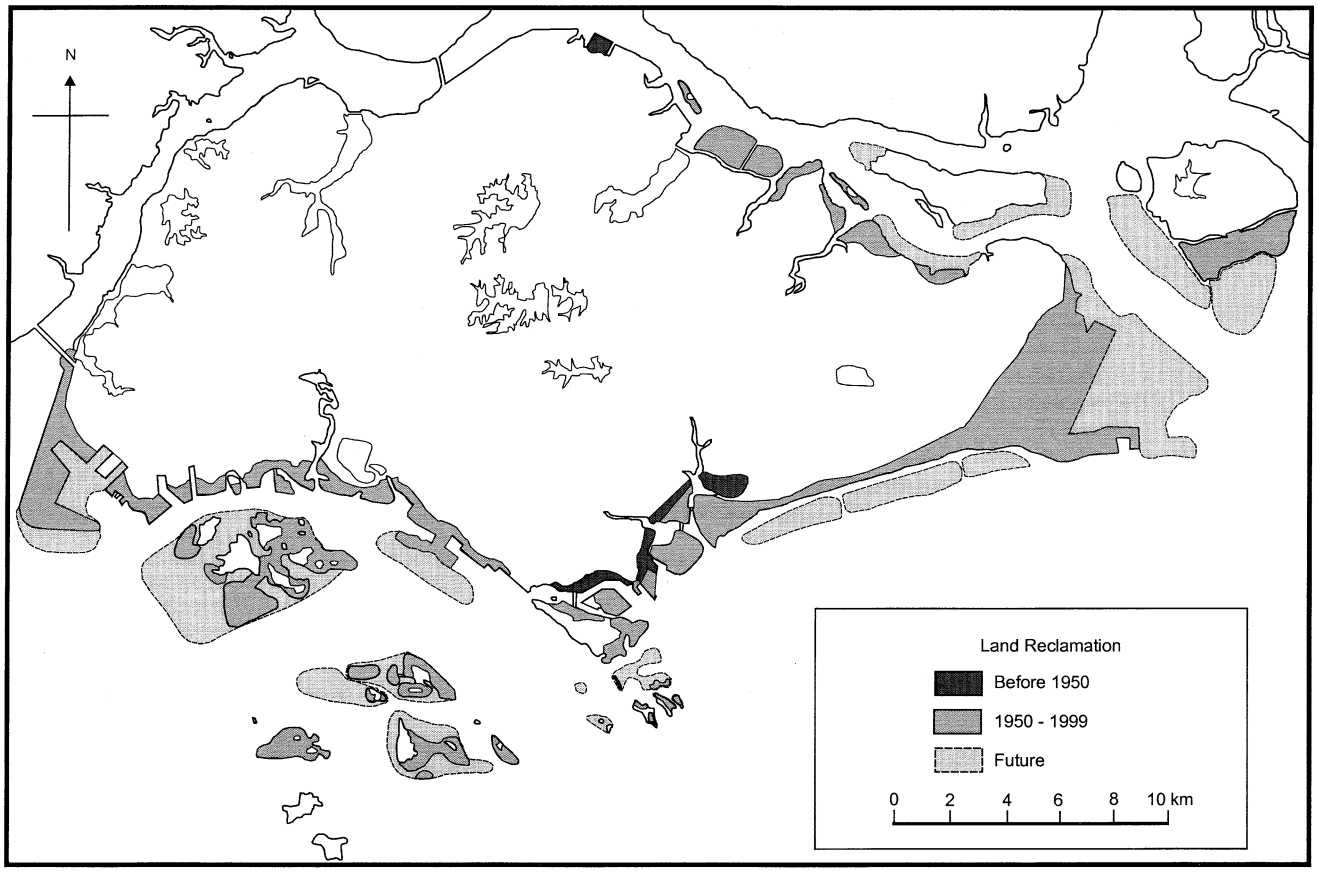


**Figure R8** Reclaimed land in Singapore.

rainstorms can halt reclamation operation. Marine conditions as influenced by climate can be equally significant, for example, water depth and wave conditions influence the operation of dredgers. Seabed conditions can vary widely and water depth and type of materials influence both settlement and stability. A low-energy environment is advantageous as fill material can be placed on the seabed and not easily scoured by wave action. The availability of power, water, and communication services at the site can influence the design of reclamation.

Much of the early reclamation efforts often capitalized on the availability of fills such as quarry waste, urban refuse, excavation spoil, building demolition spoil, dredged material from ports and navigation channels, or the byproduct of some dredging operation. It was also carried out in connection with shallow tidal, marshy, or mangrove areas. Usually, for specific reclamation projects, materials cut from hills or seabed sand have been the most common fill. But with increasing scarcity of such fill materials, alternative sources, such as marine clays were dredged from the seabed. Marine aggregates, primarily sand and gravel from offshore-submerged sources, are also used in reclamation projects. In 1989, 7.7 million $m^3$ and more than 9 million $m^3$ were used for reclamation works in Denmark and Netherlands, respectively (Bokuniewicz, 2000).

Various techniques have been in use to deal with the reclamation of coastal areas with soft foundations. For example, in Japan, the removal of the soft material and replacement by sand was the common method. The lack of sand and environmental problems, such as increased turbidity of water and the problem of disposal of dredged material, saw the end of this method for large-scale reclamation in 1975. This was replaced by the sand drain, which first came into use in 1952. From 1970–83 some 230,000 sand drains, each about 20 m long, were used for seabed foundation improvement in Japan. Driving-type sand compaction was used in 1966 in offshore construction and supplemented by the deep mixing method (DMM) from the mid-1970s (Watari *et al.*, 1994).

For its earlier phases of reclamation, Singapore obtained landfill from the cutting of hills in the construction of public housing where extensive platforms were required. In the east coast reclamation, the fill was excavated by bucket wheel excavators and transported by belt conveyors to a loading jetty for loading to barges and dumped directly into the reclaimed site. Where water depth limited the movement of barges, the fill was unloaded by a reclaimer and conveyor system. Bulldozers and dump trucks then spread, graded, and compacted the reclaimed land (Yong *et al.*, 1991). The reclaimed land required little settlement after compaction.

As materials from land become less readily available, Singapore has to import from neighboring countries or obtain them from marine resources. The typical procedure in large-scale coastal reclamation is as follows (Yong *et al.*, 1991; Chuah and Tan, 1995).

1. Seabed stabilization is first carried out in several ways by the excavation of soft material from the seabed, dredging to form a sandkey trench or the installation of sand compaction piles or vertical drains. Sand compaction piles were first used in 1989. A hollow pipe casing is driven into soft material, filled with sand, then compacted, and the casing is withdrawn. Sand piles were placed at close intervals. This method strengthens the clay seabed, obviated dredging, and thus avoids the costs of disposal.
2. A sandkey is formed from transported sand towed in by hopper barges. In some cases, where conditions are suitable, a sand wall is also constructed along the coast to be reclaimed. Sand barges build up a stockpile outside the sand wall.
3. Reclamation is carried out by direct dumping or hydraulic filling using cutter suction dredgers and pumps or trailer hopper suction dredgers. Where sand is sucked from the stockpile, it is spread into the fill area by a floating spreader. If the depth is too shallow, sand is pumped through overland pipes.
4. After filling, compaction is carried out by rollers. Shore trimming and shore protection works (geotextile placing, stone placing, and hand-pitching) complete the reclamation. The reclaimed land is usually ready for development after 1–5 years.

The above procedure has been applied to the reclamation of a group of islands located about 1 km south of Jurong Industrial Estate to form a single island zoned for petrochemical and chemical industries. The

shape of the reclaimed island is to give a maximum land area that could be possibly reclaimed and a coastline with harbor basins that have no adverse conditions on water currents, sedimentation, and navigation (Chuah and Tan, 1995).

## Ground treatment

The magnitude and rate of settlement of *in situ* soils and fills is a major concern in reclamation. The settlement depends on the type of fill, method of placement, and use of reclaimed area (Plant *et al*., 1998, p. 131). Ground treatment is any process in which the properties of the ground are improved or changed. Various methods are used to speedup settlement, each has its own merits.

Surcharging or preloading is the process in which the ground surface is loaded with additional mass. A stockpile of material is required and the material is moved from location to location until the process is completed (rolling surcharge). This procedure avoids importing vast quantities of additional material. Where rockfill is used, surcharging is an effective means of reducing future settlement in rockfilled areas (Plant *et al*., 1998, p. 417) and less disruptive to the geotextile over rockfill. Fine-grained dredged materials take up to 2–3 years or more to consolidate under self-weight before surcharging is used. Although surcharging avoids the costs of handling large quantities of surcharge fill material and its eventual disposal, the whole process can take up to a decade or more for a 200-acre site (Thevanayagam *et al*., 1994).

Vibrocompaction refers to ground treatment in which heavy vibrators are inserted into loose granular soils and then withdrawn leaving a column of compacted soil in the ground. This reduces creep and vibration-induced settlement of the ground surface during follow-up construction activities. It is a fast method of achieving a high degree of compaction for a specific material. In dynamic compaction, the ground is compacted by high-energy impacts using a tampering weight. It can be used for all fill types but its effective depth is limited to about 10 m.

To facilitate rapid settlement associated with very soft clayey material, water conduits have to be installed for easy dissipation of water. In the past, this was achieved by vertical columns of sand drains installed at a grid of about 1–3 m. In recent years, sand drains are being replaced by wick drains or band-shaped drains, which make installing faster and easier. In the reclamation of a seabed underlain by thick deposits of soft clay, soil improvement is required. One of the most popular procedures is to combine prefabricated band-shaped drains with preloading.

In the reclamation for Hong Kong International Airport at Chek Lap Kok, seabed conditions varied widely in terms of water depth, thickness of marine mud to be dredged, and underlying compressible strata. These had a strong influence on both settlement and stability of the reclaimed land. The time taken for settlement was difficult to determine as the settlement of fill after construction depends on the type of fill, method of placement, and use of filled area. Instruments monitored settlement and allowed analytical settlement models to be calibrated and updated as reclamation and follow-up works progressed. An extra 0.5 m was provided for future settlement. For ground treatment, surcharge, vibrocompaction, and dynamic compaction were used (Plant *et al*., 1998).

## Coastal protection

Land gained from sea has to be protected from erosion by waves and currents. Depending on coastal conditions, various types of halophytes can be used to protect reclaimed land. For example, marram grass (*Ammophila*) is used in Europe (Cole and Knights, 1979). In Singapore, idle reclaimed land along Changi Coast Road has been effectively colonized by beach vegetation, such as *Ipomoea pes-caprae* and trees such as *Casuarina equisetifolia*.

More often, reclaimed land is protected by shore protection works. In accordance with current international practice, seawall construction allows for some risk of damage under extreme conditions. A high factor of safety will result in a disproportionate effect on costs. As the philosophy on coastal protection changes, this is also reflected in the protection of reclaimed land. For example, in Japan, coastal protection began with seawalls, followed by groins and then detached breakwaters (Hsu *et al*., 2000).

Although Singapore is not in a high wave-energy environment, various types of coastal protection works were required for the reclaimed land depending on several variables, such as the usage of reclaimed land, ease and speed of construction, site constraints, cost of construction, and predominant wave approach. Three major groups of shore protection works for reclaimed land in Singapore can be identified.

1. Reclaimed land with beaches. Initially, a seawall was used but this was superceded by a series of breakwaters acting as headlands between which beaches can be developed. These were used in the east coast because of the low wave energy, predominant wave approach from the southeast, and net littoral drift to the west. Beaches were formed in J-shaped bays with their upcoast curves in the east and downcoast straight sectors in the west.
2. Reclaimed land for port purposes. A sand key provides the broad base for the seawall to be constructed and withstand loads, for example, in Jurong. Sheet piles are used for deep-water frontage where wharf construction is required.
3. Reclaimed land retained behind a marine retaining wall. Various types of structures are used. Generally, stone bunds are constructed with stones large enough to withstand dynamic lifting and to absorb forces of waves on their outer face. Stone bunds were constructed around some islands with gaps for beaches to form (Wong, 1985). Various prefabricated structures were also used. Caissons or huge reinforced concrete boxes were towed to sea by tugboats, then filled with sand and positioned on the seabed. These are costly and used where a rocky seabed is available. Depending on their size to be used, L-blocks of 30–70 tons require a compacted rubble foundation and are positioned by cranes. These were used in the reclamation of Marina Bay and Tanjung Rhu.

Depending on the size of area to be reclaimed, the condition of the seabed which may require stabilization, and the necessity of shore protection to protect reclaimed land from erosion, the following approaches can be identified for reclamation in Singapore. For small areas, such as offshore islands, site preparation is followed by seabed stabilization for the construction of breakwaters to prevent erosion from currents and waves and followed by the filling of sand. For large areas extending from the mainland, site preparation is followed by seabed stabilization, filling of sand, and shore protection works. For large swampy areas, settlement is a problem and additional time and costs are required for shore protection measures. Site preparation is thus followed by sand filling and shore protection works.

## New developments

Reclamation often involves work on land and sea, which is collectively referred to as land operations and marine operations, respectively. The land operation is basically civil engineering and quarrying operations and the scale of earthworks is typical of large mining operations. The marine operation usually involves dredging and coastal protection. Dredging is defined as "underwater excavation of seabed material, transportation of the materials to a discharge area, and subsequent discharging of dredged material" (Plant *et al*., 1998, p. 266). In recent years, reclamation has seen new developments in both land and marine operations.

Modern reclamation relies on some heavy specialist equipment to recover (dredge) from the burrow area, transport, and place the material over the reclaimed site. Cutter-suction dredgers and trailing-suction hopper dredgers (also called trailer dredgers) have been developed to dredge a greater volume of materials in a short time and at lower costs, often in deeper waters. A trailing-suction hopper dredger is a self-proposed ocean-going vessel fitted with special dredging equipment. The hopper capacity of these dredgers has doubled from 10,000 $m^3$ in the 1980s to 23,000 $m^3$ and set to treble to 33,000 $m^3$ in 2000 (Riddell, 2000). A cutter-suction dredger differs from a trailing-suction hopper dredger in that the former is effectively stationary during dredging, has more control over the dredging process and is also capable of dredging harder material. Depending on water depth, a cutter-suction dredger trails as dredging progresses. The dredged material is projected through a nozzle at its bow in a process called "rainbowing" as land is reclaimed. Hopper barges are for direct dumping of material and are confined to sheltered waters.

The increasing use of geosynthetics in coastal and harbor engineering has also found its place in reclamation. Geosynthetics is a generic name given to various materials that are synthesized for use with geological materials to improve or modify their behavior. One major success was the construction of storm-resistant structures over soft soils at the coast in the Netherlands (Rao and Sarkar, 1998). In Japan, geosynthetics have been commonly used for more than three decades in land reclamation involving a soft clay foundation. They are mainly used for surface stabilization to increase bearing capacity and to reinforce the base of fill and for foundation improvement to replace sand drains in facilitating drainage (Akagi, 1998). Probably the world's largest sewn single sheet of geotextile used for reclamation took place in Singapore in one phase of the reclamation for Changi Airport. A 180-ha pond, 2,000 m in length and 750 m and 1,050 m in width at both ends, created earlier by the borrowing of sand contained slurry-like material 3 to 20 m thick. The

initial spreading of sand over the pond failed as mud burst through the sand cap. Remedial measures started with the removal of some of the exposed slurry. Then, the geotextile sheet of 1,060,000 $m^2$ sewn from $5 \times 90$ $m^2$ rolls was laid across the silt pond to strengthen the foundation soil. This was supplemented by prefabricated band-shaped vertical drains to accelerate the consolidation time by shortening the drainage path (Na *et al*., 1998). This example shows that high-strength geotextile can strengthen foundation soil that is extremely soft.

The technique of vacuum consolidation is being used in reclamation. This is a process in which a vacuum is applied to a soil mass to produce a negative pore pressure, leading to increased effective stress that leads to consolidation. Although the technique was known in the early 1950s, it was not widely used until the 1980s because of high costs and implementation difficulties. Its application was made possible by recent technological advances in geotextiles and efficient and cost-effective prefabricated vertical drains (wick drains) (Shang *et al*., 1998). The technique has been field-tested for on-land vacuum consolidation in countries such as the Netherlands, France, Malaysia, Sweden, Japan, and China. It shows considerable promise as an economically viable method to replace or supplement surcharge fill and the potential to strengthen weak sediments on the seabed adjacent to or beneath water, or consolidate fine-grained hydraulic fills during construction. The technique can also be used with prefabricated horizontal drains and selective placement of dredged materials for new land reclamation (Thevanayagam *et al*., 1994). It was applied to 480,000 $m^2$ of reclaimed land in Tianjin Harbor, China, where individual sites treated with vacuum ranged from 5,000 to 30,000 $m^2$, illustrating that it was especially attractive for hydraulic fills and in reclamation sites with a shortage of surcharge fills but that have an easy access to a power supply. Currently, research on the method is on numerical modeling of the consolidation process, the application of geotextiles over larger areas, and the development of high-efficiency vacuum equipment (Shang *et al*., 1998).

During earthquakes, especially in Japan, some reclaimed land can undergo a complex phenomenon called liquefaction in which loose sandy deposits change into a liquid state. The liquefaction sites are related to the age of reclamation, the methods used, and type of material. The remediation methods depend on large-scale or localized remediation and are implemented during or after completion of land reclamation. With wide experience in this area, Japan has produced a handbook on remediation measures (Port and Harbor Research Institute, 1997) that can be used in other seismically active regions where reclamation has been carried out.

Compared with the past, environmental considerations are given serious attention in modern reclamation and associated works (Bates, 1994). The main areas of impact are at the dredging site, the transportation route, and the reclamation site. The potential adverse effects of dredging include the release of contaminants into the water, increased turbidity, disturbance to the seabed, erosion, noise, oil spillage, blanket cover, and consequent loss of habitat. To some extent, the impacts resulting from dredging and dumping may be overcome by changing the type of dredger and method of dumping. With the concern on the impacts on water quality and ecology, there is a need to develop methods to minimize environmental impact, such as modeling to examine environmental impacts of reclamation projects.

## Conclusion

Reclamation continues to be a significant means in providing land to meet the needs of expanding population and economic development, especially in small countries and coastal cities where land is scarce. It brings about a complete change in the coastal environment. Its implementation involves the input of various disciplines, for example, physical geography, geology, soil mechanics, loose boundary hydraulics, land drainage, coastal engineering in the planning and design of reclamation, and ecology, with the increasing concern on loss of natural habitats. New developments have to try to overcome the technical constraints, make reclamation low cost, take advantage of available soft material and other fills, such as incinerator ash, and to reclaim further into increasing depths.

P.P. Wong

## Bibliography


Akagi, T., 1998. Reclamation with geosynthetics. In Sarkar, S.S. (ed.), *Geohorizon: State of Art in Geosynthetic Technology*. Rotterdam: Balkema, pp. 89–96.

Bates, A.D., 1994. Dredging and dredgers. In Abbott, M.B., and Price, W.A. (eds.), *Coastal, Estuarial and Harbour Engineer's Reference Book*. London: Chapman and Hall, pp. 655–670.

Bokuniewicz, H., 2000. Marine aggregate dredging. In Herbich, J.B. (ed.), *Handbook of Coastal Engineering*. New York: McGraw-Hill, pp. 18.1–18.9.

Center for Civil Engineering Research and Codes (CUR), 1993. *Hydrology and Water Management of Deltaic Areas*. Rotterdam: Balkema.

Chuah, S.G., and Tan, D.T.L., 1995. Reclamation of Jurong Island. In *1995 Seminar on Engineering for Coastal Development (ECD 1995 Proceedings, Volume 10)*. Tokyo: The Kozai Club, pp. 111–119.

Cole, G., and Knights, B., 1979. An introduction to estuarine and coastal land reclamation and water storage. In Knights, B., and Phillips, A.J. (eds.), *Estuarine and Coastal Land Reclamation and Water Storage*. Farnborough: Saxon House, pp. 3–20.

Hsu, J.R.C., Uda, T., and Silvester, R., 2000. Shoreline protection methods—Japanese experience. In Herbich, J.B. (ed.), *Handbook of Coastal Engineering*. New York: McGraw-Hill, pp. 9.1–9.77.

Kendrick, M.P., 1994. Estuarial problems. In Abbott, M.B., and Price, W.A. (eds.), *Coastal, Estuarial and Harbor Engineer's Reference Book*. London: Chapman and Hall, pp. 615–635.

Kondo, T., 1995. Technological advances in Japan's coastal developments: land reclamation and artificial islands. *Marine Technology Society Journal*, **29**: 42–49.

Na, Y.M., Choa, V., Win, B.M., and Arulrajah, A., 1998. Use of geosynthetics for reclamation on slurry like soil foundation. In Yanagisawa, E., Moroto, N., and Mitachi, T. (eds.), *Problematic Soils*. Rotterdam: Balkema, pp. 767–771.

Pilarczyk, K.W., 2000. Design of dikes and revetments—Dutch practice. In Herbich, J.B. (ed.), *Handbook of Coastal Engineering*. New York: McGraw-Hill, pp. 3.1–3.104.

Plant, G.W., Covil, C.S., and Hughes, R.A. (eds.), 1998. *Site Preparation for the New Hong Kong International Airport*. London: Thomas Telford. p. 576

Port and Harbor Research Institute, 1997. *Handbook on Liquefaction Remediation of Reclaimed Land*. Rotterdam: Balkema.

Rao, G.V., and Sarkar, S.S., 1998. Geohorizon—overview of geosynthetics foe [sic] the environment. In Sarkar, S.S. (ed.), *Geohorizon: State of Art in Geosynthetic Technology*. Rotterdam: Balkema, pp. 1–11.

Riddell, J., 2000. Dredging: opportunities and challenges for 2000 and beyond. Terra et Aqua, No. 78, March 2000.

Shang, J.Q., Tang, M., and Miao, Z., 1998. Vacuum preloading consolidation of reclaimed land: a case study. *Canadian Geotechnical Journal*, **35**: 740–749.

Thevanayagam, S., Kavazanjian, E., Jr., Jacob, A., and Juran, I., 1994. Prospects of vacuum-assisted consolidation for ground improvement of coastal and offshore fills. In Rollins, K.M. (ed.), *In-Situ Deep Soil Improvement*. New York: American Society of Civil Engineers, Geotechnical Special Publication No. 45, pp. 90–105.

Watari, Y., Fukuda, N., Aung, S., and Yamanouchi, T., 1994. Japanese reclamation techniques for coastal and offshore areas with soft foundation. In Balasubramaniam, A.S. (ed.), *Development in Geotechnical Engineering: From Harvard to New Delhi, 1936–1994*. Rotterdam: Balkema, pp. 543–551.

Walker, H.J. (ed.), 1988. *Artificial Structures and Shorelines*. Dordrecht, The Netherlands: Kluwer Academic Publishers.

Wong, P.P., 1985. Artificial coastlines: the example of Singapore. *Zeitschrift für Geomorphologie*, **57**: 175–192.

Yong, K.Y., Lee, S.L., and Karunaratne, G.P., 1991. Coastal reclamation in Singapore: a review. In Chia, L.S., and Chou, L.M. (eds.), *Urban Coastal Area Management: The Experience of Singapore*. ICLARM Conference Proceedings 15. Manila, Philippines: International Center for Living Aquatic Resources Management, pp. 59–67.


## Cross-references


Artificial Islands
Beach Drain
Bioengineered Shore Protection
Dredging of Coastal Environments
Geotextile Applications
Polders
Shore Protection Structures
Wetlands Restoration

# REEFS, NON-CORAL

Although most modern reefs are communities of coral and coralline algae that live in clear, well-lit tropical and subtropical waters, there are many different groups of reef-forming organisms that are found on living and ancient reefs. The modern non-coral reefs thrive in a wide range of environments extending from sponge reefs in the arctic to non-photosymbiotic algae and Halimeda reefs found near methane seeping faults at depths of 600 m (Wood, 1999).

## Definitions of reefs

The word, reef, is derived from the Norwegian word, rif, which means rib. In nautical terms, reef refers to a narrow chain of rocks, shingle or sand lying at or near to the surface of the water. When early sailing ships explored the tropical waters of the South Pacific, they encountered ring-like reefs of coral that enclosed a lagoon which they called "atoll" after "atolu," the Malayalam name for the Maldives Islands. In the more restrictive modern use of the word, reef denotes a rigid, wave-resistant framework constructed by large skeletal organisms (Ladd, 1944). While living coral reefs on atolls are wave resistant and contain a framework of corals and algae, boreholes drilled beneath the reefs consist of rubble, sediment, and voids (Hubbard *et al.*, 1990). Many ancient carbonate buildups, that are referred to as reefs, show that the original coral framework is almost completely destroyed by deep burial and diagenesis. A broader definition of reef, which would encompass both modern and ancient non-coral reefs, has been proposed by Rachel Wood: "a reef is a discrete carbonate structure formed by in-situ organic components that develops topographic relief upon the Seafloor" (Wood, 1999, p. 5).

## Reef-forming organism on non-coral reefs

The earliest recognized reefs are composed of stromatolites which were found on Phanerozoic carbonate platforms dating back to 2.5 Ga. Stromatolites are finely laminated microbialites produced by photosynthetic blue-green algae (cyanobacteria) that form a range of morphologies including domes, columns, and mounds (Reitner, 1993). Ancient stromatolite reefs were constructed on preexisting carbonate ramps and rimmed shelves (Grotzinger, 1989). Living stromatolites are found in intertidal zones on Lizard Island in the Great Barrier Reef, in Shark Bay, Australia, and in submerged tidal channels on Lee Stocking Island in the Bahamas. Thrombolites, which also form reefs, are non-laminated microbial structures which often have a mottled or bioturbated appearance.

Archeocyathids were the first metazoan reef-forming organisms and are found in Lower Cambrian limestones. The archeocyathids are large sponges with double-walled inverted conical calcareous skeletons (Debrenne and Zhuravleb, 1994). The first bryozoan reefs appeared in deep cold waters perhaps related to the presence of microbial mounds in the Lower Ordovician (Pratt, 1989). Stenolaemate bryozoa colonies of clonally calcified chambers, which formed reefs in the Lower Ordovician and died out during the Permian, reappeared as gymnolaemate bryozoans in the Jurassic and expanded during the Cretaceous and Eocene. Phylloid algae are calcified algae of platy, cup, and encrusting leaf-like forms that inhabited many late Paleozoic reefs.

Rudistid reefs are common in the Jurassic to Cretaceous limestones. Rudists are heavily calcified, heterodont bivalves in which the hinge and ligament have been modified forming a complete uncoiling of both valves (Skelton, 1991). The large lower (right) valve is conical, cylindrical, or coiled and the upper (left) valve is flattened. Most rudists were semi-infauna, soft sediment dwellers, but they often colonized storm-generated debris forming large rudistid reefs.

Large colonies of the common oyster, *Crassostera virginica*, are found in intertidal to subtidal environments including sounds and estuaries where the salinity is between 5 and 30 ppt. The oyster spat becomes cemented to old oyster shells and forms mounds of oysters which are commonly known as oyster reefs. When the buried oyster beds are exposed as fossils, they take on a reef-like form, but do not resemble the modern coral reefs.

## Conclusions

Most living reefs are composed of coral and coralline algae and consist of a wave-resistant framework constructed by large skeletal organisms. A broader definition of a reef is "a discrete carbonate structure formed by in-situ organic components that develops topographic relief upon the sea floor" (Wood, 1999, p. 5). A wide variety of non-coral organisms including coralline algae, stromatolites, archeocyathids, bryozoans, rudists, and oysters formed reefs in the geologic past and many are still forming reefs today.

William T. Fox

## Bibliography


Debrenne, F., and Zhuravleb, A.Yu, 1994. Archaeocyathan affinity: how deep can we go into the systematic affiliation of an extinct group? In Balkema, E. (ed.), *Sponges in Space and Time. Proceedings of the 4th International Poriferan Congress*, Amsterdam, pp. 3–10.

Grotzinger, P.J., 1989. Facies and evolution of Precambrian depositional systems: emergence of the modern platform archetype. In Crevello, P.D., Wilson, J.L., Sarg, J.F., and Read F.F. (eds.), *Controls on Carbonate Platform and Basin Development*. Society of Economic Paleontologists and Mineralogists Special Publication 44, pp. 79–106.

Hubbard, D.K., Miller, A.I., and Scaturo, D., 1990. Production and cycling of calcium carbonate in a shelf-edge reef system (St. Croix, USVI): applications to the nature of reef systems in the fossil record. *Journal of Sedimentary Petrology*, **56**: 335–360.

Ladd, H.S., 1944. Reefs and other bioherms. National Research Council, Division of Geology and Geography, *Annual Report 4*, Appendix K, pp. 26–9.

Pratt, B.R., 1989. Small Ordovician patch reefs, laval Formation (Chazy Group), Caughnawaga, Monteral area, Quebec, In Geldsetzer, H.H., James N.P., and Tebbutt (eds.), *Reefs. Canada and Adjacent Area*, Volume 13. Canadian Society of Petroleum Geologists, pp. 506–509.

Reitner, J., 1993. Modern cryptic microbialite/metazoan facies from Lizard Island (Great Barrier Reef, Australia), formation and concepts. *Facies*, **29**: 3–40.

Skelton, P.W., 1991. Morphogenic versus environmental cues for adaptive radiations. In Schmidt-Kittler N., and Voegel K. (eds.), *Constructional Morphology and Evolution*. Berlin: Springer-Verlag pp. 375–88.

Wood, R.A., 1999. *Reef Evolution*. Oxford: Oxford University Press.


## Cross-references


Algal Rims
Australia, Coastal Ecology
Bioherms and Biostromes
Caribbean Islands, Coastal Ecology and Geomorphology
Coral Reef Coasts
Coral Reefs


# REFLECTIVE BEACHES

## Definition and classification

Reflective beaches are systems where there is minimal wave-energy dissipation by breaking and therefore most energy is reflected by the nearshore morphology. In cases of strong reflection, individual reflected waves can be seen propagating away from the foreshore. Guza (1974), in his study of beach cusp formation, was apparently the first to use the term reflective beach. He distinguished between reflective and dissipative beaches (*q.v.*) using the surf-scaling parameter, ε:

$$\varepsilon = \frac{\alpha\omega^2}{g\tan^2\beta},$$

where α is the wave amplitude at breaking, ω is the wave radian frequency ($\omega = 2\pi/L$, where $L$ is wave length), $g$ is the gravity constant, and β is the beach slope in degrees. The proportion of incident wave energy that is reflected from the beach increases as ε decreases. For beaches where ε is larger than 20, most energy is dissipated by the turbulence associated with wave breaking. Where ε is less than about 2.5, most wave energy is reflected off the foreshore, and such beaches are designated as reflective. Thus, Guza (1974) used the relative degree of reflection or dissipation of incident waves as a rationale for the classification

**Figure R9** A reflective gravel beach near Malin Head, Co. Donegal, Ireland. Note steep foreshore and cusps. Maximum height of the collapsing breakers is less than 0.5 m, with a period of about 6 s.

of beaches. This approach was subsequently subsumed under the rubric of nearshore morphodynamics.

## Nearshore morphodynamics

The concept of nearshore morphodynamics was developed to characterize systems where form and process are closely coupled through feedback mechanisms. On beaches, waves (*q.v.*) interact strongly with sediments and morphology, and the form of wave breaking is one manifestation of these interactions. For a given wave steepness, $H/L$ (where $H$ is wave height), the breaker type will change as the nearshore slope changes. On a very low gradient slope, spilling breakers should occur. As the gradient increases, there should be a progression through plunging and collapsing breakers. Finally, on very steep beaches, surging breakers should occur (Galvin, 1968). For a constant nearshore slope, the same sequence of breaker types will occur as wave steepness decreases. Breaker type is closely associated with the expenditure of wave energy in the nearshore (e.g., reflection or dissipation) and the development of nearshore morphology. The morphology, in turn, controls breaker type. These relationships are the underlying bases for the concept of nearshore morphodynamics (see summary by Wright and Short, 1984). The recognition of characteristic sets of dynamic relationships provides the basis for using morphodynamic regimes (or states) as a means for classifying beach types. For example, collapsing or surging breakers occur on reflective beaches. This contrasts with dissipative beaches (*q.v.*), where spilling breakers are common. Plunging waves tend to occur on the intermediate beach states of the morphodynamic model (i.e., systems where $20 \geq \varepsilon \geq 2.5$), where neither reflection nor dissipation dominates the nearshore energy response.

## Characteristics of reflective beaches

In cross section, morphodynamically reflective beaches display the classic form of "swell" or "summer" beach profiles (e.g., Sonu and Van Beek, 1971). According to Wright and Short (1984), other distinguishing characteristics include steep nearshore and beach slopes (tan $\beta$ between about 0.10 and 0.20), and, typically, relatively coarse sediment sizes. Coarse clastic beaches, therefore, tend to be reflective. The subaerial beach tends to be narrow with a pronounced step at the foot of the foreshore. Low-energy reflective beaches are approximately two-dimensional alongshore. Higher-energy systems frequently include well-developed beach cusps on the foreshore. These cusp systems are presumed to be caused by low-mode, subharmonic edge waves. Incident wave energy is a maximum at or near the beach face. The classic reflective system displays only one coincident set of breakers (Figure R9), and substantial energy remains at the landward extremity of uprush. On meso- and macrotidal beaches, the nearshore system may be reflective only at higher tidal stages and dissipative at low tide (Short, 1991; Masselink and Hegge, 1995). Short and Hesp (1982) have linked the reflective beach state to the formation of small foredunes that are eroded frequently. This linkage is a key concept in the development of beach-dune interaction models (e.g., Sherman and Bauer, 1993).

Douglas J. Sherman

## Bibliography


Galvin, C.J., 1968. Breaker type classification on three laboratory beaches. *Journal of Geophysical Research*, **73**: 3651–3659.

Guza, R.T., 1974. Excitation of edge waves and their role in the formation of beach cusps. Unpublished Ph.D. dissertation, University of California, San Diego, p. 102.

Masselink, G., and Hegge, B., 1995. Morphodynamics of meso- and macrotidal beaches: examples from central Queensland, Australia. *Marine Geology*, **129**: 1–23.

Sherman, D.J., and Bauer, B.O., 1993. Dynamics of beach-dune systems. *Progress in Physical Geography*, **17**: 413–447.

Short, A.D., 1991. Macro–meso tidal beach morphodynamics—an overview. *Journal of Coastal Research*, **7**: 417–436.

Short, A.D., and Hesp, P.A., 1982. Wave, beach and dune interactions in southeastern Australia. *Marine Geology*, **48**: 259–284.

Sonu, C.J., and Van Beek, J.L., 1971. Systematic beach changes on the outer banks, North Carolina. *Journal of Geology*, **79**: 416–425.

Wright, L.D., and Short, A.D., 1984. Morphodynamic variability of surf zones and beaches: a synthesis. *Marine Geology*, **56**: 93–118.

## Cross-references

Bars
Beach Features
Beach Processes
Dissipative Beaches
Rhythmic Patterns
Sandy Coasts
Surf Zone Processes
Waves

# REMOTE SENSING OF COASTAL ENVIRONMENTS

Coastal ecosystems are transitional environments that are sensitively balanced between open water and upland landscapes. Worldwide, they exhibit extreme variations in areal extent, spatial complexity, and temporal variability. Sustaining these ecosystems requires the ability to monitor their biophysical features and controlling processes at high spatial and temporal resolutions but within a holistic context. Remote sensing is the only tool that can economically measure these features and processes over large areas at appropriate resolutions. Consequently, it offers the only holistic approach to understanding the variable forces shaping the dynamic coastal landscape. Remote sensing must be able to adjust to these spatially and temporally changing conditions and also be able to discriminate subtle differences in these systems. As a result, remote sensing of coastal ecosystems is a complex undertaking that needs to incorporate not only the ability to define the observable hydrologic and vegetation features, but also the scale of measurement.

## Historical development

Since the 1960s, remote sensing has been used to describe a new field of information collection that includes aircraft and satellite platforms carrying cameras to electro-optical and antenna sensor systems (Jensen, 2000). Up to that time, camera systems dominated image collection and photographic media dominated the storage of the spatially varying visible (VIS) and near-infrared (NIR) radiation spectral intensities reflected from the earth to aircraft platforms. Beginning in the 1960s, electronic sensor systems were increasingly used for collection and storage of earth's reflected radiation, and satellites were posed as an alternative to aircraft platforms. Advances in electronic sensors and satellite platforms were accompanied by an increased interest and use of radiant energy not only from the VIS and NIR wavelength regions but also from the thermal and microwave regions. In 1983, the American Society of Photogrammetry and Remote Sensing adopted a formal definition of remote sensing as "the measurement or acquisition of information of some property of an object or phenomenon, by a recording device that is not in physical or intimate contact with the object or phenomenon under study" (Jensen, 2000, p. 3). Although, others extended this definition to encompass the new technologies established for data collection, all definitions implicitly suggest that the property measured should describe a feature occupying a finite volume at a certain spatial and temporal position.

Remote sensing can include mapping of the earth's magnetic and gravitational fields and monitoring activities based on mechanical vibrations such as marine profiling by sonar and seismic exploration (Slater, 1980; Horler and Barber, 1981), or it can be applied to fields as diverse as cosmology to medical imaging. Historically, however, remote sensing has been used primarily to describe the collection of information transmitted in the form of electromagnetic radiant energy from an aircraft or satellite that is relevant to the earth's natural resources. Following this description, most remote sensing applications can be generally described by considering, (1) the nature of the probing signal, (2) the characteristics of the sensor and sensor platform, and (3) the interaction of the signal with the target.

## Electromagnetic spectrum

The electromagnetic spectrum describes the distribution of energy per wavelength ($\lambda$) or within an interval of consecutive wavelengths referred to as spectral bands ($\Delta\lambda$). Standardized to the speed of light in a vacuum, the electromagnetic spectrum is used to categorize general similarities of electromagnetic radiation in terms of changes in wavelength. The spectrum begins at the short wavelength cosmic rays and extends to the long wavelength radio waves (Figure R10). Ultraviolet radiation below 0.3 μm is removed by atmospheric ozone absorption, and between 0.3 and 0.4 μm atmospheric scattering reduces image contrast to levels generally unacceptable for satellite remote sensing applications (Slater, 1980). From about 0.4 μm to about 0.7 μm (VIS) little absorption occurs in clear and unpolluted atmosphere, although scattering is higher in this region than at longer wavelengths. In practice, the VIS is subdivided into the blue, green, and red regions. Above 0.7 μm, remote sensing applications are concentrated in atmospheric transmitting regions or windows bridging strong absorption bands primarily related to water vapor, ozone, and carbon dioxide. The region from 0.7 to 1.3 μm defines the NIR region, and the combined VIS and NIR regions are commonly referred to as the VNIR. The middle infrared (MIR) region from 1.3 to 8.0 μm is sometimes partitioned into a shortwave infrared (SWIR) region from 1.3 to 2.5 μm dominated by reflectance and a region from 2.5 to 8.0 μm dominated by emission. The MIR contains high atmospheric water vapor and carbon dioxide absorption bands and includes an atmospheric window from about 3 to 4 μm and a region of strong absorption between 5 and 8 μm. Ozone absorption between 9 and 10 μm interrupts the thermal region extending from 8 to 14 μm. Poor atmospheric transmission and the lack of sensitive detectors and instrumentation prohibit remote sensing applications between around 14 μm and 1 mm. Starting at 1 mm and extending up to 1 m, the microwave region is subdivided into regions from the shortest (*K*) to the longest (*P*) wavelength. Beyond the microwave region begins the region of television and radio frequencies. The electromagnetic spectrum does not end abruptly, but frequencies less than 3 kHz corresponding to

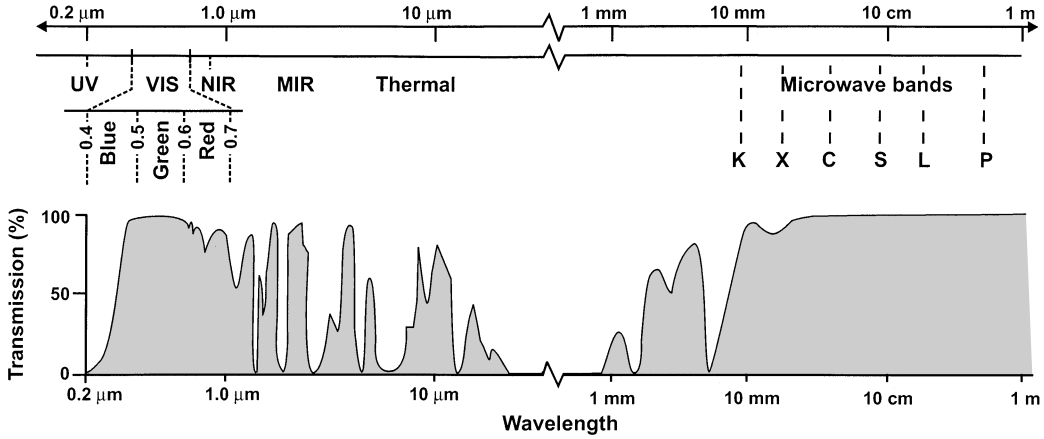


**Figure R10** The upper figure shows the general locations and ranges of various wavelength regions. Note the microwave region is used by passive microwave (passive measurement of emitted energy) and radar (active) remote sensing systems. The lower figure depicts atmospheric transmission. Satellite remote sensing applications are normally carried out in spectral regions of high transmission (shaded) and avoid regions of high blockage.

wavelengths longer than $10^5$ m are not used. Mechanical vibrations including sound and seismic waves begin at frequencies below 20 kHz. Marine profiling by sonar, the audio analog to radar, is in the 200-Hz range (Slater, 1980).

## Platforms and sensors

Aircraft color infrared photography is useful in providing detailed biophysical, high-quality information about coastal ecosystems; unfortunately, turnaround for new map production is relatively slow. Satellite remote sensing provides holistic but detailed information on a regional as well as repetitive basis, and it is the only feasible approach to successfully overcome many intractable problems related to mapping and monitoring of coastal ecosystems. Satellite remote sensors are increasing in number, in type, and in operational usefulness, and will provide the basis for integrated remote sensing applications (Lillesand and Kiefer, 1994; Jensen, 2000). Visible to thermal sensors have the longest history and have shown promise in mapping and monitoring coastal wetland type, health, biomass, and water quality. Since the late 1970s, microwave has gained importance in wetland mapping (Lewis *et al*., 1998). Microwave sensors extend the past capabilities of visible to thermal sensors in mapping coastal ecosystems by adding the potential for higher canopy penetration, more detailed canopy orientation and density information, and 24-hr-a-day collections nearly independent of weather conditions. Aircraft data will continue to provide calibration surveys, algorithm verification, testing of new sensor systems, specialized sensor collections, and in some cases local disaster response.

Remote sensing sensors measure radiant flux over bands defined by a range of wavelengths (e.g., VIS). A radiometer is a remote sensing instrument that measures radiant flux at any distance over a single band and a spectroradiometer measures over multiple bands. The specification of the instrument determines the spectral coverage, spectral, angular (or spatial or ground resolution), and radiometric resolutions. These factors clearly control the type and value of the data obtained.

Imaging and nonimaging sensors used in remote sensing use either electro-optical (VIS to thermal) or antenna detectors (microwave). Normally, nonimaging sensors are radiometers that collect accurate data over wide spectral regions where the spatial and spectral aspects are less important (Elachi, 1987). The signals returned to the sensor represent the scene spatial characteristics as rows and columns of pixels (discrete picture elements) within an image. Resampling is sometimes necessary to construct a continuous image representation of the scene (orbital and sensor characteristics), and almost always necessary to georeference the image to an earth coordinate system (e.g., latitude/longitude). Resampling tends to reduce confidence in the pixel location and blur the information contained in spatially adjacent pixels by adding a component of within-image spatial covariation. The pixel dimensions and location on the image represent an estimate of the spatial dimensions (spatially averaged ground area) and scene location that contributed to the pixel value.

Sensors commonly used can be separated into two types, active and passive. Active sensor systems both transmit and receive reflected or scattered radiant flux. The light detection and ranging (LIDAR) and radio detection and ranging (RADAR) are common active sensor systems. These systems track the time difference between the transmission of the emitted pulses of energy and the arrival of the scattered return at the sensor. The distance to or range of the target is then directly obtained from the time difference. Active systems can also control the nature of the radiation used to probe the target. For instance, the wavelength placement, bandwidth ($\Delta\lambda$), polarization, and the angle of incidence can be controlled by the sensor and sensor platform. And because the energy source is part of the system, active systems can operate day and night and in the case of radar during most weather conditions. These features allow a greater control over the application of remote sensing techniques, and their use in monitoring earth's resources is increasing.

Passive remote sensing primarily uses the sun as the source of electromagnetic energy. Planck's blackbody law describes the sun's energy distribution with respect to frequency and wavelength. A perfect blackbody absorbs and re-emits all electromagnetic radiation impingement upon it, while a partial emitter (gray body, e.g., water) is spectrally similar but of lower amplitude, and a selective emitter (e.g., quartz) is spectrally selective compared to the general shape of a blackbody. The sun's emitted radiation closely approximates a blackbody at 6,000 K where energy emissions are mostly contained between 0.3 and 2.5 μm, peaking near 0.55 μm. Solar radiation transferred through the earth's atmosphere and scattered and reflected by its surface is generally referred to as *solar reflected radiant flux* (Slater, 1980). In addition, solar heating of the earth's atmosphere and surface produces a secondary source of energy that has a distribution similar to radiation emitted from a blackbody at approximately 300 K. Energy emitted by the earth starts around 2.5 μm and peaks near 10 μm. Radiation emitted by the earth's atmosphere and surface is referred to as *self-emitted thermal radiant flux* (Slater, 1980). Radiant flux below about 2.5 μm represents solar-reflected radiant flux while above 6.0 μm it represents self-emitted thermal radiant flux. Between 2.5 and 6.0 μm, the relative amounts of each flux depend on the target reflectance, emissivity, temperature, and atmospheric transmittance. Lowered atmospheric transmittance between 2.5 and 5.5 μm normally results in the self-emitted flux dominating this region even when the surface has a high reflectance. Even though the self-emitted thermal radiant flux is very low at microwave wavelengths, the atmosphere is nearly transparent permitting successful application of passive microwave remote sensing.

## Target interactions

Surface irradiance ($I_{T\lambda}$) (e.g., solar in passive, instrument in active) interactions with earth's features can be partitioned following Kirchhoff's law (a restatement of the conservation of energy) as the proportion of $I_{T\lambda}$ reflected ($\rho(\lambda)$), transmitted ($\tau(\lambda)$) and absorbed ($\alpha(\lambda)$), that is, $\rho(\lambda) + \tau(\lambda) + \alpha(\lambda) = 1$. These interactions are commonly described as finite volume or surface averages of discrete elements, such as algal cells in water, leaves in a canopy, pebbles on the soil surface, and aerosol particles in the atmosphere. If the aggregate properties associated with these elements are independent of changes in $I_{T\lambda}$ and the method of measurement, they are referred to as inherent, the desired quantity to extract from the target radiance ($L_{T\lambda}$) (Bukata *et al*., 1995). Other definitions include the specific conditions, particularly the view ($\theta_v$) and local incident ($\theta_i$) angles (Figure R11), within the definition of inherent optical properties. Under such measurement conditions, inherent optical properties whether describing discrete scatters or averages, reflect, transmit, and absorb the same fraction of $I_{T\lambda}$ unless the material's inherent properties change. Unless the sensor is within the target volume (transmittance), a remote sensing sensor only measures the net result of the reflectance, transmittance, and absorption summed over the target (pixel) (including depth) and generalized to a single source and view (normally $\theta_v$ and $\theta_i$) as $r_\lambda$. The resultant target reflectance ($r_\lambda$) represents the measured fraction of $I_{T\lambda}$ reflected ($I_{R\lambda}$) ($r_\lambda = I_{R\lambda}/I_{T\lambda}$, range = 0–1). The source of $r_\lambda$ (and ultimately $L_{T\lambda}$) is surface and volume scattering, partitioned based on the transmittance depth (Whitt *et al*., 1990).

### VNIR and MIR

If the conditions of the measurement and $I_{T\lambda}$ are clearly specified, $r_\lambda$ is related to the averaged target properties through the averaged inherent optical properties ($\rho(\lambda)$, $\tau(\lambda)$, and $\alpha(\lambda)$) throughout the surface or volume. However, the $L_{T\lambda}$ is commonly recorded but not irradiance ($I_{T\lambda}$), thus, a factor similar to $r_\lambda$ and tied to $I_{T\lambda}$ by a geometric distribution related to $L_{T\lambda}$ is needed. In VNIR and MIR, the bidirectional ($\theta_v$ and $\theta_i$, bistatic) reflectance distribution function ($BRDF_\lambda$) describes the fraction of $I_{T\lambda}$ reflected over a solid angle ($\Omega$) at $\theta_v$, or the surface distribution of $L_{T\lambda}$ ($BRDF_\lambda = L_{T\lambda}/I_{T\lambda}$). $BRDF_\lambda$ is a function of the incident

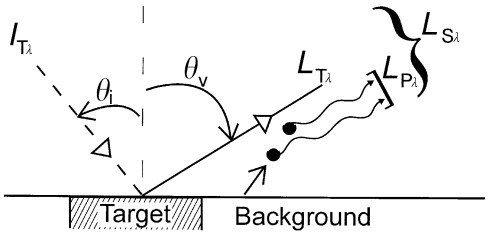


**Figure R11** $I_{T\lambda}$ depicts solar irradiance at a sun zenith angle of $\theta_i$ on a horizontal surface target, but the same depiction can refer to radiance from an active source at an incidence angle of $\theta_i$ (in this case $\theta_i$ and $\theta_v$ may be equal although the direction of the incident and reflected (backscattered) fluxes would be opposite). $L_{T\lambda}$ depicts the reflected or scattered radiance from the target at $\theta_v$, the sensor view zenith angle. $L_{P\lambda}$ depicts nontarget radiance added to $L_{T\lambda}$ from atmospheric scattering (● being the scatter center) and from areas surrounding the target (background). $L_{S\lambda}$ is the radiance at the sensor.

($\phi_i$) and view ($\phi_v$) azimuths, $\theta_i$, $\theta_v$, and $\Omega_s$ subtended by the source at a point on the surface, and $\Omega_v$ subtended by the entrance pupil of the sensor at the surface, that is, $BRDF_\lambda(\theta_I, \phi_i, \theta_v, \phi_v, \Omega_s, \Omega_v)$ (Jensen, 2000).

### Emitted energy

In thermal radiometry, the target or source emissions depend on the target contact kinetic temperature (KT) and the emissivity ($\varepsilon(\lambda)$). The $\varepsilon(\lambda)$ of a target equals $1 - \rho(\lambda)$ (when $\varepsilon(\lambda) = \alpha(\lambda)$, all transmitted incident $\Phi_\lambda$ is absorbed) and is the ratio of the emission spectral characteristics to a blackbody at the same temperature. The $\varepsilon(\lambda)$ relates KT to the self-emitted $\Phi_\lambda$ ($T_R(\lambda)$) from the target (i.e., $T_R(\lambda) = \varepsilon(\lambda)^{1/4} \cdot KT$). Because of this relationship, materials with equal KTs but different $\varepsilon(\lambda)$s will have different $T_R(\lambda)$s or in terms of the sensor, $L_{T\lambda}$s. Passive microwave intensity is the product of $\varepsilon(\lambda)$ and KT and is usually reported as brightness temperature. The $\varepsilon(\lambda)$ determines the energy from the effective emitting layer that is transferred across the soil surface, and it is dominated by surface soil moisture, and soil moisture dampens thermal and microwave emissions. In nonvegetated areas (e.g., deserts, oceans), atmospheric influences (including clouds) pose a problem to retrieval of the $T_R(\lambda)$ and therefore KT based on thermal radiometry. In vegetated areas, the vegetation adds to and attenuates the soil emissions; thus, $T_R(\lambda)$ detected at the sensor as $L_{T\lambda}$ contains emitted information proportional to both the vegetation and the soil layer. In passive microwave, the single scattering albedo and the optical depth describe microwave interactions and emissions from the overlying vegetation layer. In most cases, the effects of the single scattering albedo appear small and can be incorporated into the optical depth or set to a constant value.

### Radar

The scattering properties of discrete targets (in isolation) are described by the radar cross-section (RCS, $m^{-2}$). As in optical cross-sections, the RCS symbolizes the interaction cross-section or the target backscatter reflectivity, not the actual target area (Raney, 1998). Flux reflected or scattered to the sensor is the product of the incident radiant flux and RCS normalized by propagation losses and the area of the receiving antenna (Zebker *et al*., 1990). In typical resource applications, the radar signal recorded per pixel is the coherent summation of reflected (backscattered) energy from all scatterers (relative to the wavelength) in the distributed or diffuse target back to the sensor (Massonnet and Feigl, 1998). As such, the recorded flux depends on the target or pixel area. The backscatter coefficient ($\sigma^\circ(R, A)$ at a specific range ($R$) and azimuth ($A$) location) generated from the calibrated return and normalized by the target area (corrected for the local incidence angle) (where, $\sigma^\circ(R, A) \cdot \Delta R \cdot \Delta A / \sin\theta_i(R)$ is equivalent to RCS) represents the measured fraction of incident $\Phi_\lambda$ backscattered ($\Phi_{b\lambda}$) from the target, $\sigma^\circ = \Phi_{b\lambda}/\Phi_\lambda$ (Raney, 1998). As in reporting BRDF (albeit at one angle, monostatic), $\sigma^\circ$, at a specific wavelength, incident direction and polarization, is most closely related to the size, shape, orientation, and composition (primarily water content) properties of the diffuse target. Changes in $\sigma^\circ$ reflect the variability of these diffuse targets to send the incident energy back to the sensor (Massonnet and Feigl, 1998). A positive $\log(\sigma^\circ)$ in decibels implies focusing energy toward the sensor, while a negative number implies focusing energy away from the sensor (Elachi, 1987).

Synthetic aperture processing (focusing) creating synthetic aperture radar (SAR) (NASA, 1989) is used to improve the radar's spatial resolution. Within the processing, signal return variability is related to successive observations of the same area but from slightly different positions and somewhat different fine details in neighboring pixels with the same RCS (grainy appearance of image) (Elachi, 1987). Increasing the number of looks (statistical averages of the radar returns) reduces these effects but decreases the effective spatial resolution. Contrary to the total solar irradiance, polarimetric radar is capable of synthesizing well-defined polarization states represented in the linear case by horizontal and vertical orientations. After standard processing and image construction, phase information related to the distance between the sensor and the target can be linked to the polarimetric return (Elachi, 1987; Zebker *et al*., 1990). An interferogram is the resulting phase difference between two SAR images collected either from two antennae (bistatic) from a single platform or one antenna (monostatic) at two different times (Massonnet and Feigl, 1998). In the latter case, the direction of observation and wavelengths must be identical, and in practice, the input images are collected from the same satellite in the same orbital configuration and focusing or synthetic aperture processing (SAR) of the original image data are identical.

Both imaging and non-imaging radar sensors are commonly used in today's remote sensing applications. Altimeters use radar's ranging capabilities to measure the surface topography profile to centimeter-level precision at relatively high pixel spatial resolutions. This level of precision requires precise measurement of time and information extracted from the shape and slope of the returned pulse. Scatterometers assess the average scattering properties over large areas and within narrow spectral bands and provide directional capability by including more than one antenna (Elachi, 1987). They provide high precision backscatter measurements that cover large areas but at low pixel spatial resolutions (Cavanie and Gohin, 1995). Imaging SAR sensors are most often used for resource mapping because of their ability to provide high pixel spatial resolution data at multiple wavelengths, polarizations, and incident angles.

In all cases, objects of comparable size to the microwave wavelengths (mainly 2–30 cm in satellite imaging of earth's resources) most strongly influence the microwave scatter. At a constant incidence angle, canopy components such as leaves and stems normally interact with microwave wavelengths from about 2 to 6 cm, and trunks and limbs at longer wavelengths (10–30 cm). Longer wavelengths (>30 cm) provide more information about the surface properties but little about the canopy volume. Use of cross polarizations (e.g., horizontal send and vertical return, HV) and higher incidence angles, however, enhance volume scattering relative to lower (more vertical) incidence angles and like polarizations (e.g., VV, HH).

## Applications of remote sensing in coastal ecosystems

Polarization, angles of incidence and view, proportions of direct and scattered irradiance, and surface roughness all work to modify and build a directional reflectance character that becomes the target radiance ($L_{T\lambda}$). $L_{T\lambda}$ can be further altered from the surface to the satellite ($L_{S\lambda}$) by attenuation and addition of path radiance ($L_{P\lambda}$) (Figure R11), especially in the VIS but also in the NIR, MIR, and thermal regions and further modulated from the sensor to its representation on the image. In short, uncovering the relationship between $L_{S\lambda}$ output as a pixel in a grid-based image representation and the inherent properties of the target is often highly complex, and many times may be impossible to fully determine. Accountability can be built into the analysis by linking the image data to site-specific measurements through physical-based models. Greater accountability can diminish the reliance on gathering site-specific data and ultimately advance the operational and accurate representation of the temporal and spatial distributions of biophysical features in the scene.

The generation of the bidirectional reflectance distribution function ($BRDF_\lambda$) or radar backscatter coefficient ($\sigma^\circ$) is required when target inherent properties are sought or when the spectral contrast between the target ($L_{T\lambda}$) and its surroundings at the sensor prevents successful classification of the target. Classifications can be improved by generation of $BRDF_\lambda$ or $\sigma^\circ$; for example, biomass estimates are improved when generated from $L_{T\lambda}$ (top of canopy after atmospheric correction) versus $L_{S\lambda}$ (top of the atmosphere). Inferential relationships have more promise of extension over space and over time and the detection and mapping of subtle scene features when based on $BRDF_\lambda$ or $\sigma^\circ$. The consistent success of these detection and monitoring methods based on remote sensing data requires a rudimentary estimation of the relative extent the target material reflects, transmits, and absorbs surface irradiance ($I_{T\lambda}$) under various geometric and $I_{T\lambda}$ conditions.

### Classification

Most often, classification has relied on the differential interactions and responses of VNIR and MIR (e.g., spectral signature or $L_{T\lambda}$) to changes within the coastal scene to provide spectral classes uniquely linked to the type and state of coastal features. These classifications generally use simple image-based parametric statistical models (e.g., clustering techniques, principal component analysis, canonical correlation, discriminant analysis) that do not require detailed information about the plant, canopy, or water optical properties. The developed relationships are commonly limited to conditions existent only during the data collection, and are not necessarily extendable temporally or spatially. Integrating data from multiple remote sensors (VIS to microwave, hybrid models) has successfully improved the spatial detail of coastal vegetation classifications (Ramsey *et al*., 1998), as have newer classifications based on nonparametric statistical models (e.g., neural network

analysis) that allow greater control in linking the classification to the biophysical characteristics.

Classification of the radar images can follow the commonly used procedures of VNIR and MIR classifications (Ramsey *et al*., 1998), while also enhancing the use of neighborhood information or image texture in the classification. Radar image texture is a combination of the system and scene features. System texture (speckle) can be diminished by increasing the number of looks or can be estimated and removed by averaging the radar return over undisturbed water bodies. The improved or corrected measure is a more accurate representation of scene texture and a more pertinent input into the classification process. A more direct method is developed on rule-based logic (van Zyl, 1989; Dobson *et al*., 1995). In one method, returns associated with single or combinations of SAR sensors of different wavelengths and polarizations from sites with known structural characteristics are used to generate a progressive classification hierarchy. In another, rules based on predicted polarimetric return signatures from different features are used to classify targets within the scene.

## Biophysical features

Vegetation type classifications are not always the primary objective of the remote sensing application. Often the objective is to directly link the remote sensing data to biophysical variables that describe the coastal ecosystem. Of the biophysical variables, leaf area index (LAI) is probably the most sought, and it can be related to wetted or total biomass and in certain instances primary productivity and even $CO_2$ exchange.

In the VNIR, the ability to map canopy LAI and productivity is based on two facts (Horler and Barber, 1981; Smith and Morgan, 1981). First, although biomass and yield depend ultimately on light absorption, the usually close correlation between leaf reflectance and transmittance provides a basis for remote sensing reflectance measurements to be successfully applied in agronomic applications. Second, there is a striking attenuation difference between the red and NIR. NIR is not significantly absorbed and is nearly equivalent to above-canopy flux while the red is strongly absorbed and is therefore nearly equivalent to flux transmitted between the canopy leaves. Thus, the degree of canopy shading is related to both the LAI and the differential interactions of red and NIR as described numerically by a vegetation index (VI). In the VNIR, two types of VI are commonly used to transform remote sensing data into estimates of LAI: those based on ratio transforms and those based on orthogonal transforms. These VIs can be modified and possibly improved by altering the required input bands, or by precorrecting the image data to account for atmospheric influence, but variability remains related to the canopy $BRDF_\lambda$, or primarily to canopy structure.

Because the three-dimensional (3-D) distribution of water within the canopy has the greatest influence on microwave interactions, and because wetted biomass is related to vegetation water content, passive microwave and radar remote sensing are sensitive to LAI, and in turn, biomass variations. Similar to VNIR to MIR ratios and differences, biophysical variables such as LAI can be related to radar copolarized (e.g., HH, VV) and cross-polarized (e.g., VH) ratios and differences (Wegmuller and Werner, 1997). The vegetation biomass distribution (canopy structure) and quantity (water content) are also related to canopy optical depth that in turn is related to emission variability at microwave wavelengths (Wigneron *et al*., 1995).

## Vertical canopy profiling

Vertical canopy profiling is an indirect result of using multispectral remote sensing systems. Canopy profiling can be used to estimate canopy architecture, an indicator of species variety, phenological stage, and present and past vigor (Malet, 1996). In general, the longer wavelengths transmit further into fully formed vegetation canopies relative to shorter wavelengths. Canopy structure, or the spatial distribution and orientation of the canopy elements, however, also influences canopy penetration and must be removed or accounted for before the variable return can be used to describe the canopy architecture. Typically, NIR to MIR wavelengths transmit from 8 to 10 leaf layers (equivalent LAIs) into the canopy and VIS wavelengths from 2 to 3 LAIs. Although there are notable exceptions, active sensors offer a greater ability to profile the response from various depths within the vegetation canopy as compared to passive sensors. The use of shorter to longer radar wavelengths, multiple incident angles probing with a single band, and multiple polarizations can offer variable depths of transmittance although the analogy becomes less straightforward in canopies with convoluted branching (Ramsey, 1998). LIDAR offers the most direct canopy profiling. By using the allometric relationship between tree height and diameter-at-breast-height, LIDAR can provide volumetric representation of the canopy structure.

## Vegetation stress

One of the greatest challenges to coastal remote sensing is detecting plant stress before irreversible losses occur due to changes in inundation, flushing water salinity, and other external forces as a result of sea-level rise and shoreline alteration and protection. Although broadband VNIR to MIR remote sensing applications have detected broad indicators of vegetation stress, hyperspectral systems have identified specific spectral features related to stress from metal contamination to deficient foliar water content (Card *et al*., 1988). Radar is sensitive to vegetation stress through changes in water content, and because optical depth is linked to water content, passive microwave and thermal radiometry are closely related to plant stress. Chlorophyll_a fluorescence can also be used to assess vegetation stress by providing estimates of photosynthetic capacity (Carter *et al*., 1996). A passive technique using Fraunhofer line radiometers (FLR) detects the absorbed photosynthetic radiant flux (about 3%) re-emitted as fluorescence by taking advantage of the relatively strong Fraunhofer absorption lines in the solar irradiance (Horler and Barber, 1981; Carter *et al*., 1996). One of the strongest Fraunhofer lines is located in the chlorophyll fluorescence peak providing a convenient method for identifying plants suffering from metal toxicity and water stress. Active laser-induced fluorescence (LIF) sensors also provide the ability to assess the fluorescent properties of the leaf pigments (e.g., chlorophyll). Both passive FLR and active LIF offer new capabilities to isolate the alteration or change in dominance of specific pigments as an early indicator of vegetation stress.

## Thermal radiometry

In dry environments (e.g., nearly constant emissivity ($\varepsilon_\lambda$)), the rate of temperature change in response to variable surface solar irradiance ($I_T$) can be used to uniquely identify the target material (e.g., soil composition, mineral) (Lillesand and Kiefer, 1994). To characterize the rate materials respond to temperature changes (thermal inertia), radiant temperature ($T_R(\lambda)$) measurements are collected in the early morning and the afternoon. This temperature difference indicates the variable heat capacity of the different materials and can be used to map landcover variation. Heat capacity mapping has been applied mostly in nonvegetated regions for identifying geologic materials. Intense heat sources, however, can often be directly observed. Fires can exhibit self-emitted thermal fluxes down to about 3.0 μm, and some volcanic lava flows as low as the NIR (0.7–1.3 μm).

## Area mixtures

In any remote sensing application, all pixels are weighted mixtures of different scene features, even when the pixel nearly matches the target feature's mean spatial extent (e.g., adjacency effects, boundary pixel landcover mixtures). Mixture models are used to extract the occurrence of specific scene features from composite mixtures (e.g., trees, water, bare ground). In a linear mixture model, weighted combinations of specific scene features (e.g., spectral endmembers) are combined to completely reconstruct every spectral signature ($L_{S\lambda}$ or $L_{T\lambda}$) as represented on the image. This reconstruction allows target features to be detected and the percent occurrence in each image pixel to be determined. In nonlinear endmember analysis, the interaction between target features is included. Mixture models can be based on broadband sensor data; but most successful applications are based on hyperspectral sensor data (Adams *et al*., 1986).

## Soil moisture content

The NIR to MIR regions are used to estimate soil moisture where the increase in soil moisture (as in the presence of standing water) dampens the return to the sensor. Successful studies have relied more on direct determinations with thermal radiometry and passive microwave and radar (Idso *et al*., 1978; Ulaby *et al*., 1983; Shutko, 1992; Kostov and Jackson, 1993; Chanzy *et al*., 1995; van de Griend *et al*., 1996). As noted, decreases in moisture content are associated normally with decreases in the radiant temperature ($T_R(\lambda)$). In the thermal region, emissions are constrained to within 50 μm of the surface and this shallow depth can exhibit rapid temperature variations. Even though

monitoring diurnal temperature variations in the thermal region may improve the moisture content estimation, microwave is the only remote sensing platform and technique that can provide soil moisture with reasonable precision and consistency.

Both radar and passive microwave sensors are sensitive to non-bound water, and in general, sandy soils hold less bound water than clays. Normally, microwave is sensitive to soil moisture content within the top 2–5 cm of the soil depth (Chanzy *et al*., 1995). In exceptional conditions, radar can detect changes in moisture content at depths greater than 1 m, and passive microwave returns have been related to moisture content and groundwater at depths exceeding 1 m (Reutov and Shutko, 1992). Up to saturation, soil moisture acts to enhance the radar return at any given soil surface roughness height; in some cases, surface roughness variability can severely hamper the ability of radar to estimate changes in soil moisture (Ramsey, 1998). Radar is sensitive to soil moisture under short vegetation canopies; however, where moderately dense, the detection of soil moisture depends on the relative strength of the vegetation canopy and the incident flux interaction (Dobson *et al*., 1995). Surface roughness increases also enhance passive microwave emissions and can enhance soil emissivity differences between wavelengths. For most natural surfaces, however, roughness is not a serious limitation, and in wet soils, emissivity differences may be minor (Wang *et al*., 1987; Engman and Chauhan, 1995). In most soils, passive microwave emissions are practically independent of soil type, salinity, bulk density, and temperature variability (Shutko, 1992; Engman and Chauhan, 1995), but overlying vegetation attenuation increases as water content increases (van de Griend *et al*., 1996). In both passive microwave and radar, in general, the transmission through the vegetation canopy increases with increasing wavelength. Thus, longer wavelengths, HH polarization, and steeper incident angles are preferred for sensing soil moisture through a vegetation canopy.

## Shoreline placement

The delineation of land and water is important in coastal classifications, land loss, and shoreline displacement. Accurate mapping of coastal shoreline (defined as the high water line or wet–dry boundary) placement requires not only high spatial resolution sensors but also the spectral ability to provide contrast between open water and the regional nearshore material. Historically, optical sensors (especially photographic) have provided image data used for shoreline mapping, but more recently, radar image data have been used to construct shorelines (Lee, 1990; Ramsey, 1995). Coastline detection and automated tracing algorithms are being developed to provide dynamic shoreline construction. In the case of radar, scatter from roughened open water at times can limit the ability to differentiate land and water areas. In addition, a shoreline position is dynamic, especially in coastal regions experiencing high tidal ranges. Consequently, to truly represent the shoreline position, the variation in the tidal height relative to mean high tide and the occurrence of influencing forces such as wind set-up or set-down or abnormal river runoff must be accounted for at the time of the measurement.

## Flood monitoring

Remote sensing can detect flooding under vegetation. VNIR to MIR have been used, but microwave remote sensing offers the greatest potential for the instantaneous and consistent determination of flood extent. Within the microwave region, the most extensive history of flood detection under vegetation has been associated with radar (Ramsey, 1998). The radar return from flooded forest is usually enhanced compared to returns from nonflooded forests. The enhancement is related to the double bounce mechanism where the signal penetrating the canopy is reflected off the water surface and subsequently reflected back toward the sensor by a second reflection off a tree trunk (Hess *et al*., 1990). In contrast, diminished returns from flooded relative to nonflooded coastal marshes have been observed (e.g., Ramsey, 1995). The marsh grasses may calm the water surface accentuating specular reflection but without the grasses providing the double bounce (Ormsby *et al*., 1985). As in soil moisture mapping, flood detection can occur only if transmitted through the canopy; thus, longer wavelengths, HH polarization, and steeper incident angles are preferred.

## Topography

Coastal topography controls the hydrology of the coastal wetlands, and thereby the distribution and health of the coastal vegetation. Offshore coastal bathymetry is a result of the dynamic forces of local erosion and sedimentation and littoral drift. Mapping and monitoring the onshore topography and offshore bathymetry is of vital importance to the coastal engineer and resource manager. Historically and currently, indirect methods based on the simultaneous viewing of overlapping images (parallax) are commonly used to generate topographic information. Methods based on passive optical remote sensing also have been used to map coastal bathymetry, but these methods are limited by severe and variable attenuation by the water column materials (Ji *et al*., 1992; Lyon *et al*., 1992). Besides audio-mechanical systems (sonar), radar and LIDAR systems offer a direct and more consistent approach to surveying coastal topography and bathymetry.

After processing and most orbital contributions have been eliminated from the interferogram (radar phase difference image), slight remaining differences in the point of view of the radar sensor yield fringes that follow the topography (Massonnet and Feigl, 1998). These topographic contours can be used to generate a digital elevation model (DEM). Additionally corrected for elevation and local elevation gradient (slope) spatial variances, the interferogram can be related to finer resolution topographic changes from deformation (e.g., coastal volcanoes, surface subsidence, erosion, rebound, or deposition). In monostatic systems, success of this technique requires all scatters comprising the target (e.g., overlying vegetation, moisture content, inundation) remain unchanged between the time of the two radar image collections (Massonnet and Feigl, 1998). While successful application is problematic in vegetated environments, absolute stability, and thereby success, in dynamic and highly vegetated coastal environments is less probable. Frequent and variable flooding and the associated changes in soil and vegetation moisture contents add complexities that appear as random speckles in the interferogram. In coastal areas, these complexities may limit the absolute elevation and elevation change resolutions attainable with interferograms generated from monostatic systems.

Airborne laser altimetry (ALS) is the simplest application of LIDAR remote sensing. ALS surveys are primarily performed at 700–1,000 m above ground level in order to eliminate most atmospheric attenuation of the signal. As in radar systems, when properly calibrated to a stable platform, the time between the emitted and detected pulses is directly related to the range, and thereby to changes in the surface elevation. Vegetation interferes with the laser pulse and complicates conversion of the ALS image into a topographic surface. Reflectance of solar illumination into the sensor field of view within the laser operational bandwidth also corrupts the ALS signal. A correction for vegetation interference and contamination uses data collected near in time along multiple transects to develop a topographic precision estimate.

## Bathymetry

ALS is also used to develop coastal bathymetry maps. Most current ALS systems use two wavelengths: a green band for high water penetration to the bottom and a NIR band with little to no water penetration and almost total reflectance from the surface. Use of the two-band system helps diminish errors resulting from platform altitude variation so that the time delay difference between the two return pulses is a direct bathymetric measure. Increased turbidity, however, results in lower spatial resolutions and increased water volume backscattering of the emitted pulse creates false echoes in the record. The low altitude and fairly narrow coverage of current ALS systems hamper the operational feasibility of these systems in regional assessments. Even with these limitations, of all the electromagnetic systems, the ALS systems may provide the only feasible mechanism for rapid and consistent detailed mapping of coastal bathymetry and wetland topography.

## Water quality and submerged aquatic vegetation

Remote sensing of estuarine and coastal waters is primarily concerned with mapping the type, concentration, distribution, and dispersion of materials suspended and dissolved in the water (water quality) (Morel and Gordon, 1980; Ramsey and Jensen, 1990), and the type and distribution of submerged aquatic vegetation and bottom cover (e.g., rock, mud, sand, shell). To accurately map the water quality and bottom type, the radiant flux depth-intensity and spectral distribution must be estimated (Kirk, 1980). In a well-mixed water column, the underwater radiation environment is determined by reflection and refraction at the water–air interface (surface), absorption and scattering within the water body, and reflection from the bottom. Surface reflections of $I_{T\lambda}$, upwelling restrictions (due to refraction at the surface), added atmospheric path and background fluxes, and atmospheric attenuation result in the upwelling water volume flux (below the water surface) transferred

through the surface ($L_{T\lambda}$) normally comprising only 3–5% of the sensor signal ($L_{S\lambda}$). Corrected for water surface reflection, transmission, and atmospheric influences, $L_{T\lambda}$ can be related to the inherent bulk absorption and scattering properties of the water and water materials and bottom reflectance in the shallow waters (Morel and Gordon, 1980; Carder and Steward, 1985).

Excluding bottom reflections, the inherent bulk absorption ($\alpha(\lambda)$) and backscatter ($b_b(\lambda)$) coefficients can be related to $L_{T\lambda}$ as $L_{T\lambda}/I_{T\lambda} = \mathrm{BRDF}_\lambda = C_F \cdot b_b(\lambda)/\alpha(\lambda)$, where backscattering is scattering into the hemisphere trailing the incident flux, and $C_F$ incorporates the ratio of two subsurface upwelling fluxes and the water refractive index (Carder and Steward, 1985; Bukata *et al*., 1995). In optically complex coastal waters, bulk $b_b(\lambda)$ and $\alpha(\lambda)$ are commonly related to bulk descriptors of biomass (e.g., chlorophyll-a [Chl]), suspended materials (SMs) (e.g., detritus, suspended inorganic particles), and dissolved organic carbon (DOC) (Bukata *et al*., 1995). Use of these bulk descriptors normally provides a good and stable estimation of water quality with respect to location and time in coastal environments. The inherent bulk properties are related to the specific optical coefficients ($i$) as $b_b(\lambda) = \Sigma C_i(b_b)_i(\lambda)$ and $\alpha(\lambda) = \Sigma C_i\alpha_i(\lambda)$, where the subscript ($i$) represents one water component and $C_i$ refers to the components concentration (e.g., $\alpha(\lambda) = a_w + C_{Chl}\alpha_{Chl}(\lambda) + C_{SM}\alpha_{SM}(\lambda) + C_{DOC}\alpha_{DOC}(\lambda)$, where $a_w$ is absorption due to the water).

LIDAR systems can be used to stimulate fluorescence in chlorophyll pigments associated with phytoplankton, plants and corals, and fluorescent DOC (i.e., Gelbstoff) (Measures, 1984). As in passive optical remote sensing of water quality, the signal returned to the sensor can be corrupted by the atmosphere and by addition of reflectance from the bottom. The selection of the excitation (send) and emission (return) wavelengths is either fixed by the LIDAR system or optimized by laboratory measurements. Chlorophyll is normally determined by excitation in the low red and measuring the emission in the high red wavelength regions. Gelbstoff is linearly related to natural fluorescence (Otto, 1967) that has been used as a conservative tracer of riverine and ocean waters mixing. Natural fluorescence is normally determined by excitation in the ultraviolet and by measuring the fluorescence in the blue. As in canopy profiling, the fluorescent return can be scattered or self-absorbed before reaching the water surface, causing ambiguity in mapping the concentration of the fluorescent material. Raman intensity variability can be measured simultaneously with the fluorescent return and used to remove the effect of self-absorption, thereby creating spatially comparable fluorescent images (Bristow *et al*., 1981).

## Bottom reflectance

Seagrasses and bottom type (mud, sand, shell) mapping is an important aspect of coastal monitoring. In this case, the overlying water column attenuates the signal to and from the bottom. In both passive VNIR and LIDAR mapping, the same problems apply as in water quality monitoring; however, in this case, the overlying water column signal must be removed from or de-emphasized in the return signal (Ji *et al*., 1992; Lyon *et al*., 1992). Increasing water turbidity and absorption can severely restrict the ability of either method (passive VNIR and LIDAR) to accurately map bottom reflectance variations as does low contrast between the different bottom materials.

## Surface films and salinity

Observation of surface water features, especially surface films, has long been recognized as an indirect method of mapping convergence zones, mixing zones, and internal wave fields in optical oceanography (Klemas, 1980). The natural and extracted oils and similar substances also can be observed by SAR systems because they tend to dampen the creation of surface waves, smoothing the water surface, and attenuating the SAR returns. This differential dampening enables SAR sensors to map and monitor surface spills, and because of its nearly all weather capabilities, SAR provides capabilities many times superior to VNIR and MIR. Laser Induced Flouresence (ultraviolet excitation, visible emission) has also been used to detect and classify oil slicks and oil film thickness (Measures, 1984).

Of the possible conservative tracers of water mass mixing, salinity is the most notable. Salinity is not directly measurable with VIS to thermal systems (ignoring extremely slight dependencies), although salinity changes have been inferred from changes in other water properties, such as fluorescence and suspended particle concentrations. A more direct measure is based on the definition of salinity as the concentration of dissolved cations and anions. Changes in these concentrations change the water's ionic strength, leading to changes in the dielectric properties of the water that are most apparent at microwave wavelengths. These changes are best observed as changes in the emissivity, although to accurately observed changes, microwave emissions must be corrected for water temperature and surface roughness variations. To accomplish this correction, microwave measurements are collected at two wavelengths, obtaining a direct method to map changes in water salinity (Shutko, 1985).

## Sea surface temperature

One of the earliest uses of radiometry was to map the sea surface temperature (SST) and thereby map different water masses and physical dynamics (e.g., frontal convergence, upwelling). Along the same line, water temperature mapping of heated effluents into rivers, estuaries, and coastal oceans is used to monitor compliance of discharges. In each of these radiometric applications, the radiant temperature ($T_{R\lambda}$) is related to the 3–5 μm thick surface skin by converting via emissivity ($\varepsilon(\lambda, \text{water})$) to the skin kinetic temperature (KT). On average, surface skin temperatures are about 0.3 K cooler than bulk temperatures, but differences can range from about +1 to −1 K (Emery *et al*., 1995). Depending on the water stability or the amount of mixing, the bulk temperature can represent the well-mixed surface layer or the temperature gradient depth. Often the skin $T_{R\lambda}$ (radiometer measurements) is related to the bulk KT or SST by breaking the surface skin with buckets of water (i.e., bucket temperature). Ship intakes and moored buoys offer bulk temperature measurements at variable depths. These measurements are used to correct atmospheric influences (especially water vapor) and consequently directly relate the sensor signal ($L_{S\lambda}$) to the SST, aggregating skin effects into atmospheric correction (Minnett, 1995). A separate type of atmospheric correction relates $L_{S\lambda}$ to atmospheric attenuation and thereby to the skin KT. Atmospheric effects are inferred from spectral relationships based on multiple band measurements (e.g., $\mathrm{SST} = a_0 + a_\lambda \mathrm{KT}_\lambda$, where λ refers to one or a combination of bands) (Emery *et al*., 1995; Minnet, 1995). Alternatively, measurements of the same target but at different sensor view angles provide a direct measurement of atmospheric influences ($\mathrm{SST} = b_0 + b_{\lambda,N}\mathrm{KT}_N + b_{\lambda,S}\mathrm{KT}_S$, where N is nadir, S is oblique views, and λ refers to one band or a band combination). Based on current correction techniques, skin and bulk surface water temperatures can be estimated to less than 0.5°C. Even though less influenced by atmospheric conditions, the coarse spatial resolution associated with passive microwave systems makes them less preferred than thermal radiometry. Further, even at longer wavelengths, passive microwave measurements have shown dependence on surface roughness as a function of wind speed (Shutko, 1985; Trokhimovski *et al*., 1995).

## Sea ice

Detection and monitoring the distribution and type (first year and multiyear ice) of coastal (Arctic) sea ice is important in marine mammal ecology, climate processes, and early detection of global warming (Piwowar and LeDrew, 1996). Operational methods until recently have been applicable only to broadscale spatial inventories. More recently, optical, passive microwave, and radar sensors have provided higher spatial resolutions; however, increasing spatial resolution beyond 1 km constrains the ability to operationally monitor global or hemispheric regions. The primary factor controlling the remote sensing of sea ice is emissivity ($\varepsilon(\lambda)$), and the major factor controlling emissivity is salinity (Comiso, 1995). In thermal radiometry and passive microwave, the effective emissivity decreases from the cold saline first-year to the cold desalinated multiyear ice. Emissivity also decreases from first-year to multiyear ice due to the decreased density and increased surface roughness resulting in increased surface scatter. Added to this overall change, emissivity varies with wavelength and polarization. First-year ice is nearly independent of wavelength and polarization while emissivities of both VV and HH polarizations associated with multiyear ice increase with wavelength (Comiso, 1995). SAR returns tend to increase from first-year to multiyear ice (Drinkwater, 1995). In radar imaging, shorter wavelengths scattered from the ice surface primarily respond to dielectric differences (salinity) and roughness, while longer wavelengths (>5 cm) penetrate the ice (multiyear >> first-year) and are returned via volume scattering. Use of longer wavelengths normally results in a higher return from the relatively lower salinity and density multiyear ice than other ice types (Drinkwater, 1995). Of the three sensors, optical sensors are constrained by persistent clouds and darkness in Arctic regions, and radar returns from roughened multiyear ice surfaces are more prone to confusion with other types of sea ice than are emissions sensed by passive microwave sensors (Hall, 1998). Integrated approaches seem to provide the best results and the added benefit of comparison and validation.

## Wind speed and surface waves

Short gravity (>1.7 cm) and small capillary (<1.7 cm) waves are the surface water features observed with operational radar systems (2–30 cm wavelengths) (Elachi, 1987). Increasing near-surface wind speed increases the amplitude of these waves, intensifying surface roughness that in turn promotes increasing slope (specular or facet) reflections and point scatter (or Bragg). As wind speed is related to surface roughness, altimeter and scatterometer sensors can provide estimates of wind speed ($U$). Scatterometers provide regional coverage, but at coarse pixel resolutions, while altimeter measurements cover narrow swaths. In the case of altimeters, $\sigma^0$ is a result of near nadir specular reflections (facet) that decrease as surface roughness increases ($\sigma^0 \propto U^{-x}$) (Elachi, 1987; Dobson, 1995). Although designed for measuring open ocean winds, scatterometers have also been found useful in measuring winds in coastal and enclosed seas. $\sigma^0$ derived from scatterometer measurements increases with wind speed increases (at >25° incident angle) as $\sigma^0 \propto U^x$ ($x$ is dependent on wavelength) and are principally a result of Bragg scattering (Topliss and Guymer, 1995). Scatterometers also include multiple azimuths, providing the ability to estimate the wind direction. Wind speed accuracies derived from scatterometers are about 2 m/s with a directional tolerance of 20° (Topliss and Guymer, 1995). Compared to open ocean measurements, altimeter and scatterometer coastal measurements are more difficult to explain based on dynamic processes and are generally plagued by three types of problems: (1) contamination from land–water mixing, (2) varying wind–radar relationships, and (3) substantial influences of temporal and spatial variations in SST resulting in incorrect estimates of $\sigma^0$.

## Currents and waves

Indirect observation of convergence and divergence zones associated with currents and possibly internal waves through varying surface features is used in optical remote sensing of ocean features (Klemas, 1980). Radar systems, however, offer a nearly unimpeded source of mapping surface features related to ocean dynamics. Short gravity and capillary waves created by wind stress and mechanically (independent of wind stress) are modified (local slope and growth) by long-period gravity or internal waves and variable currents (fronts, eddies, upwelling, tidal circulation) and bottom topography (Topliss and Guymer, 1995). These spatially and periodic modulated small wave fields (bands of roughness) are detectable with altimeters, scatterometers, and SAR imaging. Dependent on the angle of incidence and wavelength, SAR returns can be dominated by either a mixture of Bragg scattering or specular reflections. SAR images are used to define wave direction and length and to map the location of convergence zones and currents.

## Water surface topography

Instantaneous sea surface height ($S_0$) observed by an altimeter is the sum of the geoid ($N$, a level surface of the earth's gravity field associated with a motionless ocean surface regarded as time invariant), the permanent dynamic topography ($\xi_0$, related to ocean circulation, $N + \xi_0$ = mean sea level), the variable topography ($\xi_v$, e.g., ocean tides and waves and swells), orbital and propagation errors (e.g., sensor attitude corrections, barometric correction), and sensor noise ($S_0 = N + \xi_0 + \xi_v +$ error + noise) (Le Traon, 1995). Wave heights from altimeter measurements are related to the shape or rise time of the returned pulse (Dobson and Monaldo, 1995). Increasing wave heights increase the slope or rise time. Large surface-wave heights or swell heights are estimated by differencing wave energy ($\propto$(wave height)$^2$) and wave energy associated with wave heights estimated from altimeter wind speeds. In principle, skewness of the generated wave height probability distribution can also be used to estimate the dominant wavelength in unimodal seas (Dobson and Monaldo, 1995).

The low-frequency harmonic rise and fall of the coastal tides can be observed with satellite altimetry with a precision of about 3–5 cm (Han, 1995). Limited sampling frequency associated with altimeter data, however, leads to aliasing shorter tidal periods into longer tidal periods causing ambiguities in tidal period evaluations. Conversely, extraction of tidal fluctuations from the surface height variability is necessary to recover long-term height variability (e.g., annual cycles). As in other coastal applications, increased problems are created by the high temporal and spatial variability in the surface height due to basin morphology (shape and shallow depths (≈100 m)), variable river runoff (buoyancy), solar heating (e.g., SST), wind stress (e.g., Eckman drift), and the surface expression of subsurface features (e.g., sea mounds or submarines).

Elijah W. Ramsey III

## Bibliography


Adams, J., Smith, M., and Johnson, P., 1986. Spectral mixture modeling: a new analysis of rock and soil types at the Viking Lander 1 site. *Journal of Geophysical Research*, **91**: 8098–8112.

Bristow, M., Nielsen, D., Bundy, D., and Furtek, R., 1981. Use of water Raman emission to correct airborne laser fluorosensor data for effects of water optical attenuation. *Applied Optics*, **20**: 2889–2906.

Bukata, R., Jerome, J., Kondratyev, K., and Pozdnyokov, D., 1995. *Optical Properties and Remote Sensing of Inland and Coastal Waters*. New York: CRC Press.

Card, D., Peterson, D., Matson, P., and Aber, J., 1988. Prediction of leaf chemistry by the use of visible and near infrared reflectance spectroscopy. *Remote Sensing of Environment*, **26**: 123–147.

Carder, K., and Steward, R., 1985. A remote-sensing reflectance model of a red-tide dinoflagellate off west Florida. *Limnology and Oceanography*, **30**: 286–298.

Carter, G., Jones, J., Mitchell, R., and Brewer, C., 1996. Detection of solar-excited chlorophyll_a fluorescence and leaf photosynthetic capacity using a Fraunhofer line radiometer. *Remote Sensing of Environment*, **55**: 89–92.

Cavanie, A., and Gohin, F., 1995. Sea-ice studies with scatterometer. In Ikeda, M., and Dobson, F. (eds.), *Oceanographic Applications of Remote Sensing*. Boca Raton, FL: CRC Press, Inc., pp. 9–366.

Chanzy, A., Bruckler, L., and Perrier, A., 1995. Soil evaporation monitoring: a possible synergism of microwave and infrared remote sensing. *Journal of Hydrology*, **165**: 235–259.

Comiso, J., 1995. Sea-ice geophysical parameters from SSM/I data. In Ikeda, M., and Dobson, F. (eds.), *Oceanographic Applications of Remote Sensing*. Boca Raton, FL: CRC Press, Inc., pp. 321–338.

Dobson, E., 1995. Wind speed from altimeters. Satellite measurement and corrections. In Ikeda, M., and Dobson, F. (eds.), *Oceanographic Applications of Remote Sensing*. Boca Raton, FL: CRC Press, Inc., pp. 223–236.

Dobson, E., and Monaldo, F., 1995. Significant wave height from altimeter. In Ikeda, M., and Dobson, F. (eds.), *Oceanographic Applications of Remote Sensing*. Boca Raton, FL: CRC Press, Inc., pp. 223–236.

Dobson, M., Ulaby, F., and Pierce, L., 1995. Land-cover classification and estimation of terrain attributes using synthetic aperture radar. *Remote Sensing of Environment*, **51**: 199–214.

Drinkwater, M., 1995. Application of SAR measurements in ocean-ice-atmosphere interaction studies. In Ikeda, M., and Dobson, F. (eds.), *Oceanographic Applications of Remote Sensing*. Boca Raton, FL: CRC Press, Inc., 381–396.

Elachi, C., 1987. *Introduction to the Physics and Techniques of Remote Sensing*. New York: John Wiley & Sons.

Emery, W., Wick, G., and Schluessel, P., 1995. Skin and bulk sea surface temperatures: satellite measurement and corrections. In Ikeda, M., and Dobson, F. (eds.), *Oceanographic Applications of Remote Sensing*. Boca Raton, FL: CRC Press Inc., pp. 145–165.

Engman, E., and Chauhan, N., 1995. Status of microwave soil moisture measurements with remote sensing. *Remote Sensing of Environment*, **51**: 189–198.

Hall, K., 1998. Remote sensing of snow and ice using imaging radar. In Henderson, F., and Lewis, A. (eds.), *Principals and Applications of Imaging Radar*. New York: John Wiley & Sons, Inc., Manual of Remote Sensing, pp. 677–703.

Han, G., 1995. Coastal tides and shelf circulation by altimeter. In Ikeda, M., and Dobson, F. (eds.), *Oceanographic Applications of Remote Sensing*. Boca Raton, FL: CRC Press Inc., pp. 45–56.

Hess, L., Melack, J., and Simonett, D., 1990. Radar detection of flooding beneath the forest canopy: a review. *International Journal of Remote Sensing*, **11**: 1313–1325.

Horler, D., and Barber, J., 1981. Principles of remote sensing of plants. In Smith, H. (ed.), *Plants and the Daylight Spectrum*. New York: Academic Press. pp. 43–64.

Idso, S., Hatfield, J., Reginato, R., and Jackson, R., 1978. Wheat yield estimation by albedo measurements. *Remote Sensing of Environment*, **7**: 273–276.

Jensen, J., 2000. *Remote Sensing of the Environment, An Earth Resource Perspective*. Upper Saddle River: Prentice Hall.

Ji, W., Civco, D., and Kennard, W., 1992. Satellite remote bathymetry: a new mechanism for modeling. *Photogrammetric Engineering and Remote Sensing*, **58**: 545–549.

Kirk, J., 1980. Spectral absorption properties of natural waters: contribution of the soluble and particulate fractions to light absorption in

some inland waters of south-eastern Australia. *Australian Journal of Marine and Freshwater Research*, **31**: 287–296.
Klemas, V., 1980. Remote sensing of coastal fronts and their effects on oil dispersion. *International Journal of Remote Sensing*, **1**: 11–28.
Kostov, K., and Jackson, T., 1993. Estimating profile soil moisture from surface layer measurements—a review. *Ground Sensing SPIE*, **1941**: 125–136.
Lee, J., 1990. Coastline detection and tracing in SAR images. *IEEE Transactions on Geoscience and Remote Sensing*, **28**: 662–668.
Le Traon, P., 1995. Basin-scale oceanic circulation from satellite altimetry. In Ikeda, M., and Dobson, F. (eds.), *Oceanographic Applications of Remote Sensing*. Boca Raton, FL: CRC Press, Inc., pp. 79–96.
Lewis, A., Henderson, F., and Holcomb, D., 1998. Radar fundamentals: the geoscience perspective. In Henderson, F., and Lewis, A. (eds.), *Principals and Applications of Imaging Radar*. New York: John Wiley & Sons, Inc., Manual of Remote Sensing, **3**: 131–181.
Lillesand, T., and Kiefer, R., 1994. *Remote Sensing and Image Interpretation*. New York: John Wiley & Sons, Inc.
Lyon, J., Lunetta, R., and Williams, D., 1992. Airborne multispectral scanner data for evaluating bottom sediment types and water depths of the St. Marys River, Michigan. *Photogrammetric Engineering and Remote Sensing*, **58**: 951–956.
Malet, P., 1996. Classifying the geometry of canopies from time variations of red and near-infrared reflectance. *Remote Sensing of Environment*, **56**: 64–171.
Massonnet, D., and Feigl, K., 1998. Radar interferometry and its application to changes in earth's surface. *Reviews of Geophysics*, **36**: 441–500.
Measures, R., 1984. *Laser Remote Sensing, Fundamentals and Applications*. New York: John Wiley & Sons.
Minnett, P., 1995. Sea surface temperatures from the along-track scanning radiometer. In Ikeda, M., and Dobson, F. (eds.), *Oceanographic Applications of Remote Sensing*. Boca Raton, FL: CRC Press pp. 461–472.
Morel, A., and Gordon, H., 1980. Report on the working group on water color. *Boundary-Layer Meteorology*, **18**: 343–355.
NASA, 1989. Instrument panel report. *SAR Synthetic Aperture Radar* (Earth Observation System). Washington, DC: Earth Science and Application Division, NASA Headquarters, IIF, p. 233.
Ormsby, J., Blanchard, B., and Blanchard, A., 1985. Detection of lowland flooding using active microwave systems. *Photogrammetric Engineering and Remote Sensing*, **51**: 317–328.
Otto, I., 1967. Investigations on optical properties and water-masses of the southern North Sea. *Netherlands Journal of Sea Research*, **4**: 532–551.
Piwowar, J., and LeDrew, E., 1996. Principal components analysis of arctic ice conditions between 1978 and 1987 as observed from the SMMR data record. *Canadian Journal of Remote Sensing*, **22**: 390–403.
Ramsey, E., III, 1995. Monitoring flooding in coastal wetlands by using radar imagery and ground-based measurements. *International Journal of Remote Sensing*, **16**: 2495–2502.
Ramsey, E., III, 1998. Radar remote sensing of wetlands. In Lunetta, R., and Elvidge, C. (eds.), *Remote Sensing Change Detection: Environmental Monitoring and Applications*. Chelsea, Michigan: Ann Arbor Press, pp. 211–243.
Ramsey, E., III, and Jensen, J., 1990. The derivation of water volume reflectances from airborne MSS data using *in situ* water volume reflectances and a combined optimization technique and radiative transfer model. *International Journal of Remote Sensing*, **11**: 979–998.
Ramsey, E., III, Nelson, G., and Sapkota, S., 1998. Classifying coastal resources by integrating optical and radar imagery and color infrared photography. *Mangroves and Salt Marshes*, **2**: 109–119.
Raney, K., 1998. Radar fundamentals; technical perspective. In Henderson, F., and Lewis, A. (eds.), *Principles and Applications of Imaging Radar*. New York: John Wiley & Sons, Inc., *Manual of Remote Sensing*, **3**: 9–130.
Reutov, E., and Shutko, A., 1992. Estimation of the depth to a shallow water-table using microwave radiometry. *International Journal of Remote Sensing*, **13**: 2223–2232.
Shutko, A., 1985. The status of the passive microwave sensing of the water—lakes, seas, and oceans—under the variation of their state, temperature, and mineralization (salinity): models, experiments, examples of applications. *IEEE Journal of Oceanic Engineering*, **OE-10**: 418–437.
Shutko, A., 1992. Soil/vegetation characteristics at microwave wavelength. In Mather, P. (ed.), *Understanding the Terrestrial Environment: The Role of the Earth Observations from Space*. Washington, DC: Taylor and Francis.
Slater, P., 1980. *Remote Sensing, Optics and Optical Systems*. London: Addison-Wesley Publishing Company.
Smith, H., and Morgan, D., 1981. The spectral characteristics of the visible radiation incident upon the surface of the earth. In Smith, H. (ed.), *Plants and the Daylight Spectrum*. New York: Academic Press, pp. 3–20.
Topliss, B., and Guymer, T., 1995. Marine winds from scatterometers. In Ikeda, M., and Dobson, F. (eds.), *Oceanographic Applications of Remote Sensing*. Boca Raton, FL: CRC Press Inc., pp. 205–221.
Trokhimovski, Y., Bolotnikova, G., Etkin, V., Grechko, S., and Kuzmin, A., 1995. The dependence of S-band sea surface brightness and temperature on wind vector at normal incidence. *IEEE Transactions on Geoscience and Remote Sensing*, **33**: 1085–1088.
Ulaby, F., Razani, M., and Dobson, M., 1983. Effects of vegetation cover on the microwave radiometric sensitivity to soil moisture. *IEEE Transactions on Geoscience and Remote Sensing*, **21**: 51–61.
van de Griend, A., Owe, M., de Ruiter, J., and Gouweleeuw, B., 1996. Measurement and behavior of dual-polarization vegetation optical depth and single scattering albedo at 1.4- and 5-GHz microwave frequencies. *IEEE Transactions on Geoscience and Remote Sensing*, **34**: 957–965.
van Zyl, J., 1989. Unsupervised classification of scattering behavior using polarimetric data. *IEEE Transactions on Geoscience and Remote Sensing*, **27**: 36–45.
Wang, J., Engman, E., Mo, T., Schmugge, T., and Shiue, J., 1987. The effects of soil moisture, surface roughness, and vegetation on L-band emission and backscatter. *IEEE Transactions on Geoscience and Remote Sensing*, **25**: 825–833.
Wegmuller, U., and Werner, C., 1997. SAR interferometric signatures of forest. *IEEE Transactions on Geoscience and Remote Sensing*, **35**: 18–24.
Whitt, M., Ulaby, F., and Sarabandi, K., 1990. Polarimetric scatterometer systems and measurements. In Ulaby, F., and Elachi, C. (eds.), *Radar Polarimetry for Geoscience Applications*. Norwood, Maine: Artech House, Inc., pp. 191–272.
Wigneron, J., Chanzy, A., Calvet, J., and Bruguier, N., 1995. A simple algorithm to retrieve soil moisture and vegetation biomass using passive microwave measurements over crop fields. *Remote Sensing of Environment*, **51**: 331–341.
Zebker, H., van Zyl, J., and Elachi, C., 1990. Polarimetric radar system design. In Ulaby, F., and Elachi, C. (eds.), *Radar Polarimety for Geoscience Applications*. Norwood, Maine: Artech House, Inc., pp. 273–312.

## Cross-references

Airborne Laser Terrain Mapping and Light Detection and Ranging
Altimeter Surveys, Coastal Tides and Shelf Circulation
Coasts, Coastlines, Shores, and Shorelines
Mangroves, Remote Sensing
Mapping Shores and Coastal Terrain
Nearshore Geomorphological Mapping
Photogrammetry
Remote Sensing: Wetlands Classification
Synthetic Aperture Radar Systems

# REMOTE SENSING: WETLANDS CLASSIFICATION

Coastal wetlands are a highly productive and critical habitat for a number of plants, fish, shellfish, waterfowl, and other wildlife. Wetlands also provide flood damage protection, protection from storm and wave damage, water quality improvement through filtering of agricultural and industrial waste, and recharge of aquifers. After years of degradation due to dredge and fill operations, impoundments, urban development subsidence/erosion, toxic pollutants, entrophication, and sea-level rise, wetlands have finally begun to receive public attention and protection (Daiber, 1986). Heightened awareness of the value of wetlands has resulted in the need to better understand their function and importance and find ways to manage them more effectively. To accomplish this, at least two types of data are required: (1) information on the present distribution and abundance of wetlands; and (2) information on the trends of wetland losses and gains.

Coastal wetlands can be conveniently divided into four major types: salt marshes, coastal fresh marshes, coastal forested and scrub–shrub wetlands, and tidal flats (Field *et al*., 1991). Each of these wetland types has different hydrologic requirements and is dominated by a different type of vegetative cover. As a result, their spectral signatures and detectability by remote sensors differ significantly. For instance, salt marshes are widely distributed along the Atlantic and Gulf coasts and are dominated by smooth cordgrass (*Spartina alterniflora*) and frequently include other grasses, such as salt hay (*Spartina patens*) and big cordgrass (*Spartina cynosuroides*). The relative purity and size of salt marshes makes it possible to map them from aircraft and satellites.

Freshwater marshes are relatively diverse and have a more mixed vegetative cover producing a more complex, composite spectral signature. Forested and scrub–shrub wetlands, characterized as woody communities, are regularly inundated and saturated during the growing season. Wooded wetlands resemble spectrally wooded uplands and are therefore difficult to distinguish from wooded upland areas. Combining RADAR data with Landsat TM helps to distinguish wooded uplands from wetlands by providing soil moisture conditions beneath the tree canopy.

## Wetlands mapping

Most of the major wetlands mapping programs, conducted by the United States Geological Survey (USGS), the National Oceanic and Atmospheric Administration (NOAA), and the Environmental Protection Agency (EPA), and other agencies, are described in Kiraly *et al*. (1990). Traditionally the US Fish and Wildlife Service (FWS) has played a key role, conducting its first nationwide wetlands inventory in 1954, which focused on waterfowl wetlands. In 1974, the FWS established the National Wetlands Inventory Project (NWI) to generate scientific information on the characteristics of US wetlands, including detailed maps and status/trend reports. The maps are available as 7.5 min quads at a scale of 1 : 24,000. Most have been digitized, converting them from paper maps to a GIS (Geographic Information System)-compatible digital line graph (DLG) format (Tiner, 1985).

The NWI program produced a new classification system and a more rigorous definition of wetlands: wetlands are transitional areas between terrestrial and aquatic systems where the water table is usually at or near the surface or the land is covered by shallow water. Wetlands must also have one or more of the following attributes: (1) at least periodically, the land supports predominantly hydrophytes; (2) the substrate is predominately hydric soil; and (3) the substrate is non-soil and is saturated with water or covered by shallow water at some time during the growing season each year (Cowardin *et al*. 1979). The classification system developed for the NWI by Cowardin *et al*. (1979) is hierarchical, progressing from systems (Marine, Estuarine, Riverine, Lacustrine, and Palustrine) and subsystems (Tidal, Subtidal, Intertidal, etc.), at the most general levels, to classes, subclasses, and dominance types (Figure R12). While suitable for use with field data and aerial photography, this classification system proved too complex for satellite remote sensors, which lacked the spatial, spectral, and temporal resolution required by such detailed mapping efforts. More recently, satellite techniques are being tested for updating the NWI maps and publishing status and trend reports every 10 years. Most coastal states have used aerial photography to map their wetlands in great detail (e.g., scales of 1 : 2,400) in order to satisfy legal or planning requirements.

## Remote sensing

Satellite remote sensing of wetlands was attempted, with limited success, as soon as the first Landsat MSS was launched. SPOT with its 20/10 m resolution and Landsat Thematic Mapper (TM) with its six reflected bands and 30 m spatial resolution significantly improved our ability to map large coastal marshes. Using Landsat TM data, NOAA has initiated the Coastal Change Analysis Program (C-CAP) in order to develop a nationally standardized database on land-cover and habitat change in the coastal regions of the United States C-CAP inventories coastal submersed habitats, wetland habitats, and adjacent uplands and monitors changes in these habitats on a one-to five-year cycle with a minimum mapping unit of several hectares. This type of information and frequency of detection are required to improve scientific understanding of the linkages of coastal and submersed wetland habitats with adjacent uplands and with the distribution, abundance, and health of living marine resources. Using a rigorous protocol, satellite imagery, aerial photography, and field data are interpreted, classified, analyzed, and integrated with other digital data in a GIS. The resulting land-cover change databases are disseminated in digital form to users (Dobson *et al*., 1995).

C-CAP developed a classification system, shown in Table R3 to facilitate the use of satellite imagery (Klemas *et al*., 1993). Two study areas in South Carolina were used to evaluate a modified C-CAP classification scheme, image classification procedures, change detection algorithm alternatives, and the impact of tidal stage on coastal change detection. The modified C-CAP Classification Scheme worked well and can be adapted for other coastal regions (Jensen *et al*., 1993). Unsupervised "cluster-busting" techniques coupled with "threshold 3 majority filtering" yielded the most accurate individual date classification maps (86.7–92.3% overall accuracy; Kappa coefficients of 0.85–0.90). The best change detection accuracy was obtained when individual classification maps were majority filtered and subjected to "post-classification comparison" change detection (85.2% overall accuracy; Kappa coefficient of 0.82). The multiple date images selected for coastal change detection had to meet stringent tidal stage and seasonal guidelines (Jensen *et al*., 1993; Jensen, 1996).

Henderson *et al*. (1999) performed a detailed accuracy assessment of coastal land-cover mapping results obtained for Long Island using Landsat TM data and the C-CAP protocol. Table R4 displays two columns of user accuracies for C-CAP classification categories obtained by Henderson *et al*. (1999). The first column shows the user accuracies for the classification based on the raw spectral data, while the second column shows the accuracies after the data was recoded and filtered using ancillary verification data sets. Table R4 indicates that originally there were considerable errors in some categories, such as the Palustrine Wooded and Cultivated. However, as shown in Table R4, incorporation of ancillary data layers (e.g., aerial photographs, NWI wetland maps, etc.) increased the user accuracies of most categories into the upper 90% range, with the lowest, "Cultivated," attaining 86% (Henderson *et al*., 1999).

**Table R3** C-CAP coastal land-cover classification system[a]

| Upland | Wetland | Water and submerged land |
|---|---|---|
| Developed land | Marine/estuarine rocky shore | Water |
| Cultivated land | Marine/estuarine unconsolidated shore | Marine/estuarine reef |
| Grassland | Estuarine emergent wetland | Marine/estuarine aquatic bed |
| Woody land | Estuarine woody wetland | Riverine aquatic bed |
| Bare land | Riverine unconsolidated shore | Lacustrine aquatic bed (basin ≥20 acres) |
| Tundra | Lacustrine unconsolidated shore | Palustrine aquatic bed basin ≤20 acres) |
| Snow/ice | Palustrine unconsolidated shore | |
| | Palustrine emergent wetland | |
| | Palustrine woody wetland | |

[a] Only the upper two levels are shown in this table. The third, more detailed level has been omitted.

**Table R4** Comparison of user's accuracy by classification category for combined raw spectral images and composite (including ancillary data) imagery

| Category | Raw spectral (%) | Composite imagery (%) |
|---|---|---|
| Bare | 92.67 | 93.00 |
| Cultivated | 70.00 | 86.00 |
| Developed | 96.67 | 98.00 |
| Grassland | 84.47 | 95.00 |
| Water | 100.00 | 99.00 |
| Palustrine wooded | 46.67 | 97.00 |
| Palustrine emergent | 85.33 | 97.00 |
| Estuarine emergent | 81.13 | 100.00 |
| Wooded | 87.33 | 89.00 |

*Source*: From Henderson *et al*., 1999. Reproduced by permission of Taylor & Francis.

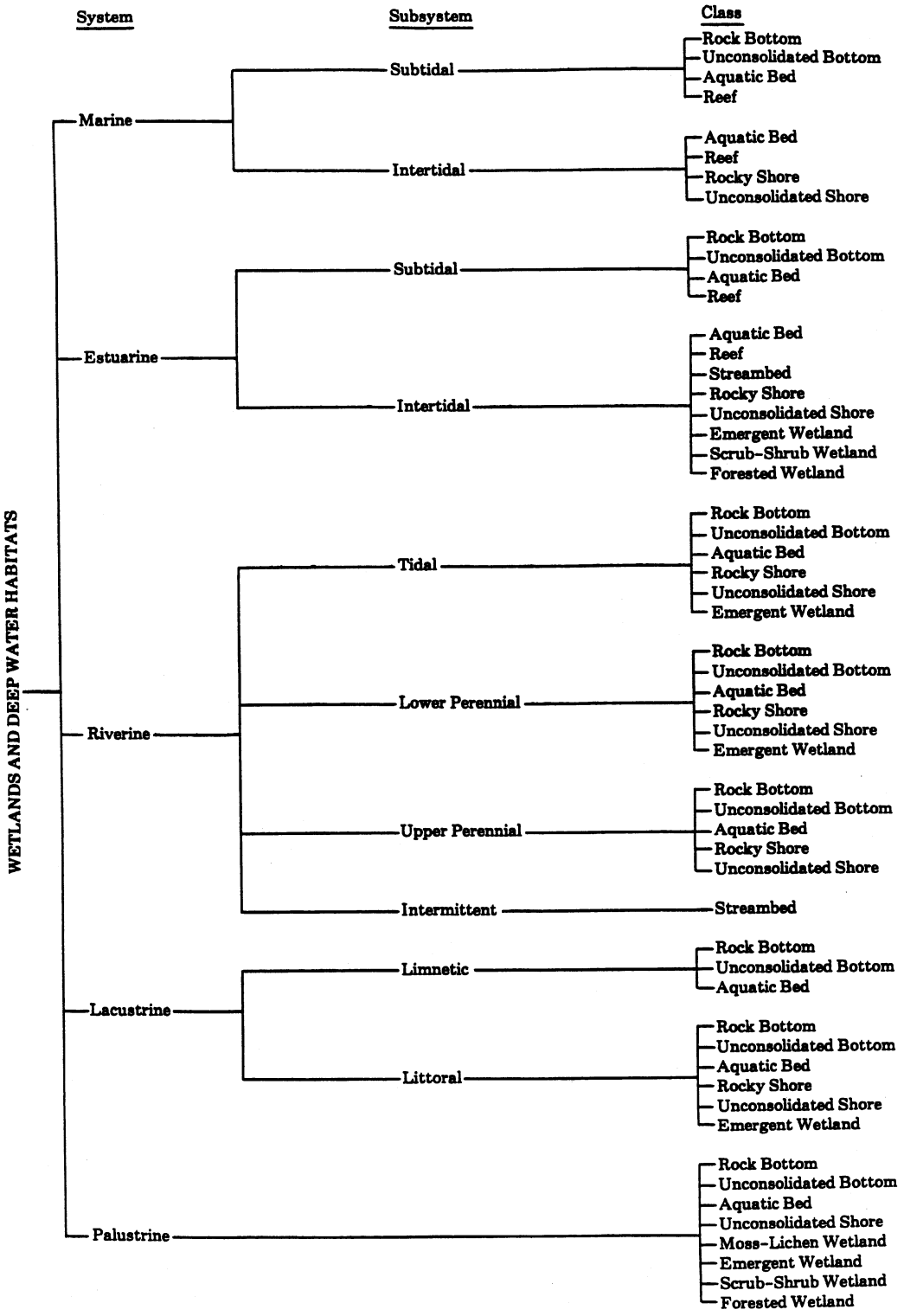


**Figure R12** Classification hierarchy of wetlands and deepwater habitats showing systems, subsystems, and classes. The Palustrine System does not include deepwater habitats (Cowardin *et al.*, 1979, Fish and Wildlife Service).

Another way to improve the accuracy of wetland classifications derived from satellite imagery is to use multiple-date (multiple season) imagery. Multi-temporal Landsat TM imagery was evaluated for the identification and monitoring of potential jurisdictional wetlands located in the states of Maryland and Delaware (Lunetta and Balogh, 1999). A wetland map prepared from single-date TM imagery was compared to a hybrid map developed using two dates of imagery. The basic approach was to identify land-cover vegetation types using spring leaf-on imagery, and identify the location and extent of the seasonally saturated soil conditions and areas exhibiting wetland hydrology using spring leaf-off imagery. The accuracy of the wetland maps produced from both single- and multiple-date TM imagery were assessed using reference data derived from aerial photographic interpretations and field observations. Subsequent to the merging of wetland forest and shrub categories, the overall accuracy of the wetland map produced from two dates of imagery was 88% compared to the 69% result from single-date imagery. A Kappa test $Z$ statistic of 5.8 indicated a significant increase in accuracy was achieved using multiple-date TM images. Wetland maps developed from multi-temporal Landsat TM imagery may potentially provide a valuable tool to supplement existing NWI maps for identifying the location and extent of wetlands in northern temperate regions.

## Summary and conclusions

Coastal wetlands are valuable natural assets and must be protected and managed more effectively. To accomplish this, timely information on wetlands distribution, abundance, and trends are required. This information can be provided efficiently by remote sensors on aircraft and satellites. Since many wetlands occur in narrow, elongated patches and have complex spectral signatures, satellite sensors on Landsat and SPOT can provide accurate wetland maps only if multi-temporal images are used or significant amounts of ancillary data employed. Fortunately, technology, cost, and need are converging in ways that are making remote sensing and GIS techniques practical and attractive for wetlands mapping and coastal resource management (Lyon and McCarthy, 1995). With the launch of Landsat 7, the cost of TM imagery has dropped by nearly a factor of 10, decreasing the cost of mapping large coastal areas. New satellites, carrying sensors with much finer spatial (1–5 m) and spectral (200 bands) resolutions are being launched and may more accurately map and detect changes in coastal habitat. Advances in the application of GIS are helping to incorporate ancillary data layers to further improve the accuracy of satellite classification of coastal wetlands and land-cover.

Victor Klemas

## Bibliography


Cowardin, L., Carter, V., Golet, F., and LaRoe, E., 1979. *Classification of Wetlands and Deepwater Habitats of the United States*. Washington, DC: U.S. Department of the Interior, Fish and Wildlife Service, Office of Biological Services.

Daiber, F., 1986. *Conservation of Tidal Marshes*. New York: Van Nostrand Reinhold Co.

Dobson, J., Bright, E., Ferguson, R., Field, D., Wood, L., Haddad, K., Iredale, H., III, Jensen, J., Klemas, V., Orth, R., and Thomas, J., 1995. NOAA coastal change analysis program (C-CAP): guidance for regional implementation. *NOAA Technical Report* NMFS 123. *A Technical Report of the Fishery Bulletin*, pp. 92.

Field, D., Reyer, A., Genovese, P., and Shearer, B., 1991. Coastal wetlands of the United States: an accounting of a valuable national resource. A Special NOAA 20th Anniversary Report. U.S. Department of Commerce, National Oceanic and Atmospheric Administration, and the National Ocean Service in cooperation with the U.S. Department of the Interior, Fish and Wildlife Service, pp. 59.

Henderson, F.M., Hart, T.F., Jr. Hearon, B.P., and Portolese, J.E., 1999. Mapping coastal ecosystems over a steep development gradient using C-CAP protocols. *International Journal of Remote Sensing*, **20** (4): 727–744.

Jensen, J., 1996. *Introductory Digital Image Processing: A Remote Sensing Perspective*, 2nd edn. Upper Saddle River: Prentice Hall.

Jensen, J., Cowen, D., Althausen, J., Narumalani, S., and Weatherbee, O., 1993. An evaluation of the coastwatch change detection protocol in South Carolina. *Photogrammetric Engineering and Remote Sensing*, **59**(6): 1039–1046.

Kiraly, S., Cross, F., and Buffington, J., 1990. Federal coastal wetland mapping programs. A Report by the National Ocean Pollutions Policy Board's Habitat Loss and Modification Working Group, Washington, DC: U.S. Department of the Interior, Fish and Wildlife Service, *Biological Report* **90**(18): pp. 174.

Klemas, V., Dobson, J., Ferguson, R., and Haddad, K., 1993. A coastal land cover classification system for the NOAA coastwatch change analysis project. *Journal of Coastal Research*, **9**(3): 862–872.

Lunetta, R., and Balogh, M., 1999. Application of multi-temporal Landsat 5 TM imagery for wetland identification. *Photogrammetric Engineering and Remote Sensing*, **65**(11): 1303–1310.

Lyon, J., and McCarthy, J., 1995. *Wetland and Environmental Applications of GIS*. Boca Raton: Lewis Publishers.

Tiner, R.W., Jr., 1985. *Wetlands of Delaware*. U.S. Fish and Wildlife Service, National Wetlands Inventory, Newton Corner, MA and Delaware Department of Natural Resources and Environmental Control, Wetlands Section, Dover, DE. Cooperative Publication.


## Cross-references


Estuaries
History, Coastal Ecology
Monitoring, Coastal Ecology
Photogrammetry
Remote Sensing of Coastal Environments
Vegetated Coasts
Wetlands


# RHYTHMIC PATTERNS

Beaches are seldom straight or smoothly curved in the longshore direction. Instead, they commonly include seaward projections of sediment, termed cusps, or embayments locally cut into the shore. Such features may be isolated, but more often occur in groups of alternating cusps and embayments that have a fairly regular spacing; they are then referred to as rhythmic patterns. There are several recognized types of rhythmic patterns, including beach cusps, sand waves, and giant cusps (Komar, 1998).

A wide range of spacings of rhythmic patterns can be found on beaches. Along the shores of ponds and small lakes the spacings between adjacent cusps may vary from less than 10 cm to 1 m. On ocean beaches with small waves, the spacing may be on the order of 2 m, while those built by large storm waves may be 50 m or more. Other rhythmic patterns, sand waves and giant cusps, have still larger spacings, typically ranging from 150 to 1,500 m, but with most being between 500 and 750 m, with the cusps projecting on average some 15–25 m seaward from the embayments.

## The classification of rhythmic patterns

In the past, the classification of different types of rhythmic patterns has been based on the lengths of their spacings. Beach cusps were considered to have the smallest spacings, less than 25 m, while sand waves and giant cusps have larger spacings. These latter terms can be considered to be nearly synonymous, different names for the same or very similar features. Research in recent years has led to a better understanding of the formation of the various types of rhythmic patterns, and this now makes it possible to develop a genetic classification that depends on the processes of waves and currents that are responsible for their formation, rather than depending simply on their spacings (Komar, 1998). Furthermore, it is clear that rhythmic patterns having a wide range of spacings can be generated by a single mechanism, and more than one mechanism may be capable of producing rhythmic patterns having the same spacing. It is clear therefore that a genetic classification is needed, one that reflects the processes of formation. Such a genetic classification is depicted in Figure R13 (Komar, 1983), one that distinguishes between beach cusps, systems of rip-current embayments and cusps, series of transverse bars that produce cusps along the shore, and crescentic bars that are chiefly an underwater feature but can produce a rhythmic pattern that extends onto the dry part of the beach. In general, this order represents an increase in cusp spacings, with the latter three mechanisms yielding what had formerly been referred to as sand waves or giant cusps.

### Beach cusps as a type of rhythmic pattern

The most easily recognized rhythmic pattern seen on beaches are the cuspate deposits of sand and gravel built by waves and known as beach cusps. Because of their marked regularity with nearly uniform spacings, beach cusps have attracted many observers and much speculation as to

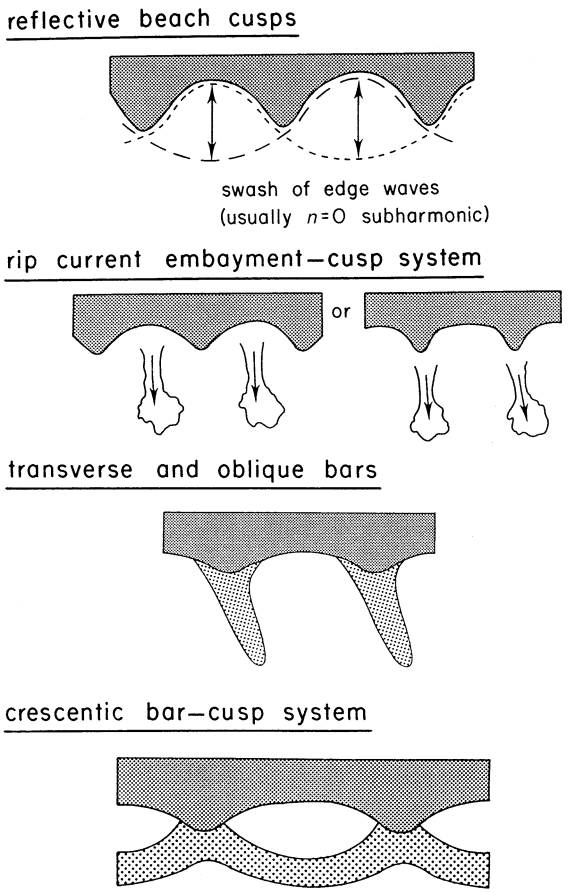


**Figure R13** A genetic classification of rhythmic patterns where the origin of the series of cusps and embayments can be attributed to different processes of waves and currents (after Komar, 1983).

their origin. Arguments still persist with regard to the processes of wave motions and sediment transport that control their formation and determine the lengths of their spacings.

Beach-cusp formation is most favorable when the waves approach normal to the beach, that is, with their crests parallel to the longshore trend of the beach. This may explain why pocket beaches are particularly favorable sites for beach cusp formation. Furthermore, regular waves having long crest lengths are particularly conducive to cusp formation; beach cusps generally are not formed by irregular, confused seas.

Various investigators have described contrasting patterns of water circulation induced by the swash of waves around the cusps and within their embayments. In some cases there is an alternating surge inward and out of the embayments. Water flows from one embayment where the wave-swash runup has been a maximum, around the nearest cusp, and into a neighboring bay where it rushes up the beach face with the next wave. Thus, the maximum runup alternates in its timing between adjacent embayments. In other cases, the arriving waves break evenly along the beach, but the wave surge then piles up against the steep cusps and is divided into divergent streams that flow into the adjoining embayments. These streams head off the wave surge that had flowed directly up into the embayment. The two side streams from the cusps on either side meet at the center of the bay, and together form a seaward flow of considerable strength. This return flow can resemble a rip current, but unlike true rip currents, the flow is discontinuous and the mechanisms of formation are quite different. These contrasting patterns of water circulation observed around beach cusps suggests that more than one mechanism may give rise to their formation.

A number of hypotheses have been proposed to account for the formation of beach cusps. For a theory to be acceptable, it must account for the uniformity of spacing within an observed series of cusps, and the way in which this spacing is related to the wave parameters. The hypothesis that has been most successful in explaining the formation of beach cusps and accounting for their spacings is one based on the presence of edge waves in the surf zone (Guza and Inman, 1975). An edge wave is a type of wave that is trapped in the surf by refraction across the slope of the beach, moving in the longshore direction as it alternately refracts while moving offshore, then bends entirely around to return to the shore, reflects from the beach, and repeats the pattern of movement. The important result is that the presence of the edge wave affects the intensity and distance of swash runup on the beach, producing a regular runup spacing along the length of shore. This hypothesis explains the formation of beach cusps as the rearrangement of the sediment into a regular pattern of alternating cusps and embayments, corresponding to the longshore wave length of the edge waves and spacing of their maximum runup on the beach. The validity of this hypothesis has been demonstrated in the controlled conditions of laboratory wave basins, and by a few studies on ocean beaches that happened to be measuring edge waves at the same time beach cusps formed (see review in Komar, 1998). In that the longshore length of edge waves is determined by the wave period and slope of the beach, this hypothesis yields a mathematical equation that predicts the beach-cusp spacing (Guza and Inman, 1975). Measured beach-cusp spacings ranging from 0.1 to nearly 100 m have been shown to agree with this mathematical relationship (Komar, 1998). Thus, there is strong supporting evidence for the edge wave hypothesis of beach cusp formation.

There is, however, an alternative hypothesis that has been proposed to account for the formation of beach cusps, the so-called "self organization" hypothesis of Werner and Fink (1993). It envisions an initially smooth, straight beach, lacking cusps, but with waves arriving and swashing up the beach face with some degree of irregularity. According to the hypothesis, this irregularity in the wave swash produces variable amounts of beach sand movement along the shore, with a tendency for the sand to preferentially accumulate in a few isolated areas. The critical aspect of this hypothesis is that the zones of accumulated sand then affect the subsequent patterns of wave runup, thereby increasing the sizes of the accumulated sand and causing them to evolve into a pattern of beach cusps having regular spacings. It is this trend toward increasing regularity to which the name "self organization" refers. The main supporting evidence for this hypothesis comes in the form of computer simulation models that demonstrate the possibility of such an evolution. While not actually having mathematical relationships that predict the eventual beach cusp spacing, the computer models demonstrate that the spacing depends on the wave period and height, and on the beach slope, and in fact the model yields cusp spacings that are similar to those predicted by the edge-wave hypothesis. This similarity in prediction has made it difficult to distinguish which mechanism is responsible for the formation of beach cusps on ocean shores. It is possible that both hypotheses can, in different situations, account for the formation of beach cusps, and in some cases may actually work together.

As noted above, the early definition of "beach cusps" restricted them to spacings of 25 m or less, but provided no explanation for their formation. Although we are still uncertain as to the specific generation mechanism, the proposed hypotheses appear to offer satisfactory explanations, so the term "beach cusps" is now used in genetic classifications like that in Figure R13. For the most part the old and new uses of the term refer to the same rhythmic pattern, but we now recognize that edge waves and perhaps self-organization can generate beach cusps that have spacings up to 100 m.

## Rip current embayments and cuspate shores

Within the series of rhythmic patterns diagrammed in Figure R13, generally the next larger form beyond beach cusps is the system of erosional embayments and intervening cusps formed by nearshore current systems that include seaward-flowing rip currents. In most instances the rip currents erode sand from the beach and transport it offshore, forming embayments at the rip-current positions, with cusps midway between. In rarer instances, particularly on steep beaches, coarse sand and gravel may accumulate at the shoreward ends of the rips, developing cusps at those positions. Rip currents, and hence the embayments and cusps, typically have spacings that range from tens to hundreds of meters. As such, the resulting rhythmic pattern corresponds to what has been referred to variously as sand waves or giant cusps.

The effect of the nearshore currents on the shore, forming series of embayments and cusps, is the surface expression of the underwater topography that is molded by the currents acting together with the waves. The seaward-flowing rip currents tend to erode channels across the full width of the beach within the embayments, segmenting the offshore bar. This leaves a system of cusps midway between rip currents, but each cusp seen on the shore is part of a shoal that extends out to the remaining segment of offshore bar.

This form of rhythmic pattern with embayments cut by rip currents is often important to property erosion in that the embayments narrow the beach width and remove most of the buffer protection offered to properties backing the beach. Although the rip embayments themselves do not usually produce much erosion of dunes and sea cliffs, they provide an area of deeper water where storm waves can approach close to shore before breaking against the coastal properties.

## Rhythmic patterns produced by welded and transverse bars

A variety of sand bars have been observed in the nearshore that run obliquely to the longshore trend of the beach. These have been termed "welded" or "transverse" bars (Figure R13). An example is shown in Figure R14 on the ocean shore of Cape Cod, Massachusetts, consisting of a series of bars and a cuspate shore that has a distinctive longshore rhythmicity of several hundred meters. Therefore, the presence of welded or transverse bars can also give rise to a rhythmic pattern.

A number of suggestions have been made for the origin of bars that trend obliquely to the shore, and for the corresponding rhythmic pattern. It has been observed that when waves break at pronounced angles to the beach, the offshore bars that were originally parallel to the shore and segmented by evenly spaced rip currents, rotate to align themselves with the incoming wave crests. This may be the origin of the welded bars and rhythmic pattern seen in Figure R14.

Another type of oblique bar is found on coasts of low wave energy, for example in lakes or along the shore of the Gulf of Mexico. Referred to as transverse bars, they tend to occur in families that run parallel to one another, directed toward the offshore. At each point where a transverse bar joins the shore, a large cusp develops on the dry beach. Transverse bars can be fairly permanent features—examples on the shores of the Gulf of Mexico have been observed to persist in aerial photographs that span 25 years, showing little or no tendency to migrate alongshore during that time. Investigations have demonstrated that this type of transverse bar affects the paths of nearshore currents, with the current being concentrated over the bar and flowing offshore along its length, thereby perpetuating the bar's existence and extending it's length.

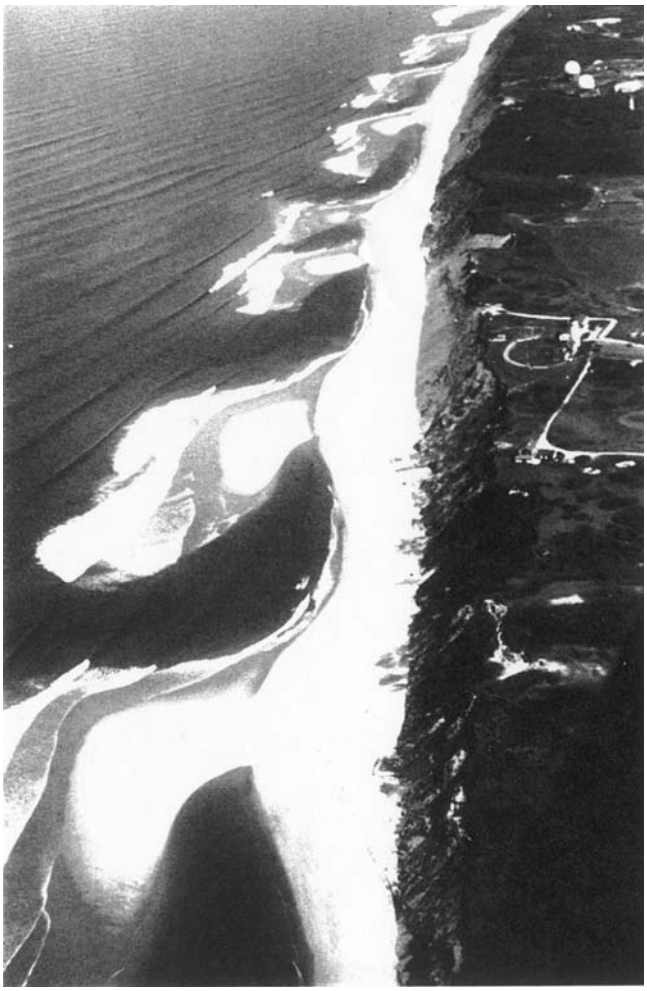

**Figure R14** A series of welded bars and associated rhythmic pattern on Cape Cod, Massachusetts (photo courtesy of David S. Aubrey, Woods Hole Oceanographic Institution).

## Crescentic bars and large-scale rhythmic patterns

Crescentic bars are one form of submerged offshore bars where rather than being linear, they have a regular lunate or crescentic shape (Figure R13), together with a uniform repetition along the length of beach. This regularity generally cannot be appreciated by observers on the dry beach, since most of the feature is underwater. However, there may be an associated series of cusps on the beach if the landward ends of the crescentic bars attach to the shore. In this instance, the presence of offshore crescentic bars leads to the development of another form of rhythmic pattern.

Crescentic bars are much larger features than beach cusps, and generally are somewhat larger than the rhythmic patterns due to rip currents or welded bars. In some instances, large crescentic bars form the outer-bar system of a beach, while the inner bar is linear and segmented by the more closely spaced rip currents. The range in lengths of crescentic bars is difficult to establish, since for many reported occurrences it is not possible to determine conclusively whether crescentic bars or some other form of rhythmic pattern is being described. Crescentic bars appear to range up to 2,000 m in length (Komar, 1998). At times there can be multiple crescentic bars on a beach, the further offshore the bars the larger their spacings. The corresponding rhythmic pattern on the beach would similarly have very large spacings between successive cusps.

Like beach cusps, the regularity in shapes and the even spacings of crescentic bars have inspired a number of suggestions as to their formation. The mechanism proposed by Bowen and Inman (1971), again by the movement of edge waves, provides the most reasonable explanation. In this case, however, important is the velocity of water movements associated with the edge waves, not their swash runup on the sloping beach which may be responsible for beach cusps. According to this mode of formation, beach sediment in the outer surf zone drifts about under the currents of the edge waves, until the sand reaches zones where the water velocity is low and the sand can accumulate. According to computer models of edge wave motions, this rearrangement of the sand would yield lunate-shaped bars that are remarkably similar to those observed on ocean beaches, a result that argues in favor of this hypothesis. Bowen and Inman (1971) conducted a series of laboratory wave-basin experiments that further confirmed this predicted sand accretion pattern, leading to the formation of crescentic bars. At this time, there is no reasonable alternative hypothesis for crescent-bar formation that satisfactorily accounts for their regularity in shapes and spacings, and for the formation of the associated rhythmic pattern.

## Rhythmic patterns, irregular shores, and coastal erosion

Depending on the mechanism, rhythmic patterns may consist of alternating cusps and embayments whose spacings range from a few meters (beach cusps), to on the order of 100 m (rip-current embayments or welded bars), and on up to 500–1,500 m (crescentic bars). If one includes series of cuspate forelands or capes like those that exist along the southeast coast of the United States, the series can be extended up to tens of kilometers. When only one type of rhythmic pattern is present on the beach, it gives rise to a fairly regular spacing of alternating cusps and embayments. However, it is common for more than one type of pattern to occur simultaneously on a beach, and the summation of what are otherwise regularly spaced patterns can lead to an irregular beach and shore. An example is shown in Figure R15, the Cape Hatteras coast of North Carolina, photographed in 1970 before the lighthouse was moved (Dolan, 1971). Apparent are the series of large cusps and embayments, with a fair degree of regularity along the length of coast covered by the photograph. However, there is a level of irregularity, with some embayments being larger than others. Although the cause in this example is uncertain, it is probable that the irregularity of the rhythmicity is produced by the summation of two rhythmic patterns, that due to a rip-current cusps/embayment system, together with a larger-scale variation due to offshore crescentic bars. Of interest in this example, the respective embayments produced by rip currents and the crescentic bars appear to have combined in the area of the Cape

**Figure R15** A rhythmic pattern of alternating cusps and embayments on the Cape Hatteras coast of North Carolina, photographed in 1970, with the largest embayment producing beach erosion and threatening the lighthouse (from Dolan, 1971).

Hatteras Lighthouse, resulting in the total loss of the beach and erosion of the dunes to the extent that the lighthouse was in danger. Therefore, an understanding of the origin and types of rhythmic patterns can be important to interpretations of the causes of coastal erosion problems.

Paul D. Komar

## Bibliography


Bowen, A.J., and Inman, D.L., 1971. Edge waves and crescentic bars. *Journal of Geophysical Research*, **76**: 8662–8671.

Dolan, R., 1971. Coastal landforms: crescentic and rhythmic. *Geological Society of America Bulletin*, **82**: 177–180.

Guza, R.T., and Inman, D.L., 1975. Edge waves and beach cusps. *Journal of Geophysical Research*, **80**: 2997–3012.

Komar, P.D., 1983. Rhythmic shoreline features and their origins, In R. Gardner and H. Scoging (eds.), *Mega-Geomorphology*, pp. 92–112, Claredon Press, Oxford.

Komar, P.D., 1998. *Beach Processes and Sedimentation*, 2nd edn. Prentice-Hall.

Werner, B.T., and Fink, T.M. 1993. Beach cusps as self-organized patterns. *Science*, **260**, 968–971.


## Cross-references


Accretion and Erosion Waves on Beaches
Bars
Beach Features
Beach Processes
Cuspate Forelands
Rip Currents
Surf Zone Processes


# RIA

A ria is a long, narrow, often branching inlet formed by marine submergence of the lower parts of a river valley that had previously been incised below present sea level. Rias are the drowned mouths of unglaciated valleys, usually bordered by steep slopes rising to mountains, hills, or plateaux (Figure R16). The term is of Spanish origin, derived from large inlets on the coasts of Galicia such as the Ria de Arosa and the Ria de Muros y Noya, fingering far inland. They are known as abers in Brittany and Wales.

Von Richthofen (1886) defined a ria as a drowned valley cut transverse to the geological strike, but the Rias of Galicia do not meet this strict definition (Cotton, 1956). Perusal of coastal textbooks indicates that the term has come to be used as a synonym for a drowned valley mouth without any structural constraint. Rias generally have a dendritic (tree-like) outline, remaining open to the sea, as in Carrick Roads (Figure R17) in southwest England, Chesapeake Bay in the United States and Port Jackson (Sydney Harbor) in Australia. The long, straight valley-mouth gulfs on the southwest coast of Ireland, such as Bantry Bay, are examples of rias, even though they follow a geological strike that runs transverse to the general coastline. Where rivers have cut valleys across geological structures there may be tributaries that follow the geological strike, submerged to form a trellised pattern, as in Cork Harbor in southern Ireland. On the Dalmatian coast of the Adriatic Sea rias are elongated straits along valleys that follow the geological strike, linked to the sea by transverse channels.

Existing rias were formed by marine submergence during the Late Quaternary (Flandrian) marine transgression, but in southwest England there is evidence of several phases of valley incision during Pleistocene low sea-level phases, alternating with earlier ria formation

**Figure R16** The ria at Aber Benoît, Brittany (photo: E.C.F. Bird: Copyright, Geostudies).

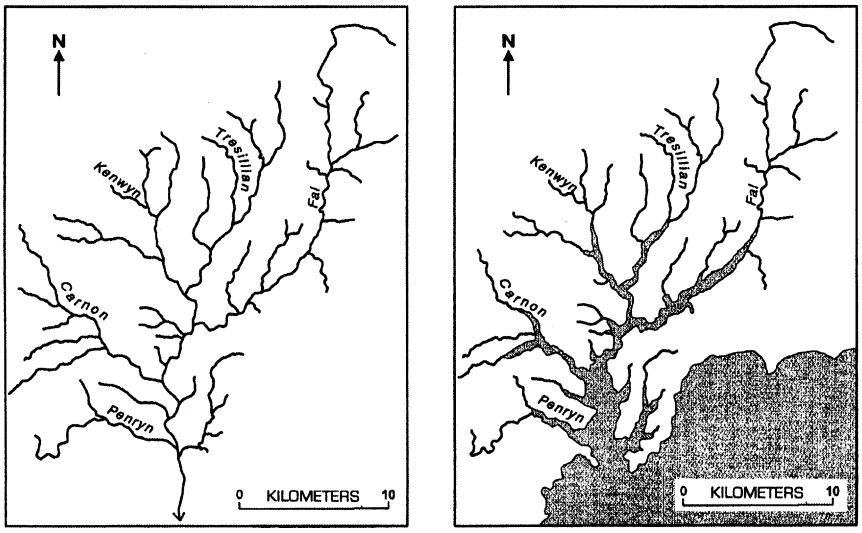


**Figure R17** The Carrick Roads ria on the south coast of Cornwall, England. (Left) the river systems as they were 20,000 years ago, during the Late Pleistocene low sealevel phase. (Right) the present outlines, after partial submergence by the Late Quaternary marine transgression. (©Geostudies).

during interglacial marine transgressions and at least one Late Pleistocene higher sea-level phase indicated by an emerged beach (Kidson, 1977).

The Galician rias are generally wide and deep (up to 30 m) marine inlets in valleys which may have been shaped partly by tectonic subsidence and the recession of bordering scarps. Subsidence has probably contributed to the persistence of the ria at the mouth of Johore River in southeastern Malaysia, which remains a wide and deep inlet, whereas other Malaysian valley mouths have been infilled as alluvial plains, some with protruding deltas. Other rias persist because they were initially deep and sedimentary filling has been slow, as on the New South Wales coast (Roy, 1984).

Rias show varying degrees of sedimentary filling, partly from inflowing rivers and partly inwashed from the sea. There are marshy deltas at the heads of the several branches of Carrick Roads in Cornwall, while other rias in southwest England have banks of inwashed marine sand, particularly on the Atlantic coast, as in the Padstow ria, where at low tide the Camel River is narrow, flowing between broad exposed sandbanks that are submerged when the tide rises. Muddy sediment has been derived from periglacial deposits on bordering slopes.

Slopes bordering rias generally show only limited cliffing on sectors exposed to strong wave action, yielding sand and gravel to local beaches. Typically' there are sandy, gravelly, and rocky embayed shores, some spits, muddy sediment and salt marshes at their heads, and sandy shoals at their entrances (Castaing and Guilcher, 1995). The Rade de Brest is noteworthy for its several bordering sand and gravel spits (Guilcher *et al*., 1957). Finer sediment is deposited in fringing tidal marshes and mudflats, and on the adjacent sea floor.

There is no clear distinction between a ria and an estuary, most rias being estuarine in the sense that inflowing rivers provide freshwater that meets and mixes with seawater moved in and out by the tide. Rias on high limestone coasts in the Mediterranean are known as calas or calanques, while those on arid coasts are termed sharms or sherms. In Chile' there is a transition southward from rias to fiords with increasing influence of glaciation on valleys.

Eric Bird

## Bibliography

Castaing, P., and Guilcher, A., 1995. Geomorphology and sedimentology of rias. In Perillo G.M.E. (ed.), *Geomorphology and Sedimentology of Estuaries*. Amsterdam, Elsevier: pp. 69–111.

Cotton, C.A., 1956. Rias sensu stricto and sensu lato. *Geographical Journal*, **122**: 360–364.

Guilcher, A., Vallantin, P., Angrand, J.P., and Galloy, P., 1957, Les cordons littoraux de la rade de Brest. *Bulletin Comité Océanographique et Etude des Côtes*, **9**: 21–54.

Kidson, C., 1977. The coast of south-west England. In Kidson, C., and Tooley, M.J., (eds.), *The Quaternary History of the Irish Sea*. Liverpool: Seal House, pp. 257–298.

Roy, P.S., 1984. New South Wales estuaries: their origin and evolution. In: Thom, B.G., (ed.), *Coastal Geomorphology in Australia*. Sydney: Academic Press, pp. 99–121.

Von Richthofen, F., 1886. *Führer für Forschungsreisende*. Hanover: Janecke.

## Cross-references

Dalmatian Coasts
Estuaries
Karst Coasts
Salt Marsh
Sharm Coasts

# RIP CURRENTS

## Definition, types, and early studies

Many of the world's beaches are characterized by the presence of strong, concentrated seaward flows called *rip currents*. Rips are an integral component of nearshore cell circulation and ideally consist of two converging longshore *feeder* currents which meet and turn seawards into a narrow, fast-flowing *rip-neck* that extends through the surf zone, decelerating and expanding into a *rip-head* past the line of breakers. The circulation cell is completed by net onshore flow due to *mass transport* between adjacent rip systems. Rip flows are often, but not always, contained within distinct topographic channels (Figure R18) and can be visually identified by darker streaks through the surf zone due to greater water depths, offshore moving foam/sediment patches, and surface turbulence created by the wave–current interactions. Rips are of great significance to coastal nearshore studies since they provide a major mechanism for the seaward transport of water and sediments, have a pronounced effect on nearshore morphology, aid in the dispersal of pollutants, and represent a major hazard to recreational beach users. It is therefore of some concern that many aspects of rip behavior, generation, and occurrence remain poorly understood. In fact, the term was first used by Shepard (1936) in order to distinguish rip currents from the misnomers *rip tide* and *undertow*, which are unfortunately still commonly used to describe rips today.

Rips are generally absent on pure dissipative and reflective beaches, but are a key component of sandy intermediate beach states as described by various microtidal beach models (e.g., Wright and Short,

**Figure R18** Enhanced time-exposure image of topographically arrested accretion rips at Palm Beach, NSW, Australia. Rip channels appear as dark areas between bars (white regions) and are approximately 150–200 m apart. Note the absence of pronounced longshore feeder channels (image courtesy of G. Symonds, R. Holman, and R. Ranasinghe).

1984) and also occur, but are not as predominant, on macrotidal beaches. Short (1985) identified three types of rip currents: (1) *accretion rips* occur during decreasing or stable wave-energy conditions and are often topographically arrested in position (Figure R18) having mean velocities typically on the order of 0.5 m/s, but exceeding 1 m/s in high-energy surf zones (Brander and Short, 2000); (2) hydrodynamically controlled *erosion rips*, which occur under rising wave-energy conditions and are transient in location, having mean flows in excess of 1 m/s; and (3) *mega-rips*, which occur in embayments under high waves (>3 m) and can extend offshore for distances of more than 1 km, attaining velocities greater than 2 m/s. All are associated with localized erosion of the shoreline and often create rhythmic *rip embayments* termed *mega-cusps*. Relatively, permanent rips located adjacent to headlands, reefs, and coastal structures such as groins have been referred to as *topographically controlled rips*.

The primary limitation to our understanding of rips has been the logistical difficulty in obtaining quantitative field measurements. The first serious scientific attempts at describing rips (Shepard *et al*., 1941; McKenzie, 1958) were largely qualitative and suggested that rips: (1) exist as a response to an excess of water built up on shore by breaking waves; (2) often display a periodic longshore spacing; (3) increase in intensity and decrease in number as wave height increases; (4) vary in location and intensity over time; and (5) flow fastest at low tide. Subsequent theoretical, laboratory, and field studies have attempted to explain these characteristics with varying degrees of success.

## Rip generation and spacing

It is generally accepted that the primary mechanism behind the formation of rip currents is the presence of longshore variations in wave height which act to produce *wave set-up* gradients that drive water alongshore from regions of high water level to regions of lower water level. Bowen (1969) showed that these gradients are intrinsically related to variations in the longshore component of *radiation stress* (Longuet-Higgins and Stewart, 1964)

$$S_{yy} = \frac{E}{2} = \frac{1}{16}\rho g H^2,$$

where $E$ is the energy, $\rho$ is the water density, $g$ is the gravitational constant, and $H$ the wave height. Bowen (1969) demonstrated that within the surf zone, the longshore gradients in set-up and radiation stress act in the same direction to produce longshore feeder currents, whereas outside the surf zone, the $S_{yy}$ gradient is balanced by a longshore variation in wave set-down and no longshore flow is produced.

Existing models for the generation of rip cell circulation have thus incorporated various mechanisms to account for the existence of longshore gradients in wave height/set-up and can be grouped into three main categories. The wave–boundary interaction model involves the modification of the wave field by non-uniform topography and/or coastal structures. The resulting convergence and divergence of wave rays due to wave refraction can produce regions of high and low waves such that rips can occur in the lee of offshore submarine canyons (Shepard and Inman, 1950), but more commonly adjacent to headlands and groins.

Wave–wave interaction models have been used to explain both longshore variations in wave height and regular longshore rip spacing. Bowen (1969) and Bowen and Inman (1969) showed both theoretically and in the laboratory that incident waves can generate synchronous edge waves which produce alternating patterns of high and low wave heights along the shore. Rips are produced at every other antinode with a rip spacing ($L_r$) equal to the edge wavelength given by

$$L_r = L_o \sin(2n + 1)\beta,$$

where $L_o$ is the deep-water incident wave length, $n$ is the edge wave mode, and $\beta$ the beach slope. Dalrymple (1975) provided a model for long, straight beaches showing that the intersection of synchronous wave trains from different incident angles can also produce longshore set-up gradients and a regular rip spacing. The third type of mechanism, an instability model, was proposed by Hino (1974) who suggested that a longshore uniformity in set-up on plane beaches is unstable to any small disturbance caused by hydrodynamic or topographic factors and that predicted rip spacing was equal to four times the surf zone width. Subsequent studies based on direct field observations have shown that this ratio can range from 1.5 to 8.

It should be emphasized that validation of the above models has primarily been restricted to laboratory experiments. Using a long-term field dataset of rip spacing obtained by remote video images, Ranasinghe *et al*. (1999) showed that the models of Bowen (1969) and Dalrymple (1975) under-predicted observed rip spacing and that there was no evidence to support instability mechanisms as being responsible for rip spacing. Furthermore, the common acceptance of the edge wave model as an explanation for rip generation and spacing should be treated with caution since synchronous edge waves have not been measured in the field and the required interaction between edge waves and incident waves of the same period is believed to be restricted to steep, reflective beaches, an environment where rips are usually absent.

Based on field observations from Narrabeen Beach, NSW, Australia, Huntley and Short (1992) found that rip spacing increases with increasing wave height and surf zone width and with decreasing sediment size and beach gradient. Short and Brander (1999) used a global dataset to show that rip spacing is related to regional wave environments. Patterns of rip spacing were consistent within west coast swell ($L_r \cong 500$ m), east coast swell ($L_r \cong 200$ m), and Fetch-limited environments ($L_r \cong 50$–$100$ m). Distinct scaling factors between the environments also applied to planimetric dimensions of the rip systems and were directly correlated to wave energy. Prediction of rip spacing and location remains problematic however, and it should perhaps be acknowledged that rip spacing is often irregular.

## Topographic control and flow characteristics

The theoretical models for rip generation described previously are based on longshore variations in wave height, but on a beach consisting of alternating bars and offshore channels, Sonu (1972) found that under conditions of uniform longshore wave height, constant and extensive wave-energy dissipation across the bars, and local and intense wave breaking over the channels created a set-up gradient toward the channels. Set-up gradients generated in this manner support field data confirmation (Aagaard *et al*., 1997; Brander, 1999) that rip flows are tidally modulated (Figure R19), since stronger flows at low tide would be expected with increased wave dissipation associated with shallower water depths over the bars.

Aagaard *et al*. (1997) used field measurements to show that rip velocity ($u_r$) can be predicted by

$$u_r = \frac{QL_r}{A_r},$$

where $Q$ is onshore mass transport and $A_r$ is the cross-sectional area of the rip channel. Based on computations for $Q$, rip velocity will increase with $H^2$ and decrease with longer wave periods, and will also increase with greater distances between rips and smaller channel areas. The latter is supported by field data by Brander (1999) who found a strong relationship between increasing rip velocity and decreasing channel area. However, the degree to which rip circulation is either controlled by antecedent topography or creates this topographic feedback effect through sediment transport processes remains unclear and it should be remembered that rips do occur on beaches without irregular topography.

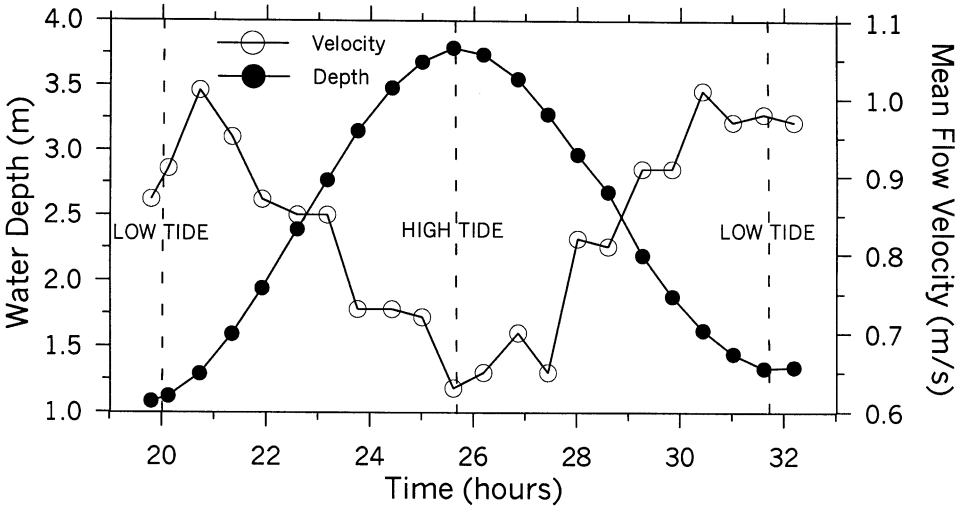


**Figure R19** Tidal modulation of rip velocity at Muriwai Beach, New Zealand showing maximum and minimum flow strengths around low and high tide, respectively. Data points represent 34-min time averages recorded 0.9 m above the bed.

Field studies have also shown that rip velocities increase steadily from the feeders to the middle of the rip-neck, with strongest flows toward the middle of the water column, decreasing away from the bed and toward the surface (Sonu, 1972). Rip flows also experience low-frequency velocity pulses on the order of several minutes, but the forcing of this behavior in response to *infragravity waves, wave groups,* or *shear waves* has yet to be determined.

Robert W. Brander

## Bibliography


Aagaard, T., Greenwood, B., and Nielsen, J., 1997. Mean currents and sediment transport in a rip channel. *Marine Geology*, **140**: 25–45.

Bowen, A.J., 1969. Rip currents. 1. Theoretical investigations. *Journal of Geophysical Research*, **74**: 5467–5478.

Bowen, A.J., and Inman, D.L., 1969. Rip currents. 2. Laboratory and field observations. *Journal of Geophysical Research*, **74**: 5479–5490.

Brander, R.W., 1999. Field observations on the morphodynamic evolution of a low-energy rip current system. *Marine Geology*, **157**: 199–217.

Brander, R.W., and Short, A.D., 2000. Morphodynamics of a large-scale rip current system at Muriwai Beach, New Zealand. *Marine Geology*, **165**: 27–39.

Dalrymple, R.A., 1975. A mechanism for rip current generation on an open coast. *Journal of Geophysical Research*, **80**: 3485–3487.

Hino, M., 1974. Theory on formation of rip current and cuspidal coast. In *Proceedings of the 14th International Conference on Coastal Engineering*. American Society of Civil Engineers, pp. 901–919.

Huntley, D.A., and Short, A.D., 1992. On the spacing between observed rip currents. *Coastal Engineering*, **17**: 211–225.

Longuet-Higgins, M.S., and Stewart, R.W., 1964. Radiation stresses in water waves—a physical discussion with applications. *Deep-Sea Research*, **11**: 529–562.

McKenzie, P., 1958. Rip-current systems. *Journal of Geology*, **66**: 103–111.

Ranasinghe, R., Symonds, G., and Holman, R., 1999. Quantitative characterisation of rip dynamics via video imaging. In *Proceedings of Coastal Sediments '99*. American Society of Civil Engineers, pp. 987–1002.

Shepard, F.P., 1936. Undertow, rip tide, or rip current. *Science*, **84**: 181–182.

Shepard, F.P., and Inman, D.L., 1950. Nearshore water circulation related to bottom topography and wave refraction. *Transactions of the American Geophysical Union*, **31**: 196–212.

Shepard, F.P., Emery, K.O., and LaFond, E.C., 1941. Rip currents: a process of geological importance. *Journal of Geology*, **49**: 337–369.

Short, A.D., 1985. Rip current type, spacing and persistence, Narrabeen Beach, Australia. *Marine Geology*, **65**: 47–61.

Short, A.D., and Brander, R.W., 1999. Regional variations in rip density. *Journal of Coastal Research*, **15**(3): 813–822.

Sonu, C.J., 1972. Field observation of nearshore circulation and meandering currents. *Journal of Geophysical Research*, **77**: 3232–3247.

Wright, L.D., and Short, A.D., 1984. Morphodynamic variability of beaches and surf zones, a synthesis. *Marine Geology*, **56**: 92–118.


## Cross-references

Bars
Coastal Processes (see Beach Processes)
Coastal Currents
Lifesaving and Beach Safety
Sandy Coasts
Surf Zone Processes
Wave–Current Interaction
Wave-Dominated Coasts
Wave Environments

# RIPPLE MARKS

## General definition and description

Allen (1978) defined ripple marks as "… regular, ridge-like structures, transverse to current, which arise and are maintained at the interface between a moving, viscous fluid (water, air) and a moveable, non-cohesive sediment (usually sand) by interaction between fluid and transported sediment." Ripple marks fall principally into two classes: aeolian ripples and water-formed ripples. Fundamental work on aeolian ripples was undertaken by Bagnold (1941) as an army officer in the Lybian desert; he considered *ripples* to be constant in size with time once formed, whereas larger types grew with time, almost without limit. Aeolian ripples are influenced by saltation bombardment of sand creating ballistic ripples which lack internal structure, and have wavelengths related to saltation length. Water-formed ripples are created by lee eddy avalanches in the direction of sediment transport, possess well-defined internal structure, and have wavelengths controlled by grain size. Thus, despite outward similarities in form, there is little overlap in the mechanisms of genesis between subaqueous and aeolian forms.

## Essential concepts and applications

Definitions based solely on morphology do not discriminate between what we "understand" to be ripple marks (small-scale bedforms) and genetically similar bedforms such as dunes, giant ripples, sand waves, or megaripples (large-scale bedforms). There appears to be a continuum in bedform morphology and sizes in both aeolian and subaqueous ripples, from the smallest forms found in silt to "giant" forms kilometers in length (Wilson, 1972; Ellwood *et al.*, 1975; Amos and King, 1984;

Ashley, 1990). So what are ripple marks, and how do they form? Darwin (1883) linked subaqueous ripples to vortices in the near-bed flow and subsequent sand transport. Exner (1925, from Allen, 1982) showed that they initiated from bottom irregularities, and were self-maintaining and self-organizing due to perturbations in the horizontal pressure gradient and sediment transport rate. They are considered to be the physical manifestations of bedload transport and the grain-to-grain interaction of the material in transport (Bagnold, 1963; Harms *et al*., 1982; Middleton and Southard, 1984) and, as such, demonstrate the emergence of order out of the chaotic movement of individual sand grains within a viscous sub-layer at the bed. This order, according to Leopold *et al*. (1964), results from the creation of a *kinetic wave* in sediment flux not unlike traffic movement on a congested highway. Early classifications were based on the shape and size of bedforms (height, wavelength, asymmetry, planform, cord coherence) which resulted in the discrimination of: small-scale ripples, large-scale ripples (superimposed by smaller forms; Allen, 1968), short-crested ripples, intermediate-crested ripples, and long-crested ripples (Inman, 1957). Each ripple type was further classified on the basis of sinuosity, bifurcation, and continuity of the crestline into: straight, sinuous, linguoid, caternary, or lunate types (Allen, 1968). Classifications of ripples based purely on metrics do not consider genesis, and hence were considered deficient in two fundamental ways: (1) they could not be predicted, and (2) they could not be used to hindcast the conditions that formed them. Fundamental observations by H.C. Sorbey, and later Gilbert (1914) showed that current-formed ripples varied with flow type and flow intensity; the product of either oscillatory near-bed currents produced by waves, by unidirectional, turbulent currents; or by a combination of oscillatory and steady currents. The majority of these forms were found to be "*flow-transverse*"; that is, the crestline oriented normal to the direction of flow. Thus, from a genetic standpoint, ripple marks were primary classified as: wave (oscillation) ripples; current ripples; or combined-form ripples (Harms, 1975). In general, wave ripples are symmetrical, sharp-crested, and two-dimensional (2-D) in planform (or brick-pattern); current ripples, by contrast are generally asymmetrical showing a continuum on planform geometry from straight, through sinuous, to linguoid (Tanner, 1967); combined-flow ripples show a complex super-imposition of forms forming three-dimensional (3-D) ripples (Amos *et al*., 1988; Arnott and Southard, 1990; Southard *et al*., 1990). Bagnold (1956) and others suggested that small-scale and large-scale ripples were genetically different; referring to the latter as "dunes." The subsequent classification of large-scale bedforms and their distinction from ripples was presented by Allen (1985).

The classic work of Allen (1968), published in a book titled simply "*Current Ripples*," links clearly and elegantly the morphology, dynamics, and internal structure of current ripples with the near-bed unidirectional flows that created them. Current ripples occur in turbulent flows between the threshold for the traction and saltation/suspension of the rippled material at Froude numbers between 0.2 and 0.6 and flow Reynolds numbers between $5 \times 10^{-3}$ and $10^{-5}$ (Tanner, 1978) and at mean grain sizes less than 600 μm. Allen (1985) reviewed the fundamental hydrodynamic research into the near-bed physical processes responsible for unidirectional bedform generation. A variety of phase-diagrams of bedform stability have resulted from this work largely expressed in 2-D: flow strength (power, pressure, or speed); and grain size (diameter, dimensionless diameter, or grain Reynolds number). Each scheme, according to Allen (1985) is "*restricted in applicability by the limitations of the database*," and are poorly understood for silt- and gravel-sized materials. Furthermore, most proposed 2-D phase relationships ignore the solid-transmitted (ballistic) part of the shear stress caused by the sand in motion (Bagnold, 1941). This ballistic contribution, important to the evolution of aeolian ripples, also appears important in the evolution of subaqueous ripples. As well, the possible feedback of ripple bed morphology into flow turbulence, and hence bed shear stress, has primary and secondary effects over that created by grain (skin) friction of an initial flat bed (Bagnold, 1963).

The classical work on the hydrodynamics of wave ripple formation, migration, and evolution was undertaken in the laboratory by Bagnold (1946) and Manohar (1955) and in the field by Inman (1957). Bagnold (1946) observed a complex interaction between the movement of sand grains, the structure of the benthic boundary layer (and in particular, the evolution of attached vortices), and ripple morphology. From these observations, rolling grain ripples, vortex ripples, and post-vortex ripples were defined; each form stable within a range of grain sizes and near-bed conditions of oscillatory flow. Later, Komar (1974) and Clifton and Dingler (1984) showed that the cord length of the wave ripples was linearly correlated to (and predictable by) either wave orbital diameter (orbital ripples), or grain size (anorbital ripples), or were transitional between the two (suborbital ripples). More importantly, the type of ripple and its orientation and cord length could be predicted from knowledge of (1) grain size, (2) water depth, (3) wave orbital diameter, and (4) wave orbital velocity (Sleath, 1984). The importance of this work lies in the power to discriminate wave conditions, and thus paleoenvironment (water depth, wave heights, etc.) in the geological past (Allen, 1981). However, one vital piece of information still remains to be introduced to understand the significance and behavior of ripple marks: the internal structure.

The link between ripple marks and internal structure came from early work on current ripples undertaken by van Straaten (1954) and later Reineck and Singh (1966) on tidal flats of the Waaden Sea. They showed conclusively that the internal structure of ripples, and the relationship to ripple form, provides a record of the evolution and migration of the ripple, and equally important, the direction and magnitude of net sediment transport. This attribute of bedforms has been explored and exploited by Harms *et al*. (1982) and later by Rubin (1987) who showed a complex suite of internal structures resulting from invariable or variable ripples. These ripples may be either transverse to the mean sand transport direction, longitudinal (parallel) to it, or oblique and may produce either 2-D or 3-D cross-bedding. Internal structures reveal that bedform superimposition is common. The cause of superimposition has been assigned to either a fluctuating flow in time (Allen, 1978), or to a multiple-boundary layer (Rubin and Hunter, 1987). However, field observation shows complex superimposed ripple patterns in nature resulting from wave–steady current interactions under storms (Amos *et al*., 1988; Arnott and Southard, 1990). These patterns are further complicated by rotation of the flows leading to complex polygonal transitional patterns in the wave-formed ripple field (Allen, 1982), which merge or diverge dependent on the angle between the two flow types. At high angles of incidence, wave ripples and current ripples coexist in a steady state defined by the partitioned (wave or current) component of the bed shear stress; each ripple type responding to the flow as if oblivious of the superimposing stress (Young and Sleath, 1990). At low angles of incidence however, the bedforms coalesce into asymmetrical wave ripples, or multifrequency ripples with parallel crests (Allen, 1982).

## Future research

Future studies on the interaction of combined flows on ripple genesis is required, particularly in relation to the net sediment transport direction and at the saltation/suspension threshold: the ripple "break-off region" (Grant and Madsen, 1982). The role of ballistic impacts to bedform evolution in subaqueous flows, also needs exploring, particularly for poorly sorted sand.

The feedback of ripple form on bed shear stress deserves attention: The late J. Ludwick once said that the world of sediment dynamics is divided into "*lumpers*" those who consider that bedforms influence the movement of sand, and "*splitters*" those who do not (assigning the frictional drag entirely to skin friction of the composite sediment grains). The literature on the relationship between form drag, turbulence, and ripple shape and size is inconsistent (Soulsby, 1997). Future work is needed on the feedback mechanism between bedform genesis and turbulence generation/dissipation within the benthic boundary layer. Only then will we know if the "*lumpers*" or "*splitters*" were right.

Carl L. Amos and Patrick L. Friend

## Bibliography


Allen, J.R.L., 1968. *Current Ripples. Their Relation to Patterns of Water and Sediment Motion*. Amsterdam: North-Holland Publishing Company.

Allen, J.R.L., 1978. Ripple marks. In Fairbridge, R.W. and Bourgeois, J. (eds.), *The Encyclopedia of Sedimentology*. Stroudsburg: Dowden, Hutchinson & Ross.

Allen, J.R.L., 1982. *Sedimentary Structures, their Character and Physical Basis*, Volume I. Amsterdam: Elsevier.

Allen, J.R.L., 1985. *Principles of Physical Sedimentology*. London: Chapman & Hall.

Allen, P.A., 1981. Some guidelines in reconstructing ancient sea conditions from wave ripplemarks. *Marine Geology*, **43**: 59–67.

Amos, C.L. and King, E.L., 1984. Bedforms of the Canadian eastern seaboard: a comparison with global occurrences. *Marine Geology*, **57**: 167–208.

Amos, C.L., Bowen, A.J., Huntley, D.A., and Lewis, C.F.M., 1988. Ripple generation under the combined influences of waves and

currents on the Canadian continental shelf. *Continental Shelf Research*, **8** (10): 1129–1153.
Arnott, R.W., and Southard, J.B., 1990. Exploratory flow-duct experiments on combined-flow bed configurations and some implications for interpreting storm-event stratification. *Sedimentology*, **60**(2): 211–219.
Ashley, G.M., 1990. Classification of large-scale subaqueous bedforms: a new look at an old problem. *Journal of Sedimentary Petrology*, **60**(1): 160–172.
Bagnold, R.A., 1941. *The Physics of Blown Sand and Desert Dunes*. New York: John Wiley and Sons.
Bagnold, R.A., 1946. Motions of waves in shallow water: interactions between waves and sandy bottoms. *Proceedings of Royal Society of London, Series A*, **187**: 1–15.
Bagnold, R.A., 1956. The flow of cohesionless grains in fluids. *Philosophical Transactions of Royal Society of London, Series A*, **249**: 235–297.
Bagnold, R.A., 1963. Beach and nearshore processes. Part I, mechanics of marine sedimentation. In Thorne, C.R., MacArthur, R.C., and Bradley, J.B. (eds.), *The Physics of Sediment Transport by Wind and Water*. New York: American Society of Civil Engineers.
Clifton, H.E., and Dingler, J.R., 1984. Wave-formed structures and paleoenvironmental reconstruction. *Marine Geology*, **60**: 165–198.
Darwin, G.H., 1883. On the formation of ripple-mark in sand. *Proceedings of Royal Society of London*, **36**: 18–43.
Ellwood, J.M., Evans, P.D., and Wilson, I.G., 1975. Small scale aeolian bedforms. *Journal of Sedimentary Petrology*, **45**: 554–561.
Gilbert, G.K., 1914. The transport of debris by running water. *Professional Papers US Geological Survey*, 86.
Grant, W.D., and Madsen, O.S., 1982. Moveable bed roughness in unsteady flow. *Journal of Geophysical Research*, **87**(C1): 469–481.
Harms, J.C., 1975. Stratification produced by migrating bedforms. *Society of Economic Mineralogists and Paleontologists Short Course*, **2**: 45–61.
Harms, J.C., Southard, J.B., and Walker, R.G., 1982. Structures and sequences in clastic rocks. *Society of Economic Mineralogists and Paleontologists Short Course*, **9**: 8–51.
Inman, D.L., 1957. Wave generated ripples in nearshore sands. *US Army Corps of Engineers, Beach Erosion Board Technical Memorandum*, 100.
Komar, P.D., 1974. Oscillatory ripple marks and their evaluation of ancient wave conditions and environments. *Journal of Sedimentary Petrology*, **44**: 159–173.
Leopold, L.B., Wolman, M.G., and Miller, J.P., 1964. *Fluvial Processes in Geomorphology*. San Francisco: W.H. Freedman.
Manohar, M., 1955. Mechanics of bottom sediment movement due to wave action. *US Army Corps of Engineers, Beach Erosion Board Technical Memorandum*, 75.
Middleton, G.V., and Southard, J.B., 1984. Mechanics of sediment movement. *Publications SEPM Short Course Notes*, No. 3.
Reineck, H.E., and Singh, I.B., 1966. Primary sedimentary structures in the Recent sediments of the Jade, North Sea. *Marine Geology*, **5**(3): 227–235.
Rubin, D.M., 1987. *Cross-bedding, Bedforms and Paleocurrents*. Tulsa: Society of Economic Paleontologists and Mineralogists.
Rubin, D.M., and Hunter, R.E., 1987. Bedform alignment in directionally varying flows. *Science*, **237**: 276–278.
Sleath, J.F.A., 1984. *Sea Bed Mechanics*. New York: John Wiley & Sons.
Soulsby, R.L., 1997. *Dynamics of Marine Sands*. HR Wallingford Report SR, 466.
Southard, J.B., Lambie, J.M., Federico, D.C., Pile, H.T., and Weidman, C.R., 1990. Experiments on bed configurations in fine sands under bidirectional purely oscillatory flow, and the origin of hummocky cross-stratification. *Journal of Sedimentary Petrology*, **60**(1): 1–17.
Tanner, W.F., 1967. Ripple mark indices and their uses. *Sedimentology*, **9**: 89–104.
Tanner, W.F., 1978. Reynolds and Froude numbers. In Fairbridge, R.W., and Bourgeois, J. (eds.), *The Encyclopedia of Sedimentology*, Stroudsburg: Dowden, Hutchinson & Ross.
van Straaten, L.M.J.U., 1954. Composition and structure of Recent marine sediments in the Netherlands. *Leidsche geologische mededelingen*, **19**: 1–110.
Wilson, I.G., 1972. Aeolian bedforms—their development and origins. *Sedimentology*, **19**: 173–210.
Young, J.S.L., and Sleath, J.F.A., 1990. Ripple formation in combined transdirectional steady and oscillatory flow. *Sedimentology*, **37**(3): 509–516.

## Cross-references

Bars
Beach Features
Beach Processes
Beach Sediment Characteristics
Beach Stratigraphy
Coastal Sedimentary Facies
Eolian Processes
Rhythmic Patterns
Scour and Burial of Objects in Shallow Water

# ROCK COAST PROCESSES

Our ability to identify and measure the effect of rock coast processes has improved with the application of modern analytical techniques, geochronometric dating, and physical and mathematical modeling, but we are still largely ignorant of their precise nature (Trenhaile, 1987; Sunamura, 1992). The relative importance of rock erosional processes is often determined on the basis of ambiguous morphological evidence. Although the processes responsible for the slow lowering of rock surfaces have been inferred from micro-erosion meter data, the technique is unable to measure the dislodgement of large rock fragments by waves and frost.

It is difficult to obtain quantitative process data because of the imperceptible changes that generally occur on rock coasts within human lifetimes, the importance of storms and other high intensity—low frequency events, the lack of access to high and frequently precipitous cliffs, and the occurrence of exposed and often dangerous environments for wave measurement and subaqueous exploration. Changes in relative sea level and climate have also caused the nature and intensity of marine and subaerial processes to fluctuate through time, and because of slow rates of erosion, rock coasts often retain vestiges of environmental conditions that were quite different from today.

## Mechanical wave erosion

Wave quarrying appears to be the dominant erosional mechanism in the vigorous storm wave environments of the middle latitudes, based on the frequent occurrence of fresh rock scars and coarse, angular debris consisting of joint blocks and other rock fragments on shore platforms and at the foot of cliffs. Weaker waves in polar and tropical regions also play important roles, however, in eroding weathered rocks and removing loose debris.

The forces exerted by waves on coastal structures depend upon their deep water characteristics, tidal elevation, and submarine topography. A broken wave may be a less effective erosional agent than a wave that breaks directly against a cliff or other steep, natural structure, but broken waves occur much more frequently. Therefore, the compression of air in joints and other structural discontinuities by broken waves is probably of much greater importance than the direct impact of waves on rocks (water hammer) and the generation of high shock pressures against near-vertical structures by breaking waves. Rock fragments and sand can be effective abrasional agents in the intertidal and shallow subtidal zones, although even large waves may be unable to agitate material sufficiently at the base of thick accumulations (Robinson, 1977). Gently sloping abrasional surfaces are generally much smoother than wave quarried surfaces, but deep grooves can develop where abrasion is concentrated along joint planes and other structural weaknesses. Potholes are approximately cylindrical depressions that form where sand or large clasts are rotated by swirling water in the surf or breaker zones. They are particularly common in the upper intertidal zone where abrasives are trapped at the foot of scarps, and in structural or erosional depressions, and they also inherit, and subsequently modify, corrosional hollows in calcareous rocks.

Air compression, water hammer, and other processes responsible for wave quarrying require the alternate presence of air and water, and they therefore operate most effectively in a narrow zone extending from the wave crest to just below the still-water level. Most mathematical models also suggest that standing, broken, and breaking waves exert the greatest pressures on vertical structures at, or slightly above, the water surface. Wave erosion on a rock coast must therefore be greatest at the elevation that is most frequently occupied by the water surface. Over long periods of time, the tidally controlled water surface is most frequently at, or close to, the neap high and low tidal levels, and wave action is increasingly concentrated within the neap tidal levels as the tidal range decreases (Trenhaile, 1987, 1997) (Figure R20).Therefore, in

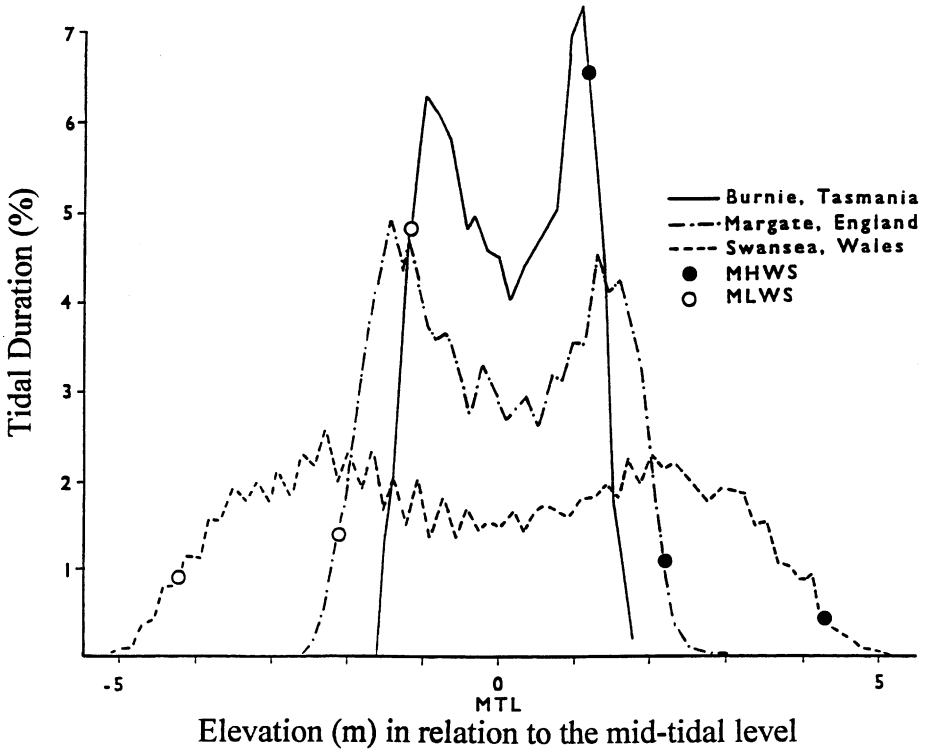


**Figure R20** Tidal duration distributions—the amount of time that the water surface is at each intertidal elevation. MHWS and MLWS are the means of the high and low water spring tidal levels, and MTL is the mid-tidal level. (After Carr and Graff, 1982.)

controlling the elevation of the water surface, tides allocate the expenditure of wave energy and direct the work of mechanical wave erosional processes within the intertidal zone.

Although mechanical wave erosion is vertically distributed according to the tidal distribution of the water surface, it may be skewed toward the upper portions of the tidal range because of the occurrence of deeper water, and therefore higher waves, at high tide, and because large storm waves operate when sea level is meteorologically raised above the tidal level. In areas with low tidal ranges, this latter effect could elevate the zone of maximum erosion above the level of the high spring tides. Furthermore, as only vigorous storm waves, which operate at higher elevations than weak waves, are able to erode resistant rocks, whereas weaker waves, operating at lower elevations, are able to erode less resistant rocks, the difference between the level of greatest erosion and the most frequent tidal level may increase with the resistance of the rock (Trenhaile, 1987).

## Weathering

Coasts are particularly suitable environments for physical and chemical weathering owing to alternate wetting and drying in the spray and intertidal zones, and the presence of salts. It is normally assumed that physical weathering is most important in high latitudes and chemical and biological weathering in low latitudes, in part because of the occurrence of suitable climates, but also because of fairly weak waves in these areas. Weathering also weakens rocks in the vigorous storm–wave environments of the middle latitudes, however, and it may be an essential precursor for the dislodgement and removal of rocks by weak waves in sheltered areas.

Physical weathering mechanisms include the alternate expansion and contraction of clay minerals under cycles of wetting and drying, temperature-dependent adsorption of water, thermally induced changes in volume, and frost action. The alternate expansion and contraction of clay minerals experiencing tidal- and weather-induced cycles of wetting and drying causes discontinuities to develop in shales and other argillaceous rocks, and also in the rocks that are adjacent to them. Clay minerals within small rock capillaries have negative charges that attract the positively charged ends of water molecules. This can breakup fine-grained, clay-rich rocks, which adsorb water and expand as temperatures rise, and desorb and contract as temperatures fall (Hudec, 1973). Temperature-dependent wetting and drying may be responsible for much of the field evidence that has traditionally been attributed to frost action, although several theories suggest that the two mechanisms could act together to generate more deleterious pressures within rocks than are generated by either mechanism acting alone. Thermally induced changes in volume also reduce the strength of some rocks. In southern Wales, for example, the expansion of limestones and the contraction of mudrocks under dry, hot conditions are responsible for diurnal variations in joint widths of up to 0.5 mm (Williams and Davies, 1987).

Although much remains to be determined about the mechanisms involved in frost action, we do have a general sense of the conditions that are most suitable for their operation. Coastal regions may be almost optimum environments. High levels of saturation can be attained in the supratidal and intertidal zones, and because intertidal rocks can freeze in air during low tide, and thaw in water during high tide, they experience many more frost cycles than in areas further inland. Intertidal frost action may also be particularly effective because of rapid changes in temperature caused by the sudden emergence and submergence of the rocks. Whereas rock temperatures rapidly increase when they are inundated in seawater, however, at least 5–6 h are needed for rocks to dissipate released latent heat and to cool to the freezing point of air. It is questionable whether critical levels of saturation can be maintained in the rocks over this period in the upper portion of the intertidal zone, and effective frost action in the lower portion of the intertidal zone may be inhibited by limited exposure to low air temperatures (Robinson and Jerwood, 1987). Although the presence of salts in solution can inhibit frost action, several studies have suggested that the greatest rock deterioration occurs in solutions that contain between 2 and 6% of their weight in salt; this suggests that frost action may be particularly effective in rocks that are saturated with seawater.

Frost- and temperature-dependent wetting and drying can only be effective erosional agents where there are suitable rocks, and waves that are strong enough to remove the coarse debris and prevent progressive burial of the cliff. Tidally induced frost action is inhibited at high latitudes by low water temperatures, but water and air temperatures suggest that it may occur at various times of the year in cool temperate regions (Trenhaile, 1987). Normal frost action, resulting from changes in air temperature, may also be more effective in the midlatitudes than in higher latitudes, where there are less frequent fluctuations about the freezing point. Atmospheric and tidally induced frost cycles are therefore probably most effective in cool, storm wave environments, and

waves and frost also tend to be most effective on the same types of rock; strong wave action may therefore obscure or inhibit the effects of frost action in exposed areas.

Chemical and salt weathering are most important in warm temperate and tropical regions. Chemical weathering requires a good supply of water to promote chemical reactions, and more crucially, to remove the soluble products. Chemical reactions are accelerated by high temperatures in the tropics, but the lack of liquid water rather than low temperatures is probably primarily responsible for the fairly low rates of chemical weathering in high latitudes. Mechanical salt weathering occurs through the growth of crystals from solutions in rock capillaries, and crystal hydration and temperature-induced expansion. Chemical and salt weathering contribute to the formation of tafoni and honeycombs, the smoothing and lowering of shore platforms by the suite of processes collectively referred to as water layer levelling, case hardening, and the impregnation of joint planes by dissolved ions to form frame- or box-like structures, and the formation of various types of weathering pits (Trenhaile, 1987). The existence of a permanent level of saturation in the intertidal zone, separating a weak, weathered oxidation zone from a strong and largely unweathered saturated zone below, has been a basic tenet of Australasian workers for almost a century. Present evidence suggests that rocks can only be permanently saturated below the low tidal level, however, where they are constantly submerged.

There is continuing debate over the processes responsible for the sharp pinnacles, ridges, grooves, and circular basins that are characteristic of coastal limestones in the spray and splash zones. Although these features are similar to karren formed by freshwater on land, surface seawater is usually saturated or supersaturated with calcium carbonate. It has been suggested that solution could occur in rock pools at night, when the carbon dioxide produced by faunal respiration is not removed by algae. Lower pH then causes calcium carbonate to be transformed into more soluble bicarbonate. Solution can be inhibited or prevented by other biochemical processes, however, including dissolved organic substances coating rock surfaces and building complexes with calcium ions. Although chemical solution does appear to be possible in seawater, recent studies have provided support for the contention that marine karren and other characteristic features of limestone coasts are primarily bioerosional in origin.

## Bioerosion

Bioerosion is the removal of the substrate by direct organic activity. It is probably most important in tropical regions, where there are fairly weak waves and an enormously varied marine biota living on coral, aeolianite, and other calcareous substrates. A wide range of techniques are used to breakdown rocks. Microflora and fauna that lack hard parts may use only chemical mechanisms, but other fauna secrete fluids that chemically weaken the rock, before mechanically abrading them with teeth, valvular edges, and other hard parts.

Microflora bore into rock and they change the chemistry of the water that is in contact with it—indeed cyanophyta (blue-green) and other algae may be the most important biological agents on rock coasts. Algae, lichen, and fungi are pioneer colonizers in the intertidal and supratidal zones and they allow subsequent occupation by gastropods, echinoids, chitons, and other grazing organisms that effectively abrade rock surfaces as they feed on epilithic and the ends of endolithic microflora. Grazing organisms are of enormous importance in some environments. For example, it has been estimated that they are responsible for about one-third of the surface erosion in the mid-tidal zone on Aldabra Atoll where sand is available for abrasion, and as much as two-thirds where sand is absent (Trudgill, 1976). At least 12 faunal phyla contain members that bore into rocks, especially in the lower parts of the intertidal zone. They include *Lithotrya* and other boring barnacles, sipunculoid and polychaete worms, gastropods, echinoids, *Lithophaga* and other bivalve molluscs, and Clionid sponges. Borers directly remove rock material, and they also weaken the remaining rock, making it more vulnerable to mechanical wave erosion and weathering. In the tropics, carbonate rocks favor chemical borers, but mechanical borers are active on a variety of substrates in temperate and cool seawater environments. There is a great deal of published data on bioerosional rates of erosion (Trenhaile, 1987), but they are of variable reliability and relevance. Nevertheless, most reported rates of erosion on vertical and horizontal limestone surfaces are between about 0.5 and 1 mm $yr^{-1}$, which may reflect the maximum boring rate of endolithic microflora.

## Ice

Until recently, it was generally believed that coastal ice is an ineffective erosional agent in the coastal zone, but its potential contribution to the development of rock coasts in cold environments is now being reassessed. The formation of subhorizontal shore platforms in the South Shetland Islands has been attributed to fast ice freezing to the underlying bedrock, quarrying by grounded ice and stranded ice rocked by the tides, and abrasion by rocks frozen into the ice base (Hansom and Kirk, 1989). Ice-push, by wind-driven floating ice loaded with rock fragments, also assists gelifraction and frost wedging in quarrying gneissic joint blocks in macrotidal Ungava Bay. Much of the ice-foot melts in place and does not contribute to debris removal, but it may facilitate deep frost penetration by providing a thermal barrier to sporadic warming by tidal water. Frost weathering and the effects of ice abrasion, dislodgement, and quarrying are also considered to be the main processes responsible for the formation of wide, subhorizontal platforms in the upper St. Lawrence Estuary (Dionne and Brodeur, 1988). Although there is clear evidence of the erosive efficacy of shore ice in this area, weak slates and shales, high tidal range, strong currents, and large erratic blocks provide particularly suitable conditions for frost and ice action, and it remains to be determined whether these cold region mechanisms assume similar roles in less favorable places.

## Mass movement

Active marine cliffs possess short rather than long-term stability because of undercutting, oversteepening, and the removal of basal debris by wave action. Mass movements therefore play an important role in the development of cliffed coasts, and there is a close relationship between the morphology of cliffs and the type of mass movement that takes place on them. Mass movements range, according to local circumstances, from the quasi-continuous fall of small debris to infrequent but extensive landsliding. Although rock falls are more frequent than deep-seated slides, they are generally much smaller. Falls occur in well-fractured rocks, especially where notches are cut into the cliff foot by waves, or, as in the tropics, by solution or bioerosion. Rock columns defined by joints or bedding planes also topple or overturn by forward tilting. Rock and slab falls, sags, and topples are essentially surficial failures induced by frost and other types of weathering, basal erosion, hydrostatic pressures exerted by water in rock clefts, and the reduction in confining pressures resulting from cliff erosion and retreat.

Deep-seated mass movements are triggered by groundwater build-up and basal undercutting. Translational slides usually occur where there are seaward dipping rocks, alternations of permeable and impermeable strata, massive rocks overlying incompetent materials, or argillaceous and other easily sheared rocks with low bearing strength. Slumps or rotational slides are common in thick, fairly homogeneous deposits of clay, shale, or marl. Sliding takes place in rocks that have been weakened by alternate wetting and drying, clay mineral swelling, or deep chemical weathering. Slides tend to occur during or shortly after snowmelt, or prolonged and/or intense precipitation. Water from septic systems, irrigation, runoff disruption, beach depletion through the building of coastal structures, and other human activities are playing increasing roles in some areas (Griggs and Trenhaile, 1994). The damming of rivers has also reduced the bed load reaching the coast, depleting beaches and exposing cliffs to more vigorous wave action.

Alan S. Trenhaile

## Bibliography

Carr, A.P., and Graff, J., 1982. The tidal immersion factor and shore platform development. *Transactions of the Institute of British Geographers*, **7**: 240–245.

Dionne, J.-C., and Brodeur, D., 1988. Frost weathering and ice action in shore platform development with particular reference to Québec, Canada. *Zeitschrift fur Geomorphologie, Supplement Band*, **71**: 117–130.

Griggs, G.B., and Trenhaile, A.S., 1994. Coastal cliffs and platforms. In Carter, R.W.G., and Woodroffe, C.D. (eds.), *Coastal Evolution*. Cambridge: Cambridge University Press, pp. 425–450.

Hansom, J.D., and Kirk, R.M., 1989. Ice in the intertidal zone: examples from Antarctica. In Bird, E.C.F., and Kelletat, D. (eds.), *Zonality of Coastal Geomorphology and Ecology*. Essener Geographische Arbeiten, **18**: pp. 211–236.

Hudec, P.P., 1973. Weathering of rocks in Arctic and Sub-arctic environment. In Aitken, J.D., and Glass, D.J. (eds.), *Canadian Arctic Geology*. Saskatoon: Geological Society Association of Canada. *Canadian Society for Petroleum Geologists Symposium*, pp. 313–335.

Robinson, D.A., and Jerwood, L.C., 1987. Frost and salt weathering of chalk shore platforms near Brighton, Sussex, UK. *Transactions of the Institute of British Geographers*, **12**: 217–226.
Robinson, L.A., 1977. Erosive processes on the shore platform of northeast Yorkshire, England. *Marine Geology*, **23**: 339–361.
Sunamura, T., 1992. *Geomorphology of Rocky Coasts*. Chichester: John Wiley.
Trenhaile, A.S., 1987. *The Geomorphology of Rock Coasts*. Oxford: Oxford University Press.
Trenhaile, A.S., 1997. *Coastal Dynamics and Landforms*. Oxford: Oxford University Press.
Trudgill, S.T., 1976. The marine erosion of limestone on Aldabra Atoll, Indian Ocean. *Zeitschrift fur Geomorphologie, Supplement Band*, **26**: 164–200.
Williams, A.T., and Davies, P., 1987. Rates and mechanisms of coastal cliff erosion in Lower Lias rocks. In Kraus, N. C. (ed.), *Coastal Sediments '87*. American Society for Civil Engineering, pp. 1855–1870.

## Cross-references

Cliffed Coasts
Cliffs, Erosion Rates
Cliffs, Lithology versus Erosion Rates
Karst Coasts
Mass Wasting
Notches
Shore Platforms
Weathering Processes in the Coastal Zone